# A High Resolution Radar Altimeter to Measure the Topography of Ice Sheets

*A* Thesis Presented

by

Rudolf A. Pawul

Submitted to the Graduate School of the
University of Massachusetts Amherst in partial fulfillment
of the requirements for the degree of

Master of Science

March 1997

Department of Electrical and Computer Engineering

A HIGH RESOLUTION RADAR ALTIMETER TO MEASURE THE TOPOGRAPHY OF
ICE SHEETS

*A* Thesis Presented

by

RUDOLF A. PAWUL

Submitted to the Graduate School of the
University of Massachusetts Amherst in partial fulfillment
of the requirements for the degree of

MASTER OF SCIENCE

March 1997

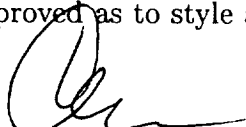Department of Electrical and Computer Engineering

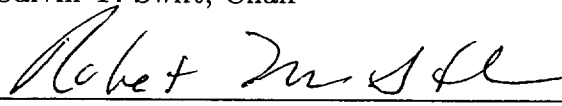A HIGH RESOLUTION RADAR ALTIMETER TO MEASURE THE TOPOGRAPHY OF ICE SHEETS

*A* Thesis Presented
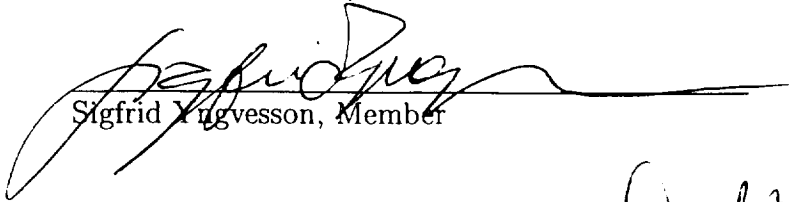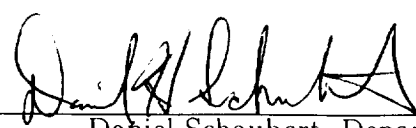
by

RUDOLF A. PAWUL

Approved as to style and content by:

_____
Calvin T. Swift, Chair

_____
Robert E. McIntosh, Member

_____
Sigfrid Yngvesson, Member

_____
Daniel Schaubert, Department Head
Electrical and Computer Engineering

To my family

ACKNOWLEDGMENTS

My graduate studies at the University of Massachusetts Microwave Remote Sensing Laboratory have been a rewarding experience and there are many people who deserve thanks for their involvement. First, I would like to thank Dr. Calvin Swift. His knowledge and guidance has been invaluable for my development as an engineer and with all the difficulties I have encountered, he never lost patience with me, something I greatly appreciate. Both he, and Dr. Robert McIntosh have assembled an excellent research facility and honored me with the opportunity to learn from them. I must again thank them both for the opportunity to continue working with them at Quadrant Engineering. I greatly appreciate Dr. Sigfrid Yngvesson for serving on my thesis committee.

There are many MIRSL colleagues who have contributed to this thesis, as well as my professional development. Dr. Ellen Ferraro not only taught me the basics when I arrived at MIRSL, but has graciously continued to advise me well after she left the lab. Dr. Jim Carswell has been a great teacher and friend, and without his support I would not be writing these acknowledgments. Eric Knapp assisted in too many ways to describe and Matt Grund also deserves many thanks. I would like to thank to Claire Hopley for greatly improving the readability of this thesis.

From my trip to Greenland, I would like to thank Bill Krabill, Earl Frederick, and Serdar Manizade for their help with data processing, as well as their friendship. The flight crew was unbelievably helpful and everyone involved made a green first year student feel like he belonged. I will never forget all their kindness.

Of course, I wish to thank my parents and family. Without their generosity, love and support, nothing I have ever done could have been possible. Finally, I want to thank my fiancee and best friend, Katie, for her love and support and for sharing her life with me.

ABSTRACT

A HIGH RESOLUTION RADAR ALTIMETER TO MEASURE THE TOPOGRAPHY OF
ICE SHEETS

MARCH 1997

RUDOLF A. PAWUL

B.S.E.E., UNION COLLEGE

M.S.E.C.E., UNIVERSITY OF MASSACHUSETTS AMHERST

Directed by: Professor Calvin T. Swift

This thesis is a reference for the Advanced Application Flight Experiment (AAFE) altimeter. The transmitter and receiver subsections are described and measurements of their current state is provided. During the 1994 NASA Greenland Experiment, the altimeter experienced several hardware malfunctions. The process of returning the radar to its fully operational state is presented in detail and necessary design modifications are explained. An updated radar user's manual is included along with various circuit designs which need to be implemented. The thesis is intended to provide an incoming graduate student with a solid foundation of the fundamentals of AAFE altimeter operation.

TABLE OF CONTENTS

LIST OF FIGURES

# CHAPTER 1

## INTRODUCTION

In 1974 the Hughes Aircraft Company designed the Advanced Application Flight Experiment (AAFE) altimeter for the NASA Wallops Flight Facility. It was constructed to provide three measurements: altitude, wave height, and reflectivity of radar signals from the ocean surface. Altitude measurements with a resolution of ten centimeters or less, at a data rate of one measurement per second, was the main objective [1].

After several years of successful oceanographic experiments, the AAFE altimeter fell into relative disuse. However, as the scientific community developed interest in monitoring the volume of glacial ice, attention was turned towards modifying the AAFE altimeter for Arctic ice mapping. Such interest stems from the impact of the mass balance of the Greenland on Antarctic ice sheets on longterm changes in the global climate and the global sea level [2].

In 1990 the altimeter was transferred to the Microwave Remote Sensing Laboratory (MIRSL) at the University of Massachusetts. At the time, it was unsuitable for conducting remote sensing measurements from an aircraft platform. The foremost difficulty was its limited number (24) of range gates, which corresponded to a range window of approximately 10 meters. This made automated tracking impossible, and even manual tracking would have been extremely difficult. In addition, the data acquisition and control systems were grossly obsolete.

As a result, MIRSL refurbished the altimeter, adding a modern data acquisition system that not only increased the range window to 88 meters, but also allowed continuous data acquisition for multi - hour flights. The increased range window

made possible the development of an automated tracking system and the storage of entire surface return waveforms, which could be re-tracked by various methods during post processing [3]. With these enhancements, the AAFE altimeter successfully participated in the 1991, 1993, and 1994 NASA Arctic Ice Mapping experiments over Greenland, obtaining valuable data.

However, from reasonable wear and tear with time (the transmitter and receiver systems are largely unmodified from the 1974 fabrication), as well as possible shipping damage during the 1994 Greenland experiment, the AAFE altimeter has experienced performance degradation. Thus, MIRSL has undertaken a series of upgrades. The main focus of this thesis will be on this "second generation" of improvements, as well as extensive hardware documentation since the large number of modifications makes the current documents inaccurate.

After a chapter on basic radar altimetry, a section details the state of the AAFE altimeter before the recent modifications. This section explains the problems that motivated the upgrade and serves as a basis for measuring the performance improvements now being enjoyed. The subsequent chapter itemizes the hardware alterations and describes the necessary new components, and their incorporation into the relevant altimeter subsystems. It also documents the performance enhancements. Following a brief segment on data from from the 1994 Greenland experiment, the thesis concludes with suggestions for future endeavors.

# CHAPTER 2

## BASIC ALTIMETRY THEORY

In its most basic form, radar altimetry consists of sending out a short pulse of energy and accurately determining the time it takes to scatter from the ground and back into the receiver. Since a radar altimeter is typically a nadir-looking instrument, the distance to the surface directly below the radar is given by

$$h = \frac{ct}{2},$$ (2.1)

where h is the height above the surface, c is the speed of light (3.0 x $10^8$ meters per second), and t is the round-trip time, as measured by the altimeter. The minimum range resolution, $\Delta R$, of the resulting measurement is limited by the width of the transmitted pulse, T, such that

$$\Delta R = \frac{cT}{2}.$$ (2.2)

Therefore, it is advantageous to transmit as narrow a pulse as possible.

If $P_t$ is the power transmitted by the altimeter, the received power $P_r$ can be determined from the radar range equation, which can be expressed in the following simplified form:

$$P_r = \frac{P_t K}{R^4},$$ (2.3)

where R is the range to the target and K is a lumped constant including the antenna gain, radar cross section of the target and the effective area of the antenna. The average power transmitted by the altimeter is given by

$$P_{av} = \frac{P_t T}{T_{PRF}},$$ (2.4)

where $T_{PRF}$ is the time between pulses. For a fixed value of $P_{av}$, it is therefore an advantage to transmit a wide pulse. As a result, some engineering compromise must

be made to accommodate both an accurate measurement of range and an acceptable range within which the instrument can operate.

One acceptable compromise is to use pulse compression, which enables a radar to radiate a greater amount of energy yet still obtain the range resolution of a short pulse. This is accomplished through increasing the signal bandwidth by frequency modulating the signal within the pulse envelope [4].

The AAFE altimeter uses a common form of pulse compression: a linearly frequency modulated pulse or "chirp" pulse. Figure 2.1 shows an example of such a pulse. Figure 2.2 shows a frequency versus time plot of the same pulse. Such a chirp pulse may be generated in a variety of ways. Two of the most common make use of either a surface acoustic wave (SAW) device, or a digital chirp synthesizer. These are described in greater detail in later sections, which focus on their use in the AAFE altimeter.

Pulse compression radars must also utilize a method to "de-chirp" the transmitted pulse upon reception. One way to accomplish this task is to pass the received pulse back through a matching SAW device, compressing all the frequency components back together in time [5]. The resulting output is the autocorrelation function of the chirped pulse. As shown in figure 2.3, this is a sinc function with a pulse width $\tau = \frac{1}{B}$ and amplitude $\sqrt{BT}$, where T is the actual transmitted pulse width of the chirp. The quantity $\tau$ can be thought of as the "effective" pulse width. Although a pulse of width T is originally transmitted, when the return is analyzed, it has already been transformed to the sinc pulse, having a shorter time duration, $\tau$.

This process illustrates the figure of merit for a pulse compression radar called the compression ratio. It is defined as

$$CR = \frac{T}{\tau}. \qquad (2.5)$$

4
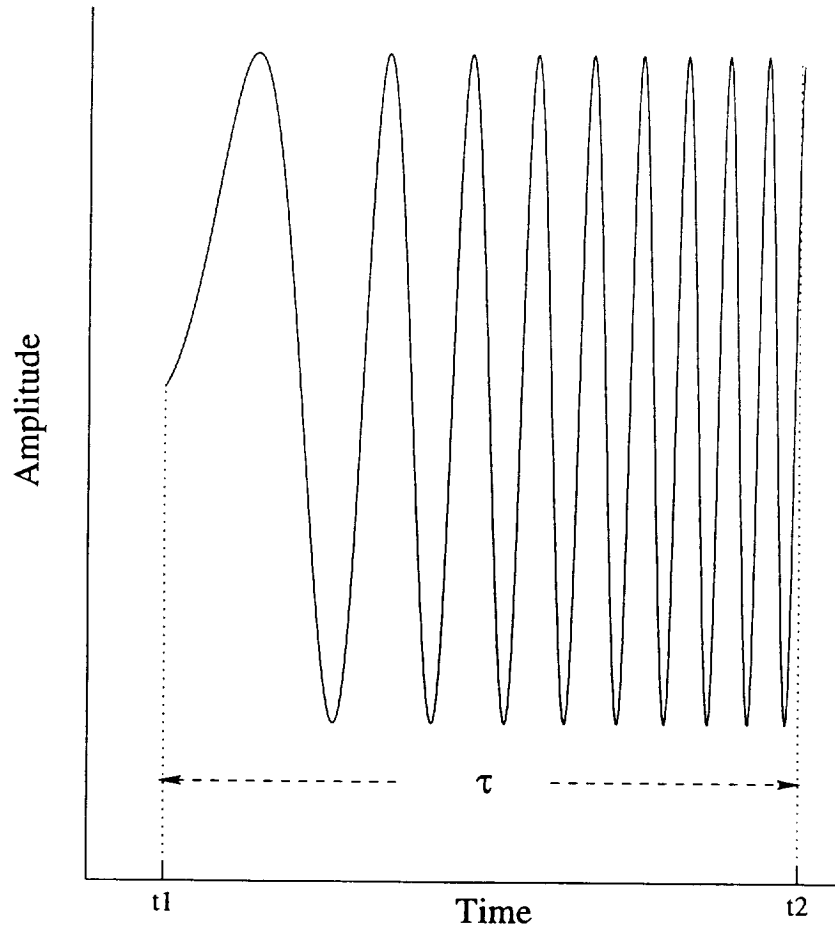
Figure 2.1 Time domain representation of a "chirp" signal.
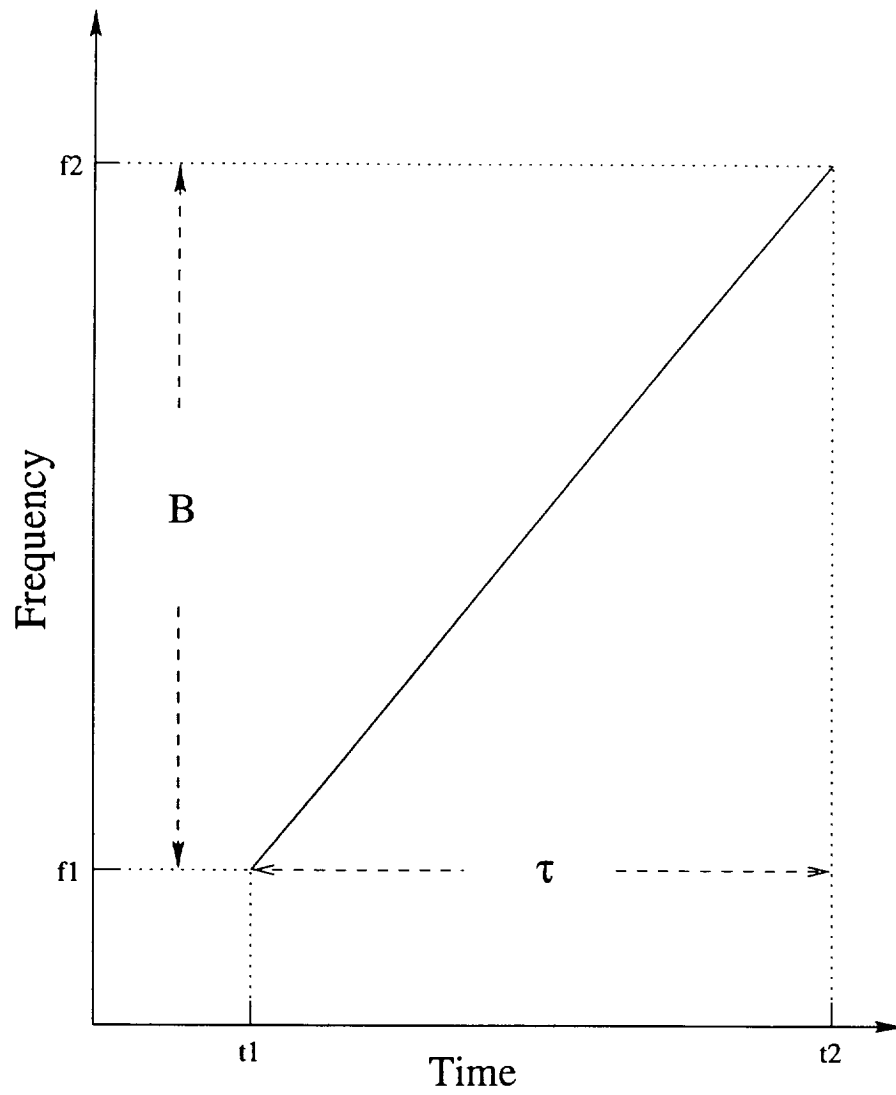
Figure 2.2 Frequency versus time representation of a "chirp" signal.
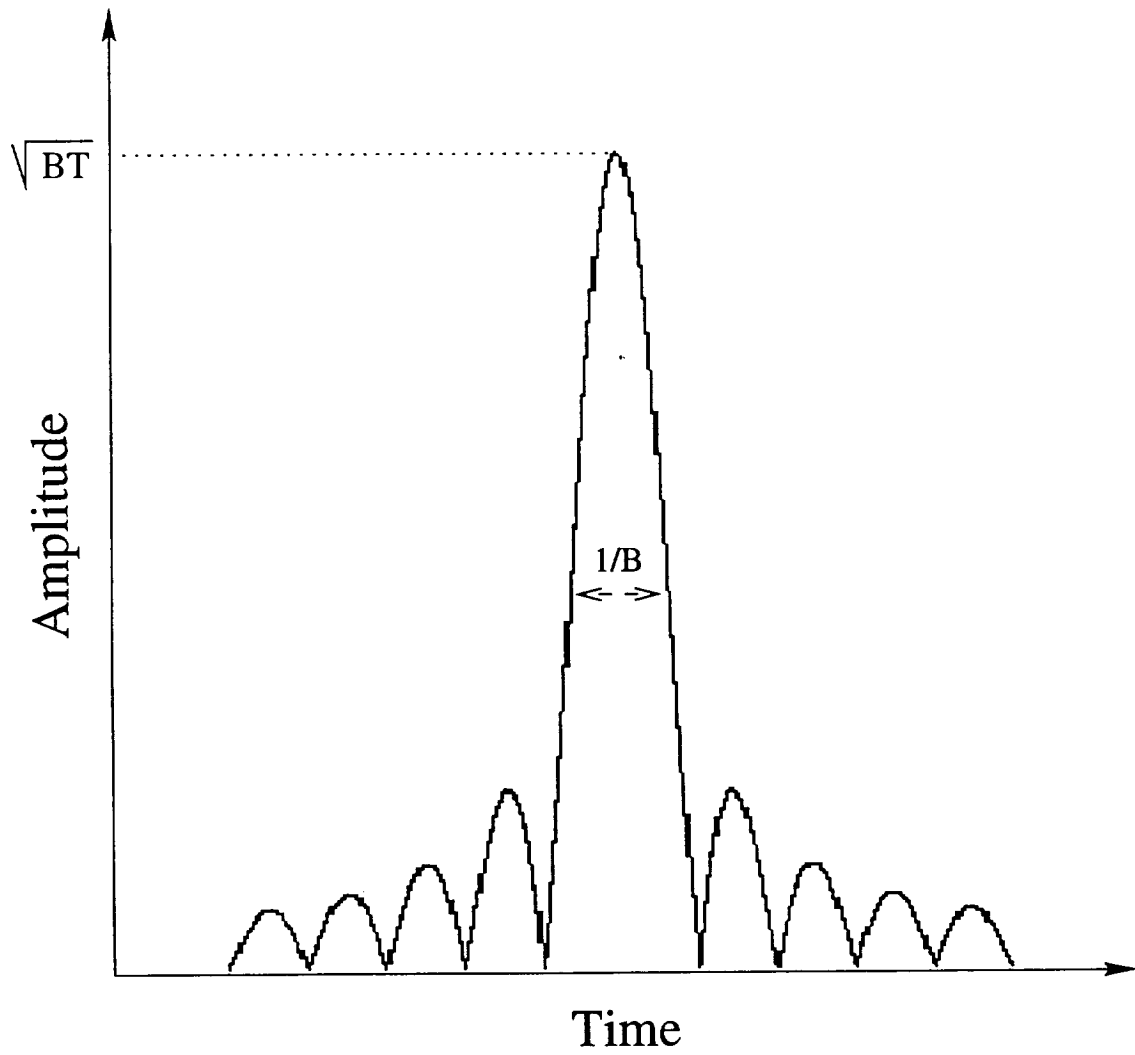
Figure 2.3 Example of a SAW device de-chirped pulse.

Using the relationship between the effective pulse width, $\tau$, and the bandwidth of the chirp signal, it may also be stated as

$$CR = BT. \qquad (2.6)$$

These two forms of the compression ratio show the improvement achieved for both the range resolution and average power transmitted.

Of greater relevance to the AAFE altimeter, however, is the dechirping technique of full deramping. This procedure involves mixing the received chirp with a delayed replica of itself, thus translating any shifts in time into offsets in frequency [3]. As a result, the converted waveform must ultimately be analyzed in the frequency domain. Depending on the time at which the transmitted pulse arrives at the deramping mixer and the time at which the dechirping pulse is sent to the mixer, the resulting mixer output can be divided into four cases. These are illustrated in figures 2.4 and 2.5. Figure 2.4a shows the timing of the transmitted and received pulses of the radar, while each of the following sub-figures are representations of the different timing cases of the dechirping pulse, normalized to their governing step functions.

In figure 2.4b, the replica chirp arrives early at the mixer input, resulting in the mixer output illustrated in figure 2.4c. Figures 2.4d and 2.4e show the best-case scenario where the dechirp signal and the received signal arrive simultaneously at the mixer input. When the replica arrives late as shown in figure 2.5b, the output assumes the form shown in 2.5c. Finally, in figures 2.5d and 2.5e, the dechirp arrives too early and too late, respectively, to acquire the received pulse. Note that the pulse width, T, of the received pulse and the dechirp pulse are assumed equal to model the performance of the AAFE altimeter; however, the analysis still holds without this assumption.

8
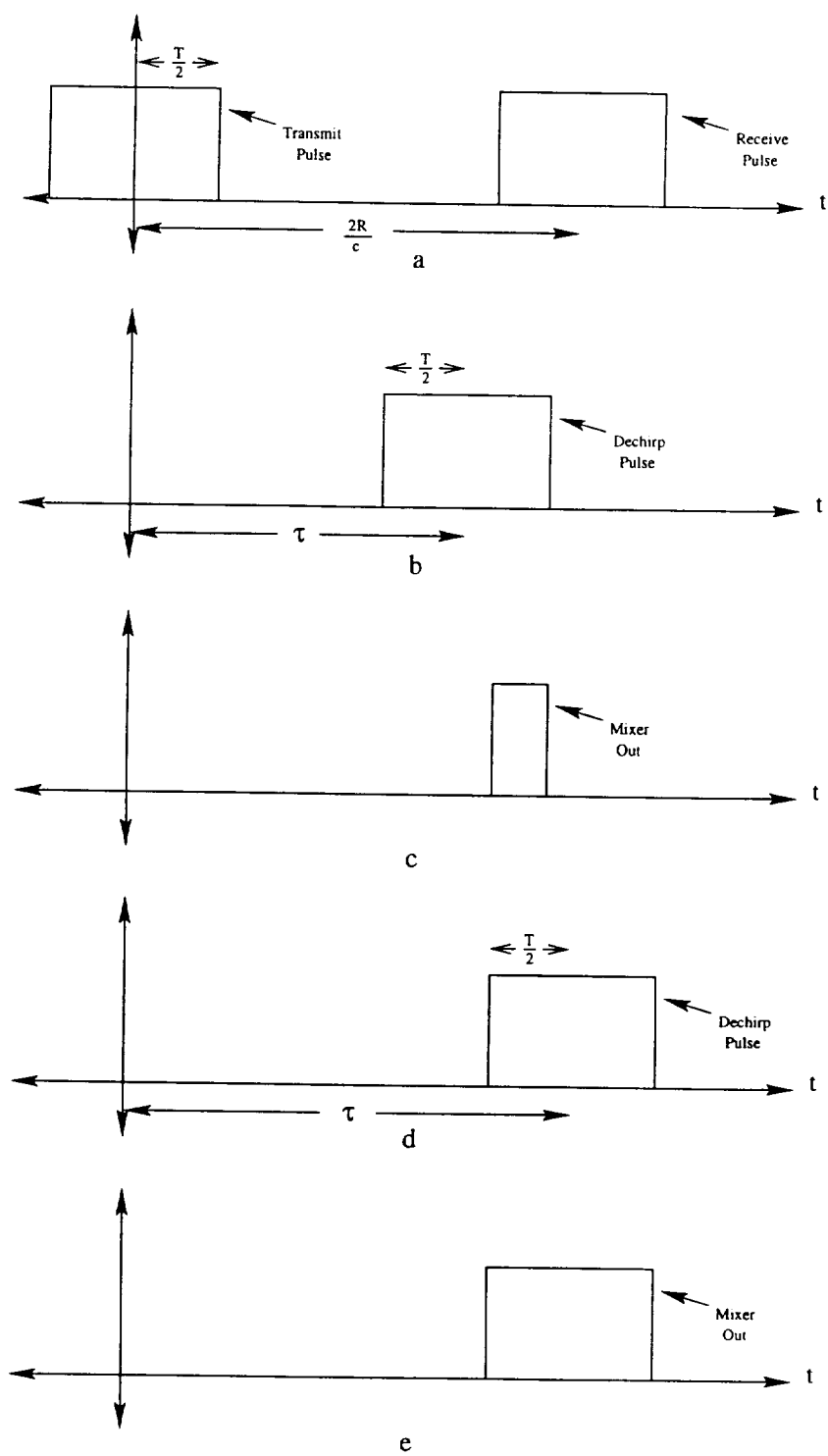
Figure 2.4 Timing analysis of the full deramping de-chirping method.
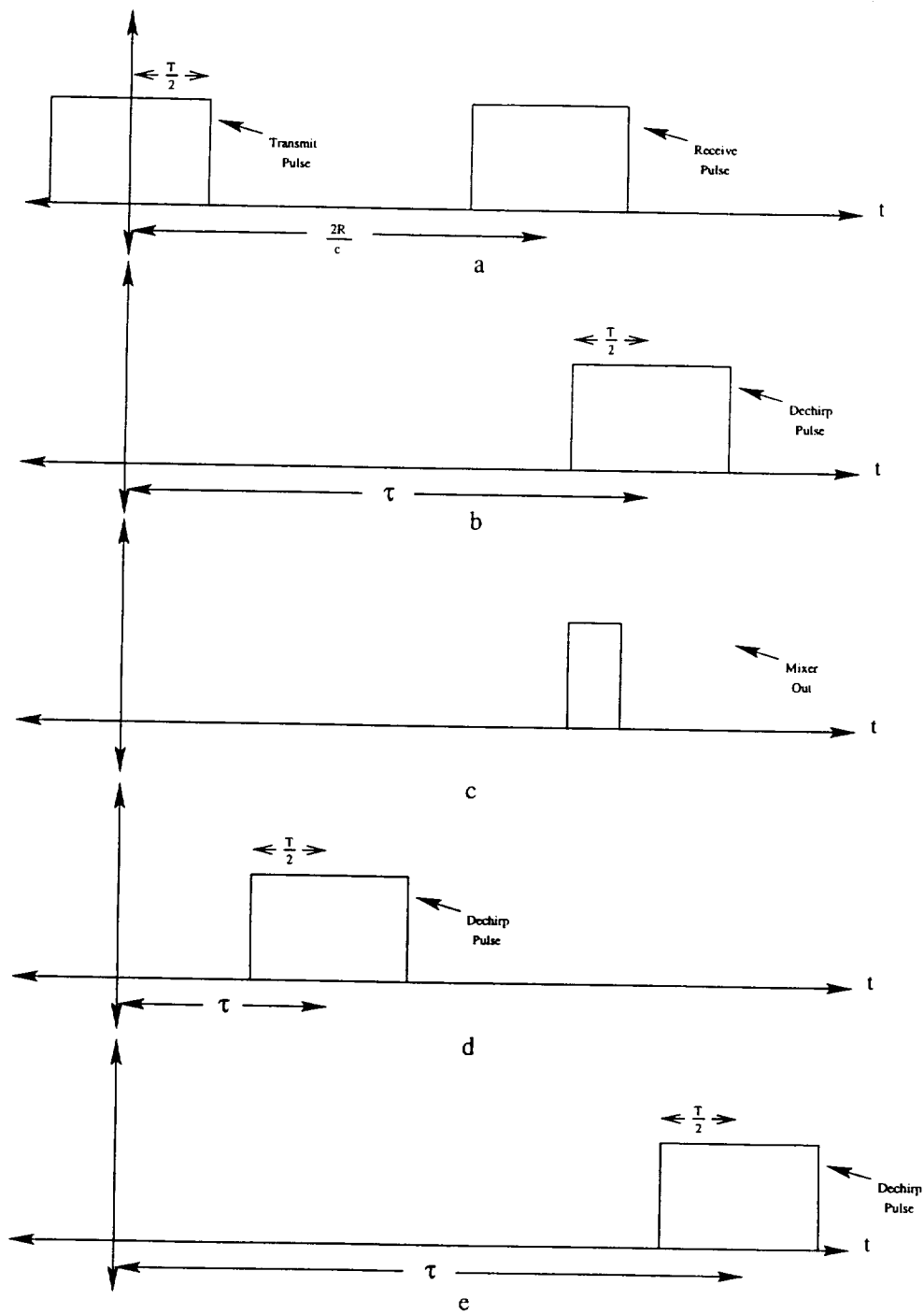
Figure 2.5 Timing analysis of the full deramping de-chirping method continued.

A transmitted chirp, with frequency $f_o$, bandwidth B, and pulse width T, can be expressed as

$$s_t(t) = e^{j2\pi f_o t} e^{j\pi \frac{B}{T} t^2} [u(t + \frac{T}{2}) - u(t - \frac{T}{2})]. \tag{2.7}$$

Accounting for the round trip delay time of $\frac{2R_o}{c}$, it can be shown that the deramped signal takes on the form

$$s_t(t) = e^{j2\pi t[f + \frac{B}{T}(\tau - \frac{2R_o}{c})]} [u(t - \frac{2R_o}{c} + \frac{T}{2}) - u(t - \frac{2R_o}{c} - \frac{T}{2})] \times$$

$$[u(t - \tau + \frac{T}{2}) - u(t - \tau - \frac{T}{2})].$$

$$\tag{2.8}$$

Then, using the previous timing analysis, and setting

$$s(t) = e^{j2\pi t[f + \frac{B}{T}(\tau - \frac{2R_o}{c})]}, \tag{2.9}$$

the full deramped return signal can be expressed as:

$$s_r(t) = \begin{cases} 0 & \tau \leq \frac{2R_o}{c} - T \\ s(t)[u(t - \frac{2R_o}{c} + \frac{T}{2}) - u(t - \tau - \frac{T}{2})] & \frac{2R_o}{c} - T \leq \tau \leq \frac{2R_o}{c} \\ s(t)[u(t - \frac{2R_o}{c} + \frac{T}{2}) - u(t - \frac{2R_o}{c} - \frac{T}{2})] & \tau = \frac{2R_o}{c} \\ s(t)[u(t - \tau + \frac{T}{2}) - u(t - \frac{2R_o}{c} - \frac{T}{2})] & \frac{2R_o}{c} \leq \tau \leq \frac{2R_o}{c} + T \\ 0 & \tau \geq \frac{2R_o}{c} + T. \end{cases}$$

As stated earlier, the information contained in the return must now be extracted in the frequency domain. By evaluating the Fourier Transform

$$S_r(f) = \frac{1}{T} \int_{-\infty}^{\infty} s(t) e^{-j2\pi f t} \tag{2.10}$$

of the time domain return, we obtain

11

$$S_r(f) = \begin{cases} 0 & \tau \leq \frac{2R_o}{c} - T \\[2mm] e^{j\pi f'(\tau + \frac{2R_o}{c})} \frac{\sin[\pi(\tau - \frac{2R_o}{c} + T)f']}{\pi T f'} & \frac{2R_o}{c} - T \leq \tau \leq \frac{2R_o}{c} \\[2mm] e^{j2\pi f' \frac{2R_o}{c}} \frac{\sin[\pi T f']}{\pi T f'} & \tau = \frac{2R_o}{c} \\[2mm] e^{j\pi f'(\tau - \frac{2R_o}{c} - T)} \frac{\sin[\pi(\tau - \frac{2R_o}{c} - T)f']}{\pi T f'} & \frac{2R_o}{c} \leq \tau \leq \frac{2R_o}{c} + T \\[2mm] 0 & \tau \geq \frac{2R_o}{c} + T, \end{cases}$$

where

$$f' = f_o - f + \frac{B}{T}\left(\tau - \frac{2R_o}{c}\right).$$

Thus, the return signal is expressed in the form of a sinc function whose center frequency depends on the round-trip time to the surface, $\frac{2R_o}{c}$.

The added performance achieved by pulse compression does not come without a penalty. The increased bandwidth of the receiver results in a greater input noise power as determined by

$$P_n = kT_oB, \tag{2.11}$$

where $P_n$ is the input noise power, k is Planck's constant (1.38 x $10^{-23}$), $T_o$ is the ambient temperature in Kelvin, and B is the expanded bandwidth of the receiver. However, due to the Gaussian statistical properties of the noise, one can somewhat reduce its degrading effects on the return signal by averaging the returns of several pulses together.

In addition, it has been shown that with a known surface composition and a prior understanding of the altimeter's response to such a surface, a greater range resolution can be achieved. Radar altimeter return waveforms from the ocean surface have been well-categorized, and the AAFE altimeter was instrumental in the study of altimeter response characteristics over glacial ice under the operation of Dr. Ellen Ferraro. The total return power of the AAFE altimeter was modeled by Ferraro as an

incoherent sum of a surface scattering component, a volume scattering component, and the noise floor given by

$$P_r(\tau) = a + AP_{rs}(\tau) + BP_{rv}(\tau), \tag{2.12}$$

where $a$ is the noise floor contribution, and A and B are the percentages of surface and volume return power respectively. $P_{rs}(\tau)$ was evaluated by assuming a transmitted impulse and using the radar range equation

$$P_{rs}(t) = \frac{P_t\lambda^2}{(4\pi)^3} \iint \frac{\delta(t - \frac{2R}{c})G^2(\theta)\sigma^o(\theta)}{R^4} dA, \tag{2.13}$$

where $G^2(\theta)$ and $\sigma^o(\theta)$ are functions representing the gain of the radar antenna and backscatter coefficient for the surface, respectively. Detailed analysis provided a form to which AAFE altimeter waveforms could be fit:

$$P_{rs}(\tau) = \frac{C_o}{H^3 s^2} e^{(t_p/t_s)^2} e^{-(2\tau/t_s)} erfc(\frac{t_p}{t_s} - \frac{\tau}{t_p}), \tag{2.14}$$

where

$$C_o = \frac{P_t\lambda^2 G_o^2 \Gamma(0^o)}{32\pi^2}, \tag{2.15}$$

$$\tau = t - \frac{2H}{c}, \tag{2.16}$$

$$t_p = \sqrt{2}\sqrt{(\frac{2\sigma_h}{c})^2 + \sigma_p^2}, \tag{2.17}$$

$$t_s = \frac{2H}{c} \frac{1}{\frac{8ln2}{\theta_B^2} + \frac{1}{s^2}}. \tag{2.18}$$

$C_o$ is a constant, erfc is the complementary error function, H is the height above the surface, $\eta_v$ is the volume backscatter coefficient, $\sigma_h$ is the rms surface height and $\sigma_p$ is the standard deviation of the system point target response.

Similarly, using the volume scattering radar range equation [Swift 1985],

$$P_{rv}(t) = \frac{P_t \lambda^2 T^2}{(4\pi)^3} \iiint \frac{\delta(t - 2(\frac{R_o}{c} + \frac{R-R_o}{c_s}))G^2(\theta)}{R^4} e^{-4\alpha(R-R_o)} \eta_v dV, \qquad (2.19)$$

the resulting return power due to volume scattering can be expressed as

$$P_{rv}(\tau) = \begin{cases} \frac{C_1}{\beta c - 2\alpha c_s}(e^{-2\alpha c_s \tau} - e^{-\beta c \tau}) & \tau > 0 \\ 0 & \tau < 0, \end{cases}$$

where

$$C_1 = \frac{P_t \sqrt{2} \lambda^2 T^2 G_o^2 \eta_v}{32\pi^2 H^3}, \qquad (2.20)$$

$$\beta = \frac{8 ln2}{H\theta_B^2}, \qquad (2.21)$$

$$\tau = t - \frac{2H}{c}, \qquad (2.22)$$

and

$$c_s = \frac{c}{\sqrt{\epsilon_{snow}}}. \qquad (2.23)$$

In glacial ice regions that contain a higher percentage of liquid water, equation 1.12 will be dominated by the surface return component due to limited surface penetration. These regions are called "wet-zone" regions. Conversely, in "dry-zone" regions, there is no liquid water content so sub-surface volume scatterers contribute more to the return. In the intermediate zone, often known as the percolation-zone, the liquid water content varies depending on season and on location within the zone. Analysis of returns within this zone are further complicated by a volume backscatter coefficient that depends upon position ($\rho$ and h). As a result, the expression for return power due to volume scatterers must be modified. Figure 2.6 gives examples of AAFE return waveforms from a variety of ice sheet compositions in Greenland. The changes in shape of the waveform can be attributed to varying contributions of surface and volume scatterers. [3]

14
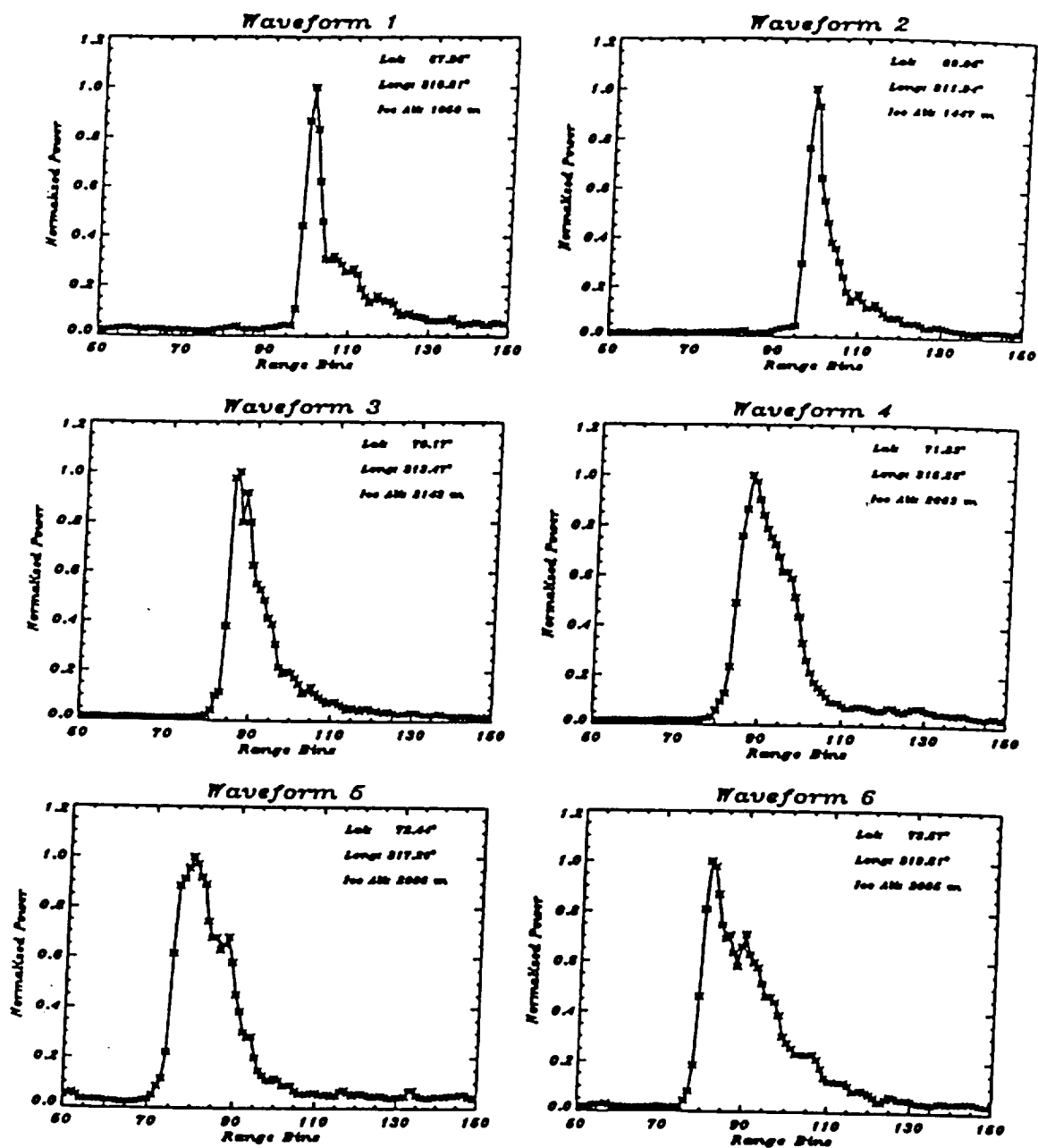
Figure 2.6 Six altimeter return waveforms from the Greenland ice sheet [Ferraro, 1994].

# CHAPTER 3

## HARDWARE DESCRIPTION

Figure 3.1 shows a general block diagram of the AAFE altimeter. The transmitter subsystem generates a 13.9 GHz chirp with a 360 MHz bandwidth. The control subsystem coordinates the timing of all the switches in the transmitter and receiver. Dechirping of the surface return takes place in the receiver subsystem, whose output is then sampled by the data acquisition subsystem. Output from the data acquisition subsystem is passed to the computer subsystem, which saves it to disk. The computer subsystem, comprised of a Hewlett Packard (HP) personal computer running both HP basic and HP Unix, facilitates communication between the control and data acquisition systems and provides a user interface for the radar operator.

Since the complete refurbishment of the AAFE altimeter in 1990, other modifications have been added. Because much of the system has remained unchanged from 1990, the refurbished state will be used as a reference point for the detailed hardware description. This will better illustrate the rationale for the more recent modifications.

Figure 3.2 shows a general block diagram of the refurbished transmitter subsystem. A more detailed diagram is presented in figure 3.3, where numbers found above and below the lines between adjacent components correspond, respectively, to the frequency in MHz and peak power measurements in dBm of the signal at the current point. Power measurements for continuous wave signals were made with an HP spectrum analyzer and low-loss test cable.
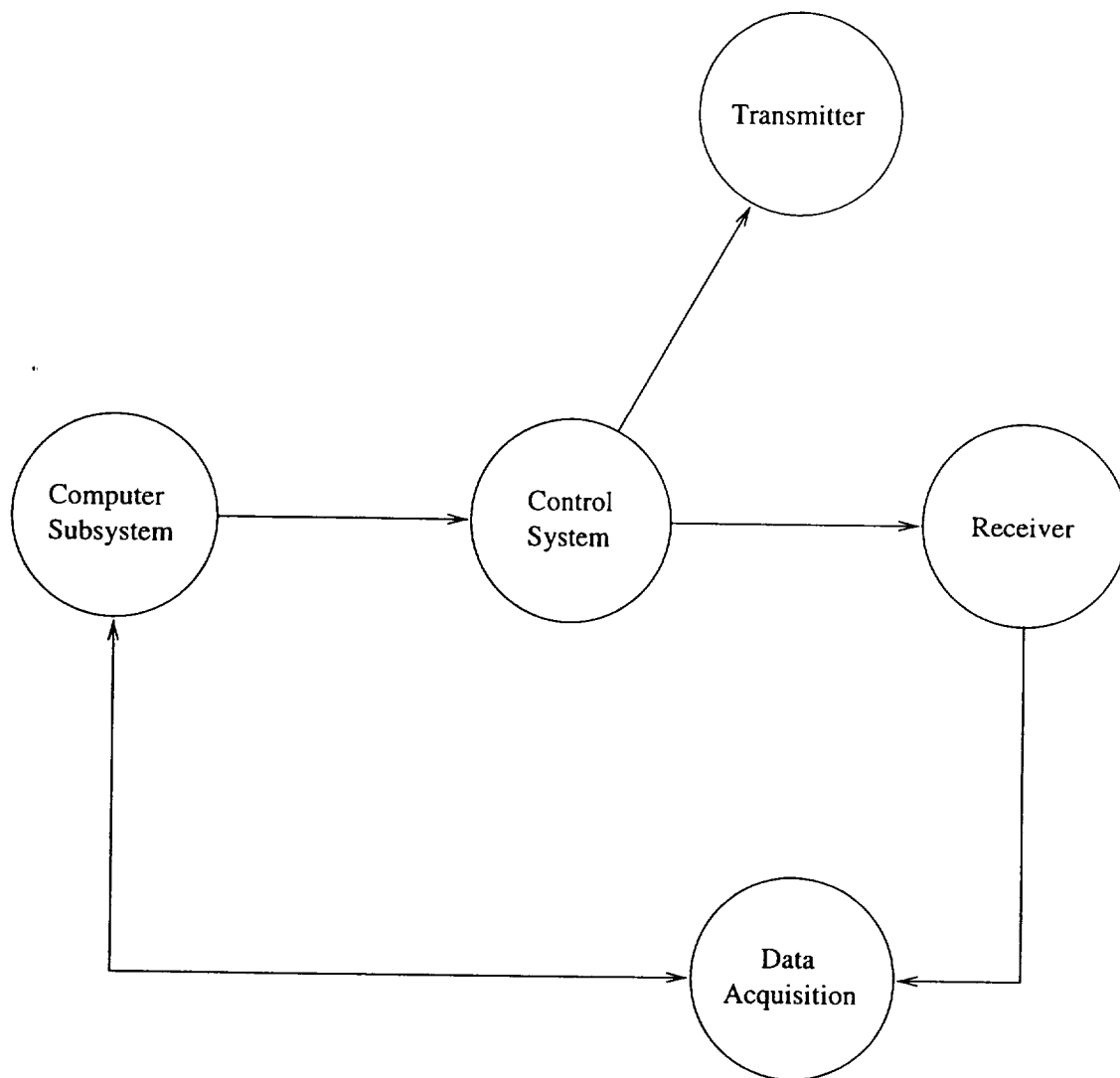
Figure 3.1 General block diagram of the AAFE altimeter's major components.

The spectrum analyzer was also used for pulsed signals, using the duty cycle of the signal to obtain a peak power figure. For example, a power measurement of a +3 dBm, 3.1 $\mu$second pulse, at a pulse repetition frequency of 750 Hertz would be approximately -23.3 dBm using the spectrum analyzer. This value is a measurement of the average power of the pulse. Since the duty cycle is 0.2325%, subtracting its value in dB

$$DutyCycle(dB) \quad = \quad 10log[\frac{3.1x10^{-6}seconds}{1/(750Hertz)}] \quad \approx \quad -26.3 \qquad (3.1)$$

results in the original peak power of +3 dBm.

Chirped pulses, illustrated with an arrow over their frequencies, were measured using a peak power meter. A peak power meter returns the total power over an entire band, which is ideal for a broad frequency chirped pulse. Sensors for the power meter are only usable over a small power range. As the approximate power level of signals was known beforehand, signal levels could be modified to this range via a well-characterized amplifier or attenuator and readings adjusted accordingly for accurate measurements. Power meter measurements were taken of continuous wave and "regularly" pulsed signals whenever possible to discover and eliminate any sources of error.

All frequencies for the AAFE altimeter are generated from the 108 MHz source as combinations of 540 MHz and 27 MHz signals resulting from the frequency multiply and divide components, as shown in figures 3.2 and 3.3. The ×5 and ÷4 are obtained from a custom Hughes Aircraft component modified from some previous design. This component also includes the 108 MHz source and is labeled "U19" in the Hughes documentation and the hardware itself.

The 540 MHz signal is then split three ways. One is mixed with the 27 MHz signal to create the third intermediate frequency that is passed into the receiver subsystem. The second 540 MHz signal encounters a series of switches (the burst

18

generator), which pulses it to a width of 5 ns. Next, the pulsed signal passes through a series of amplifiers to bring it to a power level of approximately +20 dBm. This amplification is needed to drive the Reflective Array Compressor (RAC) device.

The RAC is a type of Surface Acoustic Wave (SAW) device and is used to add the bandwidth necessary to create a chirp signal. This greater bandwidth is achieved by converting the "burst" pulse to an acoustic signal and presenting the signal with a series of shallow grooves in the delay path as shown in figure 3.4 [4]. The grooves are fabricated so that the propagation delay of each 180 degree path depends on frequency. Higher frequency components of the burst pulse travel further than lower frequency components, and thus leave the device later in time. When the burst pulse leaves the RAC device, its pulse width has been elongated to 3.1 $\mu$sec and its bandwidth has been increased to 180 MHz. There is no amplitude weighting on the RAC device so the side-lobe level of the received signal will be -13.2 dB [4]. In addition, the RAC device attenuates the signal considerably as a result of the two waveform conversions per excitation. It is common for the device to become extremely hot to the touch.

Due to the lossy nature of the RAC device, the output chirp must be significantly amplified before reaching the frequency doubler. Since the doubler is only a mixer that appropriately filters the output products, the level at which it is driven greatly affects its performance. Both the center frequency and bandwidth are doubled to create a waveform with a 360 MHz bandwidth centered at 1080 MHz. Using equation 1.2, this gives the AAFE altimeter a minimum range resolution (before waveform re-tracking) of

$$\Delta R \quad = \quad \frac{c \ T_{effective}}{2} \quad = \quad \frac{c}{2(360 MHz)} \quad \approx \quad 42cm. \qquad (3.2)$$

However, operating the altimeter at a full pulse width of 3.1 $\mu$sec requires that the aircraft platform be flying at a minimum height of approximately 465 meters.

Figure 3.2 Transmitter block diagram of the refurbished AAFE altimeter.
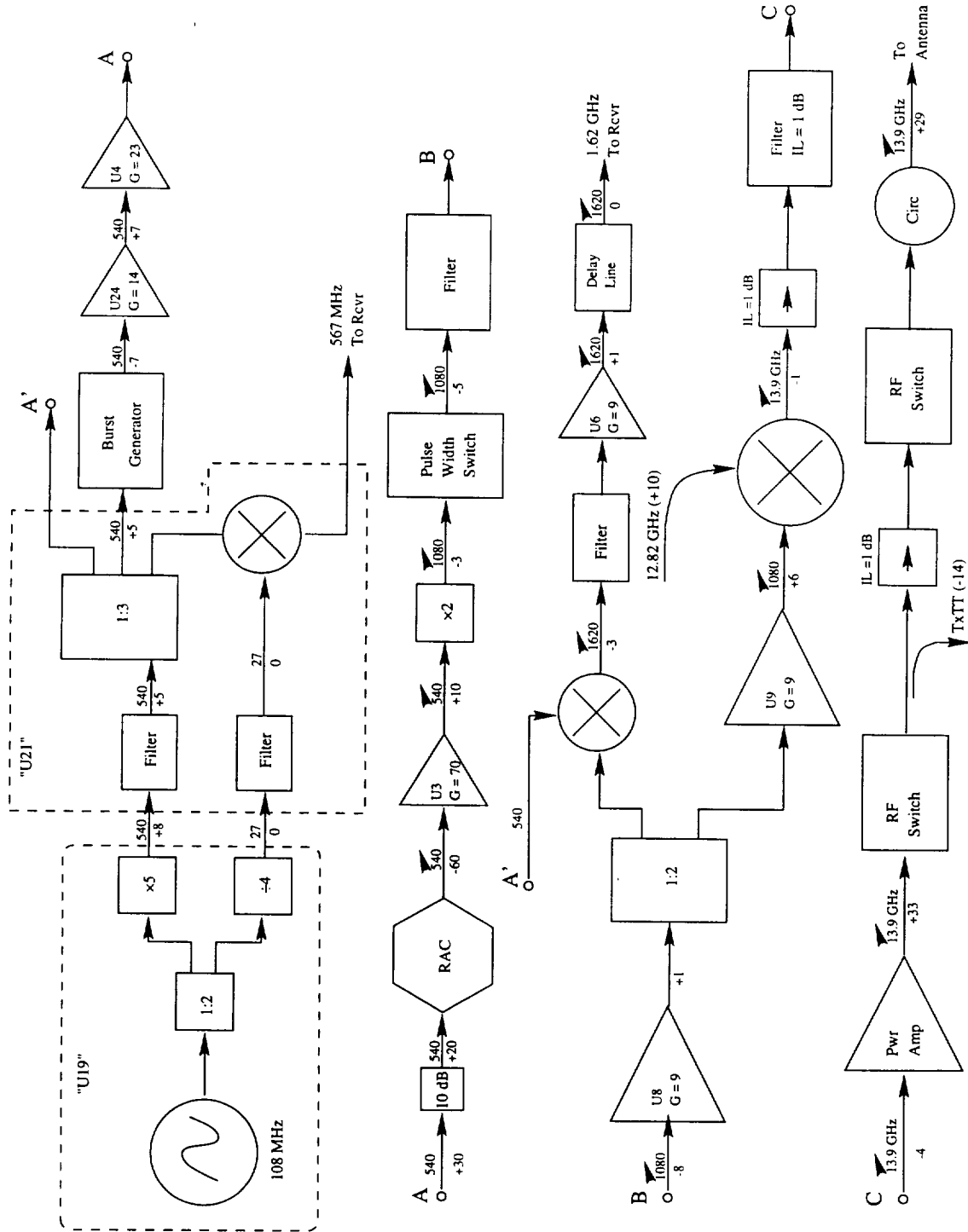
Figure 3.3 Detailed transmitter block diagram of the refurbished AAFE altimeter.

21
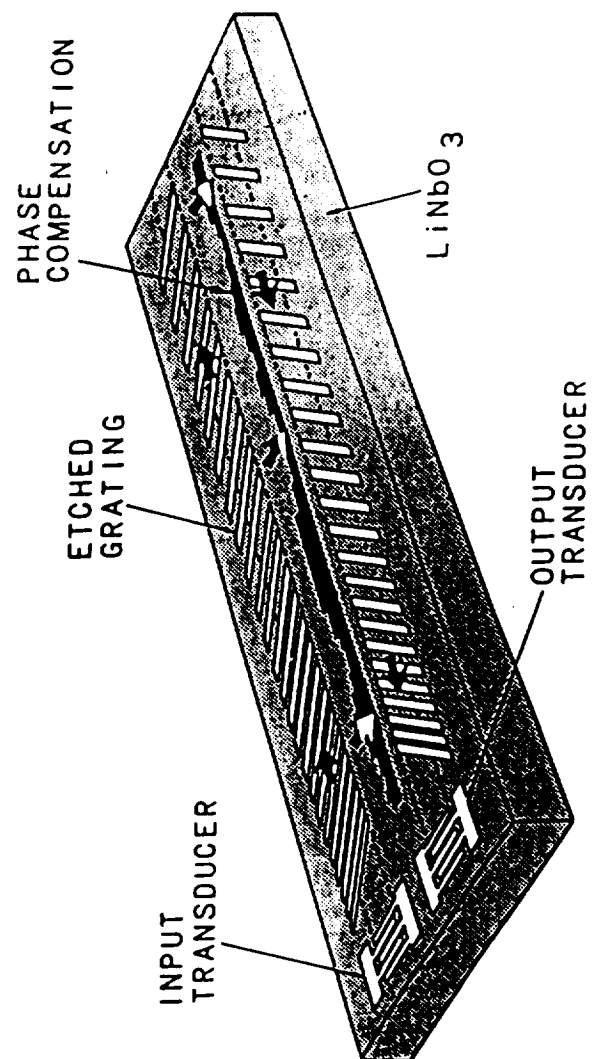
Figure 3.4 Simplified representation of a Reflective Array Compressor (RAC) device [1].
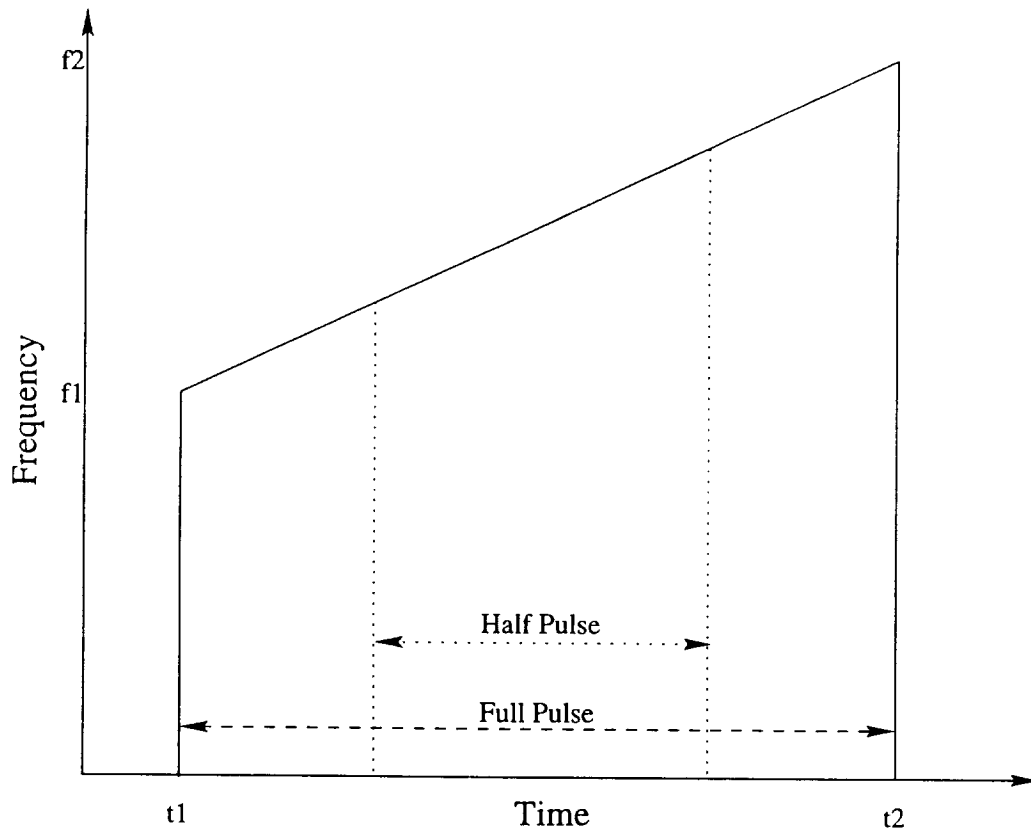
Figure 3.5 Operation of pulse width switch in transmitter subsystem.

This distance corresponds to the time at which the trailing edge of the transmit pulse is leaving the antenna and the front end of the pulse is reaching the antenna after reflecting off the surface. Under some applications, and certainly for any ground-based testing, operation must be possible within a shorter distance to the target (or surface). A pulse width switch was installed after the frequency doubler for this purpose. Control signals for the pulse width switch are appropriately timed to maintain a constant center frequency, independent on pulse width, as illustrated in figure 3.5. Cutting the pulse width in this manner trades range resolution for a greater range of operation.

Upon exiting the pulse width switch, the chirped pulse is again filtered and amplified (to recover unavoidable system losses) before passing through a power

splitter. One of the splitter outputs is mixed with the last of the three 540 MHz signals. This path generates the second intermediate frequency, which is sent into the receiver. Operating in a full pulse mode, this is a 1.62 GHz pulse, with a 360 MHz bandwidth. Before reaching the receiver, it encounters a delay line comprised of a coil of semi-rigid cable. The length of this coil is set to mimic the system time delays experienced by the other output of the splitter, whose path leads to the antenna port.

A 12.82 GHz crystal oscillator is mixed with the second of the splitter outputs. At this point, the signal attains its final center frequency of 13.9 GHz. A second output from the crystal oscillator is sent directly into the receiver, where it is the first intermediate frequency. The 13.9 GHz signal is amplified to 2 Watts (+33 dBm) via the power amplifier before reaching one of two RF switches. After this switch, part of the signal is coupled (30 dB) to form the "test target" which is passed into the receiver, depending on the state of the calibration switch. This "test target" simulates a return from the surface when the AAFE altimeter is in calibration mode.

Finally, the signal passes through the second RF switch, which provides isolation when the altimeter is not transmitting, then the circulator, and is transmitted by the antenna. The circulator enables the use of one antenna for both the transmitter and receiver and provides 30 dB of isolation. Most frequently, the antenna used is a rectangular horn 56 cm in length with a 9.1 cm by 6.6 cm aperture. It has a gain of 21.6 dB and a 3 dB beam width of 15.6 degrees [1]. The waveguide attachment for this antenna was slightly damaged after the 1994 flight experiments, but has been subsequently repaired. A plot of a current reflection measurement, taken with a network analyzer in the MIRSL laboratory, is shown in figure 3.6.

Two other antennas are available to the AAFE altimeter, both intended to investigate the effect of beam width on the surface return waveform. In order to participate in a so-called "big foot" flight experiment, typically flown at higher

24

0.0

M9

M9=-24.601E+00   M10=-24.996E+00

I1=13.670E+09   I1=14.125E+09

I2=■   I2=■

M9   M10

dB(S22)

-50.0

13.5  GHz   ~TASET..FREQ   14.5  GHz
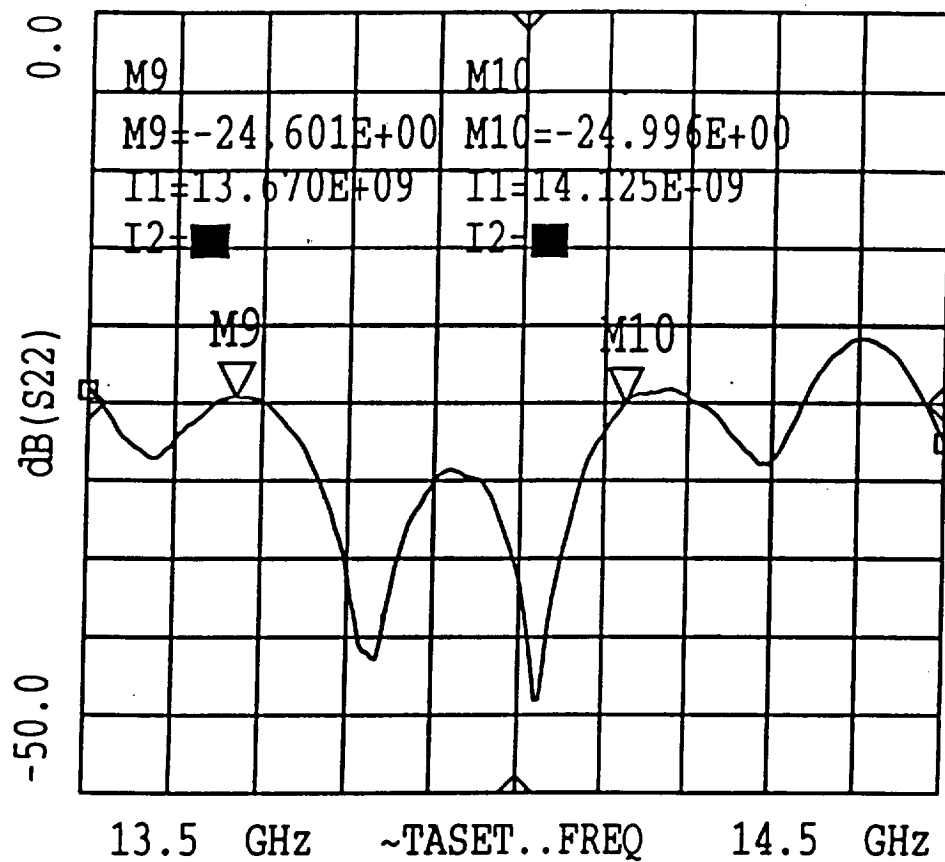
Figure 3.6 Reflection measurement of AAFE antenna after repair.

altitudes, a 31.2 degree beam width rectangular horn was outfitted. This beam width produces a much greater surface footprint, accentuating the contributions of volume scatterers on the return waveform [3]. The second antenna is a patch phased array with a beam width of 4 degrees and a gain of 34 dB.

A general block diagram and more detailed block diagram of the refurbished state of the AAFE altimeter receiver subsystem can be found in figures 3.7 and 3.8, respectively. Peak power measurements are represented in dBm and were obtained with altimeter in calibration mode, as in the transmitter block diagram . The signal labeled "from antenna" has been passed through a waveguide circulator, twelve inches of rectangular waveguide and a waveguide-to-coax adapter.

The 30dB coupler is necessary for the calibration mode of the AAFE altimeter. In the calibration mode, the "TxTT" signal is coupled in to mimic a return from the surface. During normal operation, returns via the antenna are passed through the coupler and immediately mixed down to a 1080 MHz chirped pulse. The output of this mixer encounters a manual variable attenuator. It has a range of attenuation from 1 to 69 dB and is used to prevent saturation of the front end amplifiers which follow it.

A power splitter/combiner stage follows the amplifiers. One of the outputs of the power splitter is delayed and recombined with the other splitter output, depending upon the state of the switch in the delay path. The non-delayed output is attenuated to match the loss in the switch and delay line. If the switch is closed, a second "target" is sampled by the data acquisition system 102 nanoseconds after the original. This is only used for test purposes in calibration mode and is most useful for verifying operation of the data acquisition system. In normal radar operation mode, the test target switch is always open.

Upon exiting the test target switches, the return signal is amplified and filtered before reaching the deramping mixer. In transmit and receive mode, the second
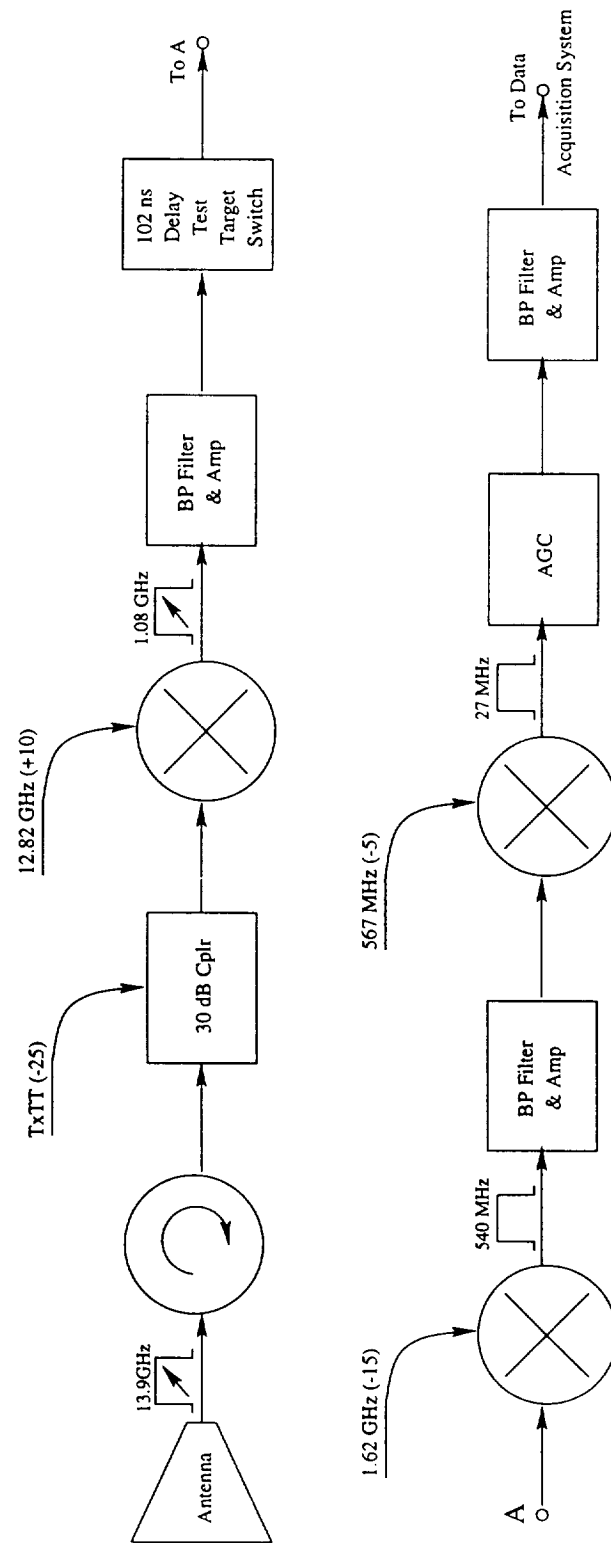
Figure 3.7 General block diagram of the AAFE altimeter receiver subsystem.

27
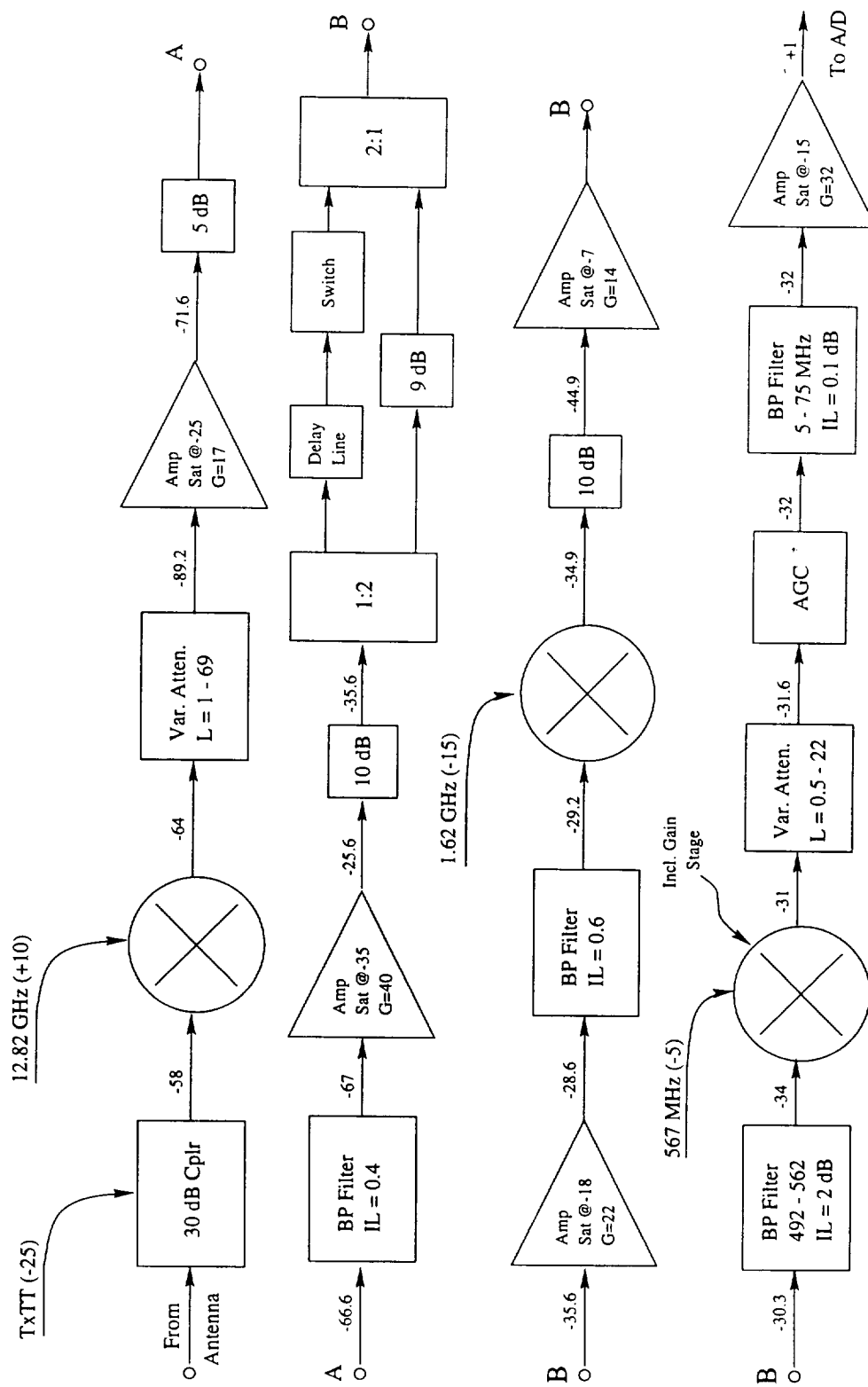
Figure 3.8 Detailed block diagram of the AAFE altimeter receiver subsystem.

A

5 dB

-71.6

Amp
Sat @-25
G=17

-89.2

Var. Atten.
L = 1 - 69

-64

12.82 GHz (+10)

-58

30 dB Cplr

TxTT (-25)

From
Antenna

B

2:1

Switch

9 dB

Delay
Line

1:2

10 dB

-35.6

-25.6

Amp
Sat @-35
G=40

-67

BP Filter
IL = 0.4

A    -66.6

B

Amp
Sat @-7
G=14

-44.9

10 dB

-34.9

1.62 GHz (-15)

-29.2

BP Filter
IL = 0.6

-28.6

Amp
Sat @-18
G=22

B    -35.6

- +1

To A/D

Amp
Sat @-15
G=32

-32

BP Filter
5 - 75 MHz
IL = 0.1 dB

-32

AGC

-32

-31.6

Var. Atten.
L = 0.5 - 22

-31

Incl. Gain
Stage

567 MHz (-5)

-34

BP Filter
492 - 562
IL = 2 dB

B    -30.3

mixer input is generated in the transmitter at a time determined by the computer software tracking system. When in calibration mode, the second mixer input is generated from the same transmit pulse as the calibration "TxTT" signal. If the output of this mixer is to be within the range window of the receiver, its frequency will be between 492 and 562 MHz. This output signal is no longer chirped, but remains pulsed.

The return signal is once again amplified and filtered before the final mixing stage. This is another custom Hughes component and it includes an additional amplifier as well as mixer. A turn-screw manual variable attenuator follows this mixer and precedes a programmable variable attenuator or "automatic gain control" (AGC). The AGC is used to prevent saturation of the analog to digital converter (ADC) within the data acquisition system and is controllable from the computer user interface. The return is now between 5 and 75 MHz and is filtered and amplified before entering the data acquisition system, where it is averaged, fast-Fourier transformed, and passed to the computer subsystem to be displayed and stored to disk.

## 3.1   Hardware Performance

The AAFE altimeter has experienced some significant performance degradation due to reasonable wear and tear and possible shipping damage. As a result, MIRSL has undertaken a series of additional upgrades. Before the 1994 Greenland experiment and during transport for installation on the NASA remote sensing aircraft, a variety of "minor" components failed to operate properly. Among these components was the intermediate frequency generator in the transmitter subsystem (labeled "U21" in the Hughes documentation). A block diagram for the intermediate frequency generator is included in figure 3.9.
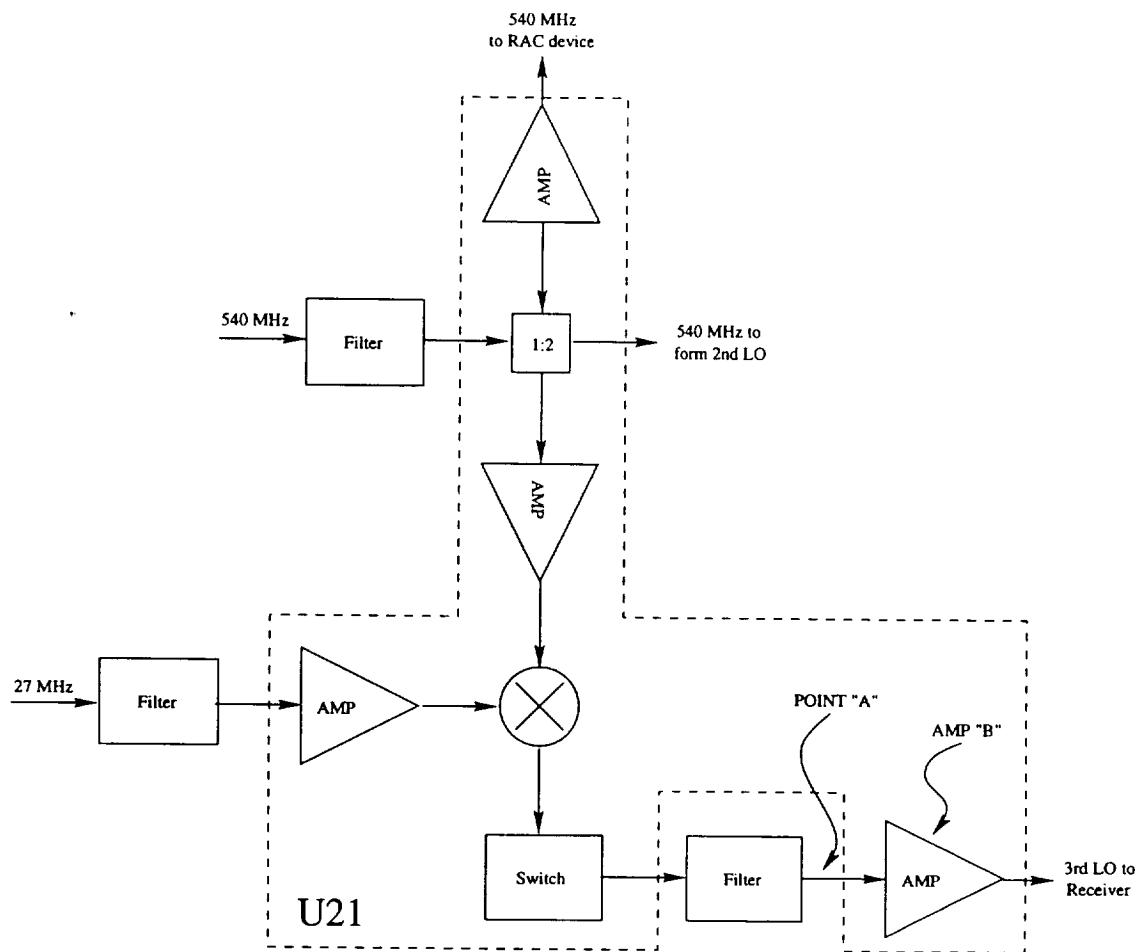
Figure 3.9 Detailed block diagram of the intermediate frequency generator.

The purpose of the "U21" component is to take inputs of 27 MHz and 540 MHz and produce two 540 MHz and one 567 MHz outputs at appropriate power levels for use in other parts of the transmitter. However, the outputs were suffering from extreme spurious signal contamination as illustrated by the 567 MHz output in figure 3.10. Examination of this signal at point A in figure 3.9, showed that it was relatively free of the 27 MHz harmonics after filtering. As a result, an additional amplifier was installed to replace amplifier B within "U21" so that the 567 MHz output was not reintroduced to any interference. The two 540 MHZ outputs were improved by the addition of narrow band pass filters.

Another significant component failure involved the automatic gain control (AGC) circuit within the receiver subsystem. The AGC was another custom Hughes component modified for use in the AAFE altimeter. Close inspection revealed the charring of some discrete circuit elements, as well as brittle solder connections. A Lucas Weinschel programmable attenuator was installed as a replacement to prevent saturation of the analog to digital converters in the data acquisition system. Attenuation steps of 1 dB, to a maximum of 127 dB are available.

All of the above component failures can detract from the overall system performance. However, none could degrade the shape and quality of the return waveform to the degree witnessed during the 1994 Greenland experiment. Once the altimeter returned to the MIRSL laboratory, investigation showed that the reflective array compression (RAC) device, which is the main component of the pulse compression system, was malfunctioning badly, hence the drop-off in performance.

Figure 3.11 shows the state of the RAC device output in 1990. This plot is taken from an HP spectrum analyzer and shows a relatively steady amplitude level over the entire 180 MHz bandwidth of the device. The shape of the chirp signal is symmetric about the center frequency, which is at a power level of approximately 1 dBm. Figure 3.12 illustrates the current state of the RAC device output. The most

31
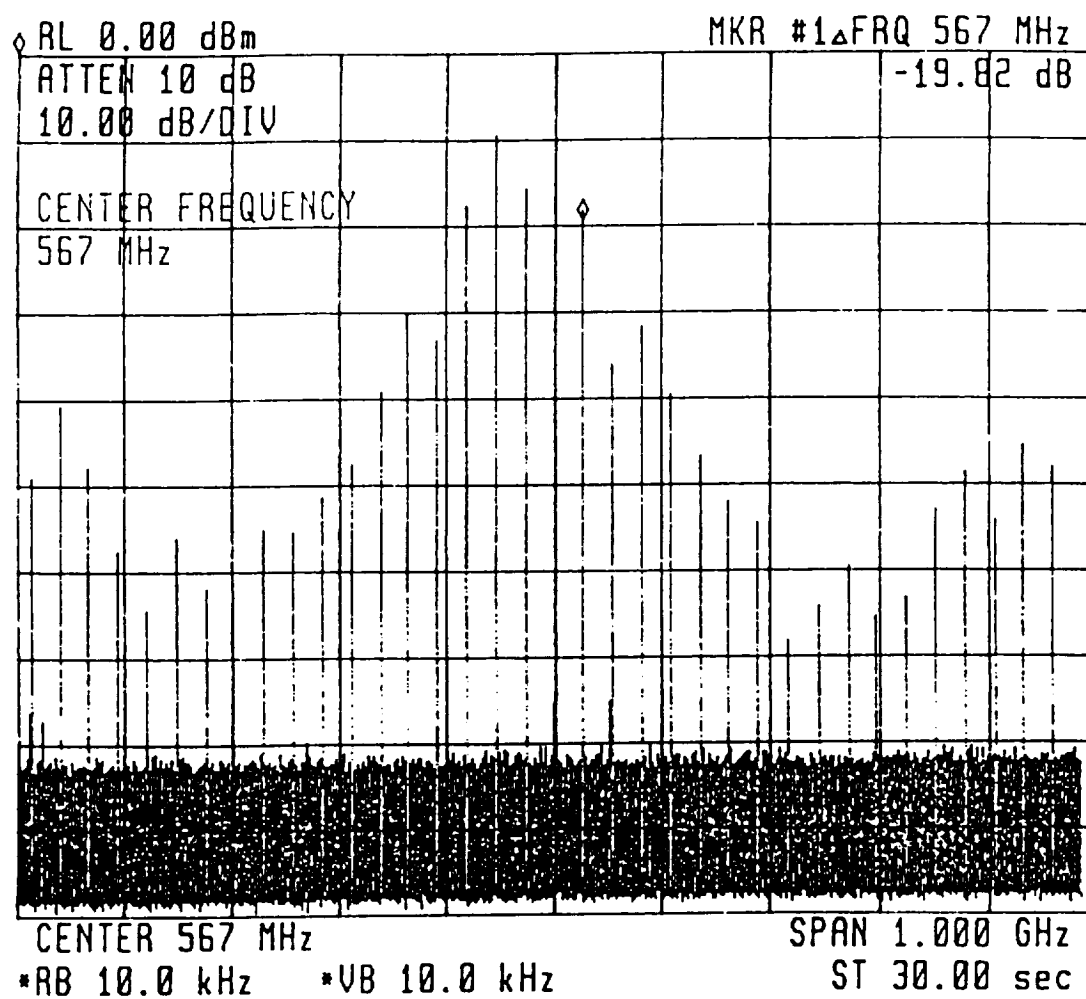
Figure 3.10 Contaminated intermediate frequency generator output.

prominent feature of this plot is the great "crevice" in the center of the frequency band of the device. At its worst point, nearly at the center frequency, the amplitude drops 20 dB from its expected value. To ensure the validity of this plot, the RAC device was tested on an HP network analyzer ($S_{21}$) and with a point-by-point test in frequency using a frequency synthesizer and spectrum analyzer. A continuous wave frequency was fed to the input of the RAC and its amplitude was recorded using the spectrum analyzer. This method essentially mimics the network analyzer, but gives the operator a more tangible reading of the operation of the device. The network analyzer plot in figure 3.13 and the point by point test results in figure 3.14 both confirm the failure of the RAC device. Figure 3.15 shows that the input signal to the RAC device in 1990 was equivalent to the input signal for the current tests.

Investigation of the RAC device itself shows no visible signs of stress or failure. However, an untrained eye could not determine any damage to the crystal etchings and many of the component parts cannot be manipulated without further damaging them. There are signs of custom modifications to the original design as was witnessed with the intermediate frequency generator. These modifications are again roughshod and could be the source of failure as they are less robust than the original component workmanship.

Unfortunately, the RAC device is a high precision, application-specific component and is not only expensive, but also not widely available. However, as digital technology has improved since 1974, an alternative to the surface acoustic wave (SAW) device now exists in the digital chirp synthesizer. This device mimics the functionality of its analog counterpart, while offering features that the SAW, RAC and other pulse compression devices cannot provide. First of these, is greater chirp to chirp reliability. Each chirp is rendered digitally for less variation between the transmit chirp and the deramping signal. Most attractive, however, is the flexibility of a digital chirp synthesizer. Whereas the analog devices are manufactured
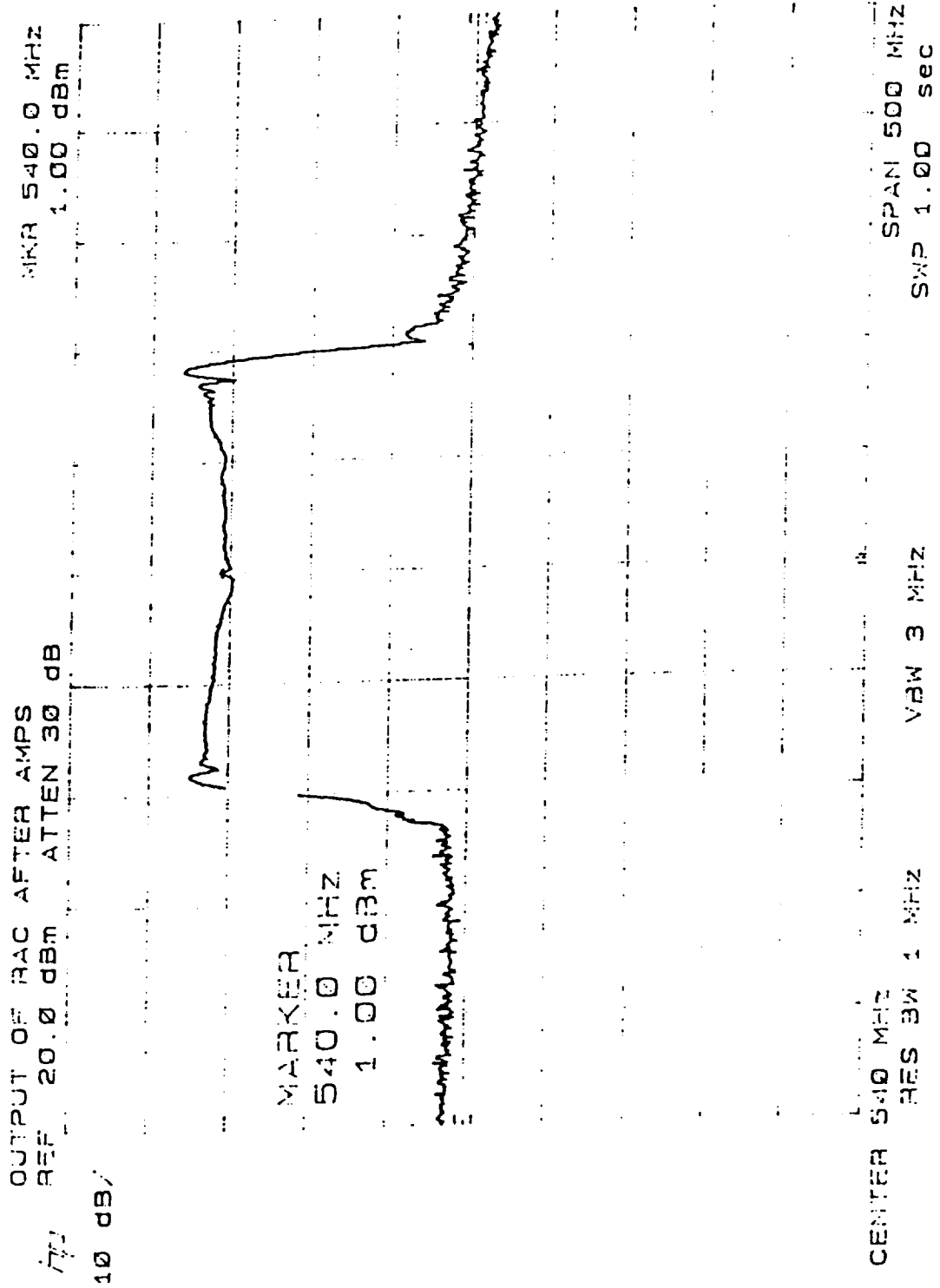
Figure 3.11 Spectrum analyzer plot of the original condition of the RAC device.
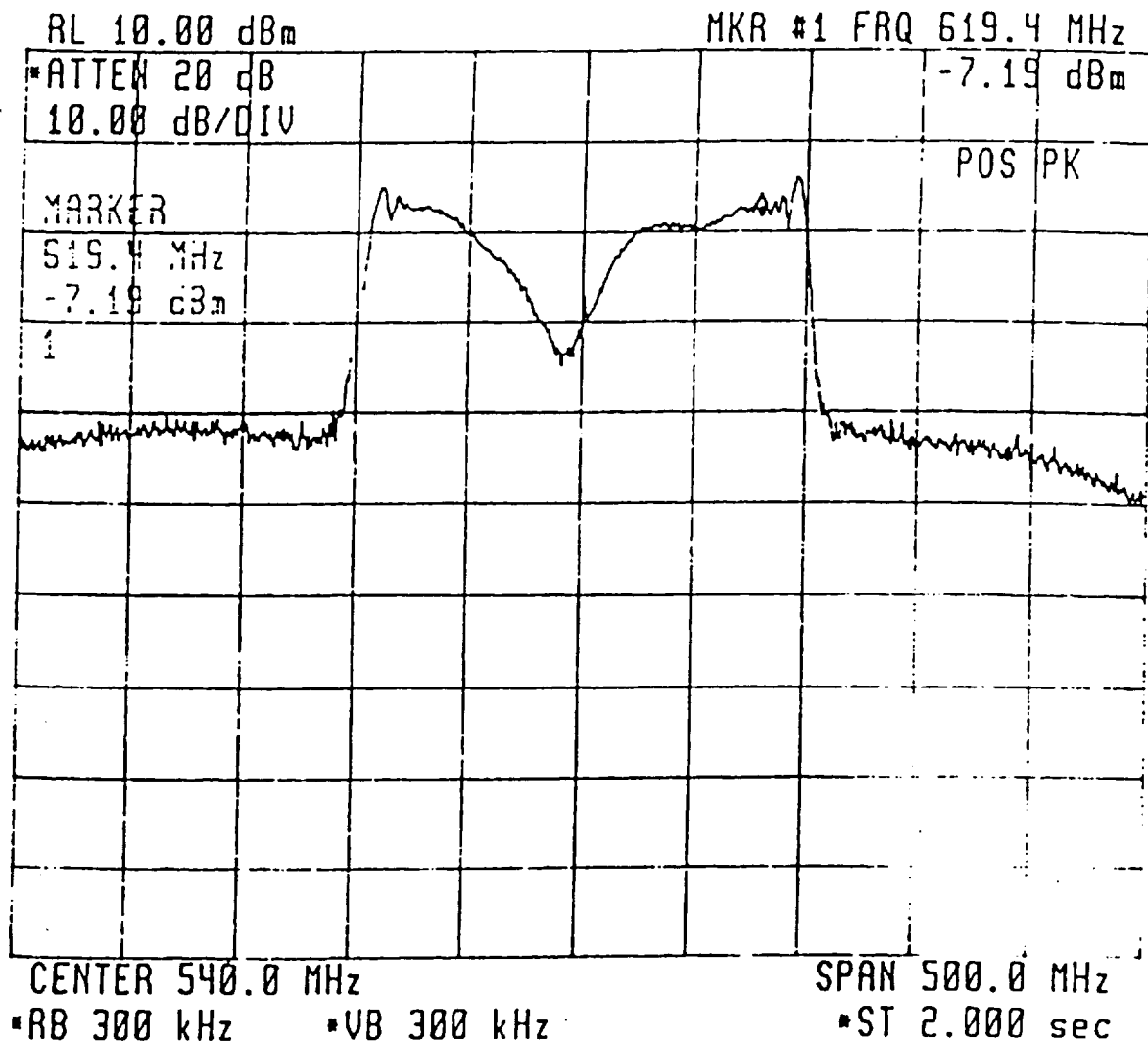
Figure 3.12 Spectrum analyzer plot of the current condition of the RAC device.

to specifications and can never be modified, the digital chirp synthesizer can be reprogrammed in seconds to manipulate its center frequency or bandwidth. Even phase properties can be chosen and modified, so the chirp synthesizer can be shared by a variety of projects without sacrificing design considerations. The effect of pulse compression parameters on overall system performance can also be investigated. In addition, the digital chirp synthesizer is solid-state and is much more robust than etchings in crystal. Finally, the costs of analog and digital pulse compression devices are comparable, so a digital solution was chosen to replace the RAC device.

Before a specific digital chirp synthesizer could be chosen, the performance specifications necessary for the AAFE altimeter had to be determined. Of greatest importance were bandwidth, amplitude level flatness, spectral purity, and frequency switching. At least 180 MHz had to be attainable and to achieve the level of amplitude flatness shown in figure 3.11, variations of no more than 3 dB could be tolerated.

To determine the requirements for frequency switching, software was written to simulate the return signal deramping process in the receiver subsystem. Figure 3.16 shows the frequency versus time plot of a digital chirp pulse. Switching speed for the device is determined by the time between frequency steps in the chirp pulse. For an analog device, this time is obviously zero. The simulation software, "mixes" a mathematical representation of an AAFE surface return, generated by a digital transmit pulse, with a mathematical representation of a digitally generated deramping signal. The result is fast Fourier transformed and displayed.

Figures 3.17, 3.18, 3.19, and 3.20 show the results for 3 common grades of digital chirp synthesizers and the analog representation, respectively. The analog plot is shown for comparative purposes. Each plot has an output level maximum centered at approximately 532.8 MHz, which corresponds to the 62 nanosecond delay of the deramping signal as follows:

36

S21    log MAG

REF 0.0 dB

1  10.0 dB/

▽ −84.871 dB

hp

START
430.0 MHz

START  0.430000000 GHz
STOP   0.650000000 GHz
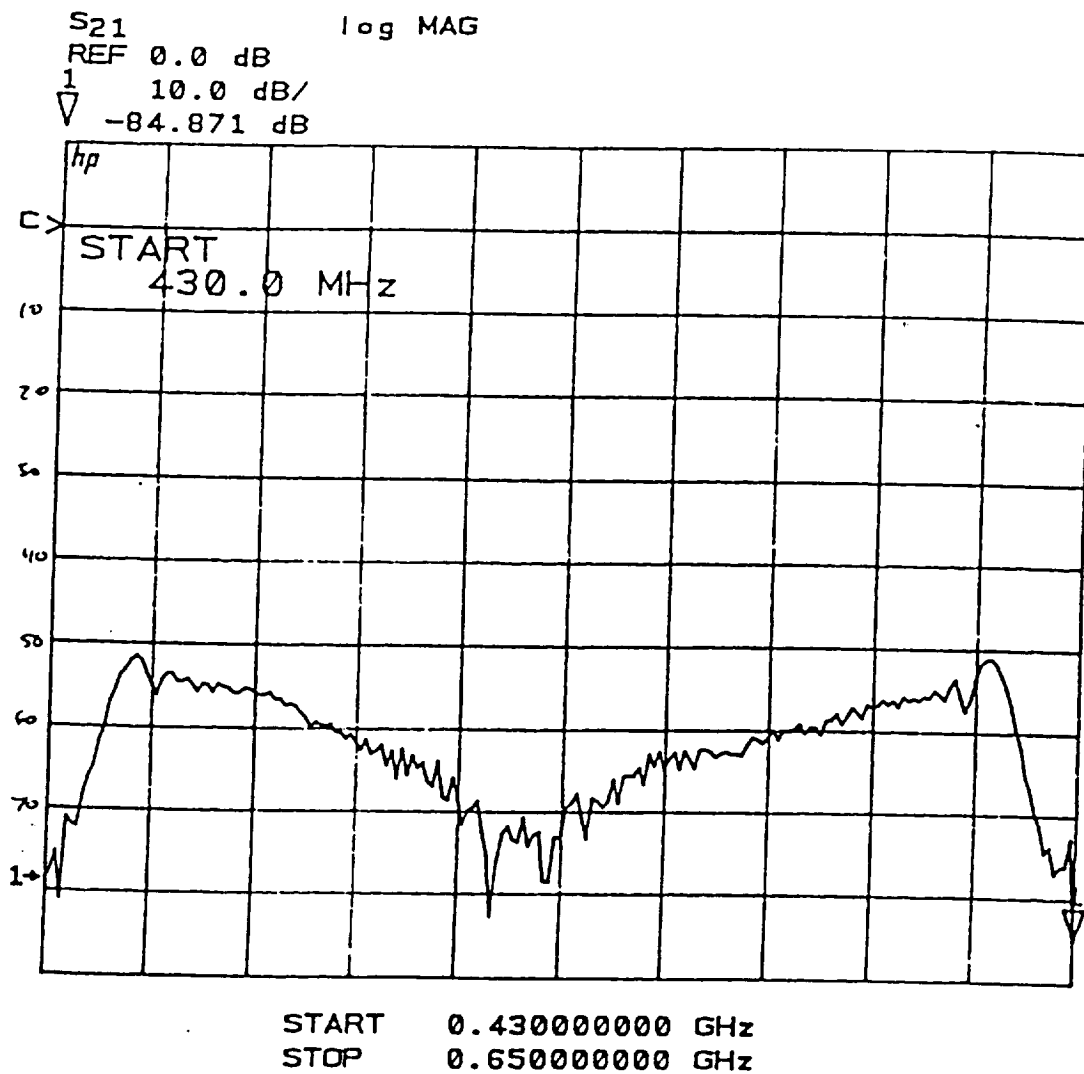
Figure 3.13 Network analyzer test of the RAC device.
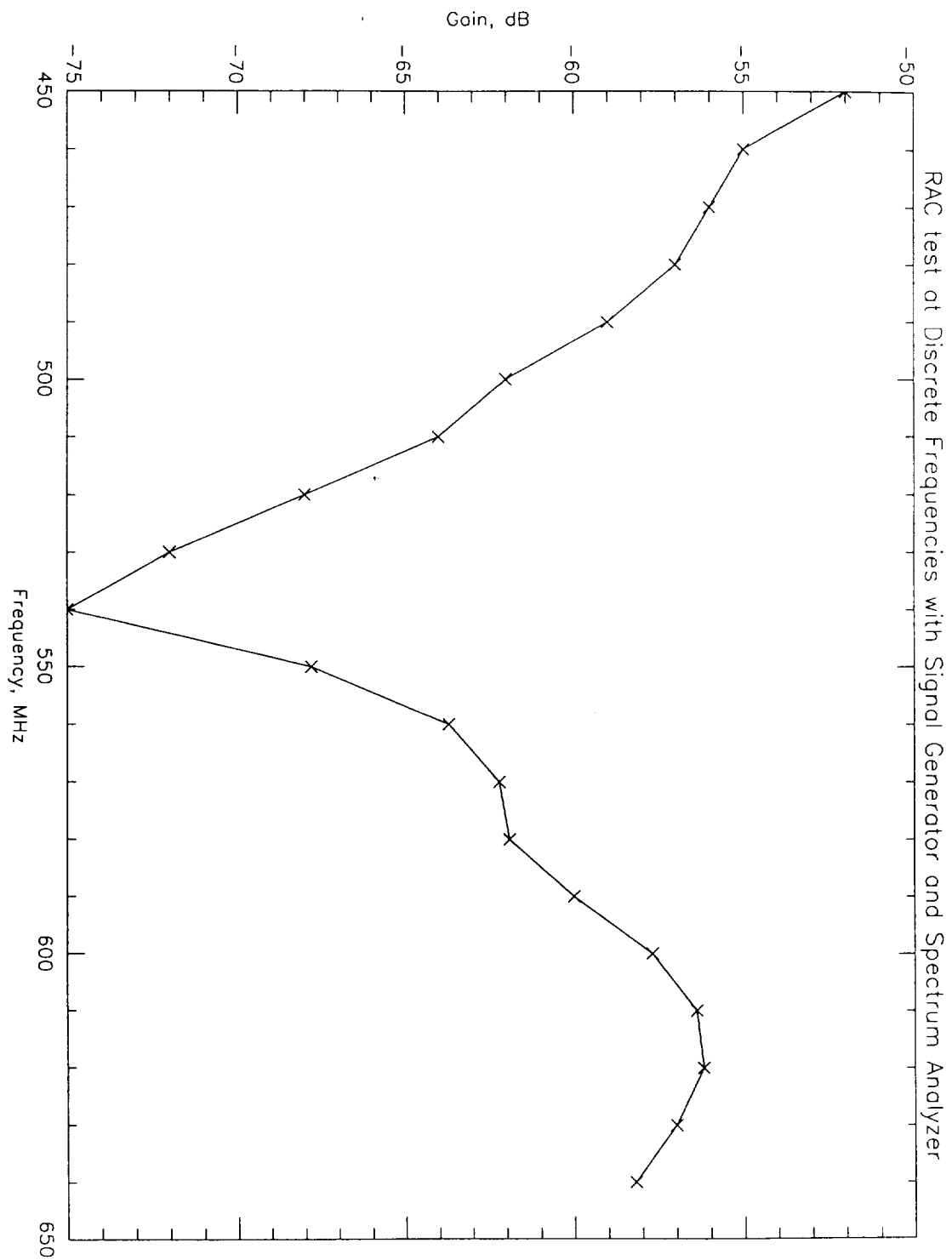
Figure 3.14 Manual synthesizer/spectrum analyzer test of the RAC device.

OUTPUT OF AMP J4

REF 10.0 dBm    ATTEN 20 dB

MKR 540 MHz
-10.30 dBm

10 dB/

MARKER
540 MHz
-10.30 dBm

CENTER 540 MHz
RES BW 3 MHz          VBW 3 MHz

SPAN 1.00 GHz
SWP 1.00 sec

RL 10.00 dBm                        MKR #1 FRQ 573 MHz

ATTEN 20 dB                              20.28 dBm
10.00 dB/DIV

POS PK

SWEEP TIME
2.000 sec

CENTER 540 MHz                    SPAN 1.000 GHz
RB 300 kHz    VB 300 kHz         ST 2.000 sec
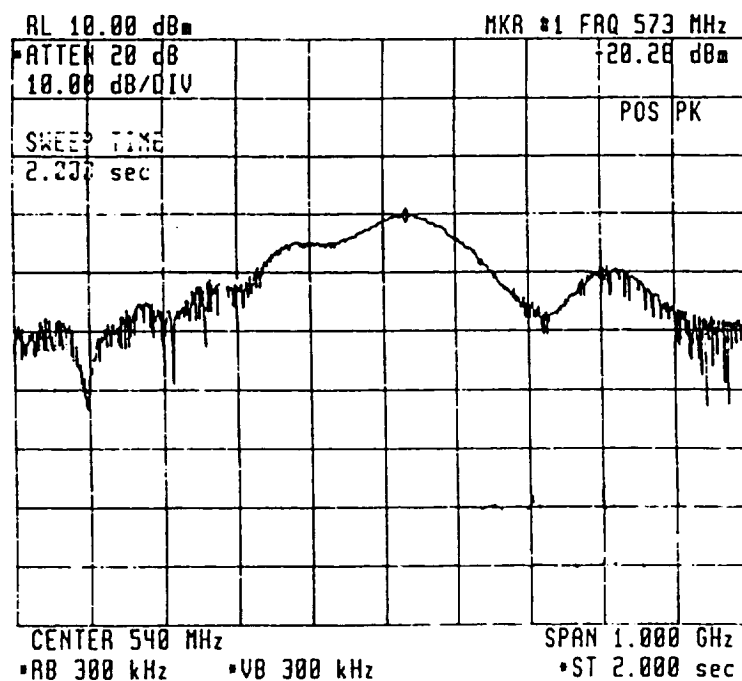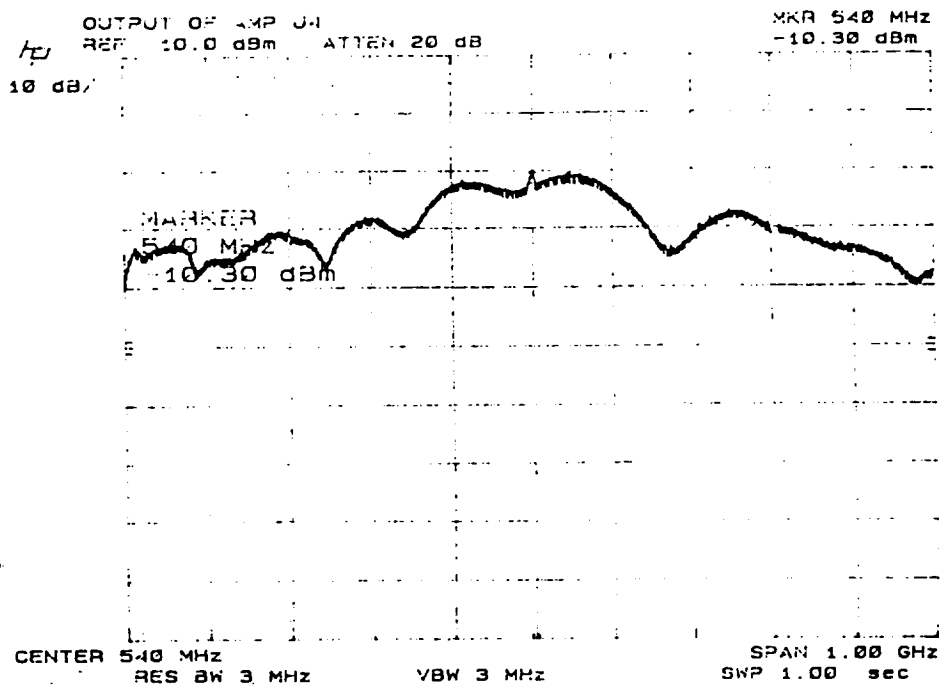
Figure 3.15 Inputs to the RAC device (1990 above, current below).

39
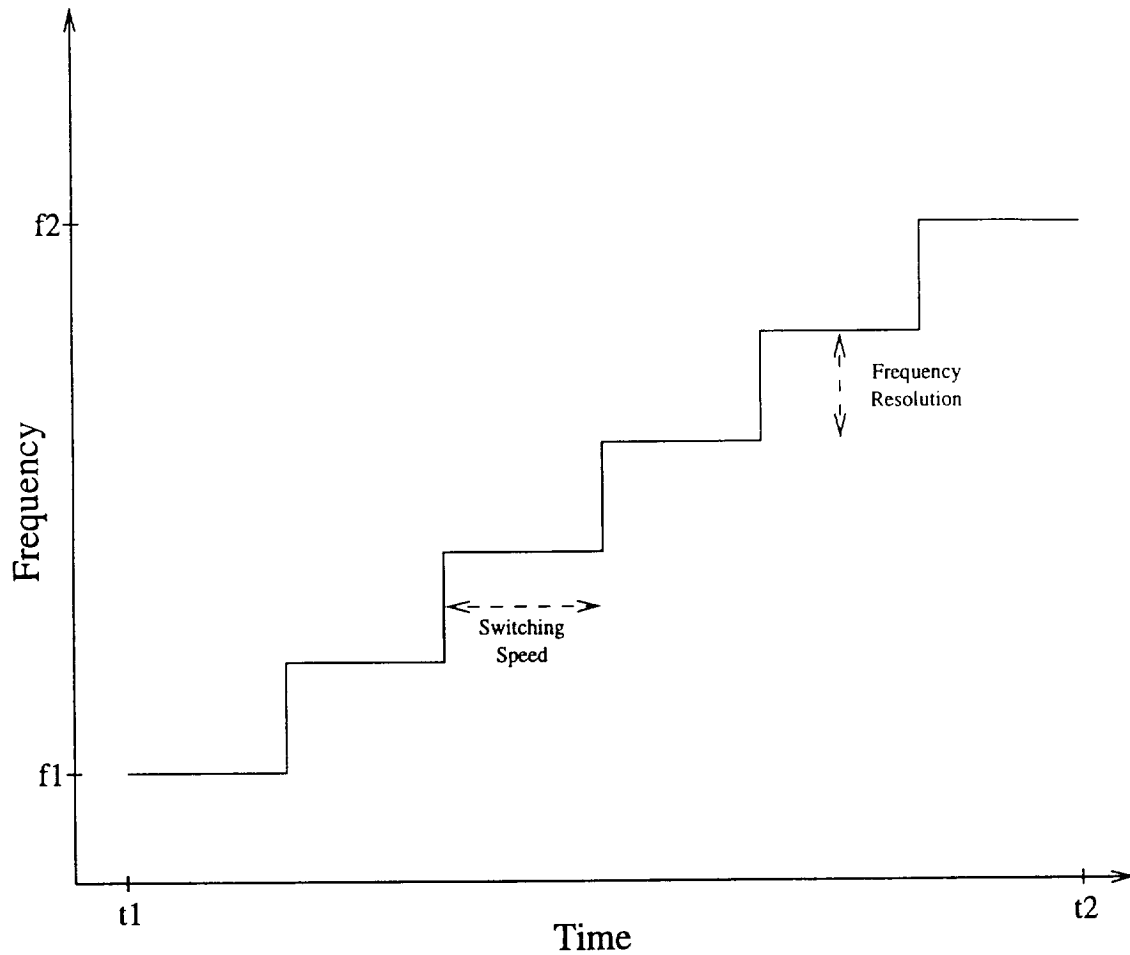
Figure 3.16 Frequency versus time representation of a digital chirp.

$$F_{CENTER} = 540MHz + \frac{360MHzBW}{3.1\mu seconds} \times -62nsec = 532.8MHz. \tag{3.3}$$

However, both the 31 and 62 nanosecond switching speed grades of digital chirps have unacceptable power levels of spurious harmonics. If returns from these signals were to be tracked, they would skew power level weightings to give a false reading about the center of the return and, therefore, range to the surface.

After weighing performance versus cost, the Sciteq DCP-1A/LPF was chosen as the best solution. The DCP-1A has a 500 MHz reference clock enabling a switching speed as low as 2 nanoseconds, and 24 data bits provide frequency resolution less
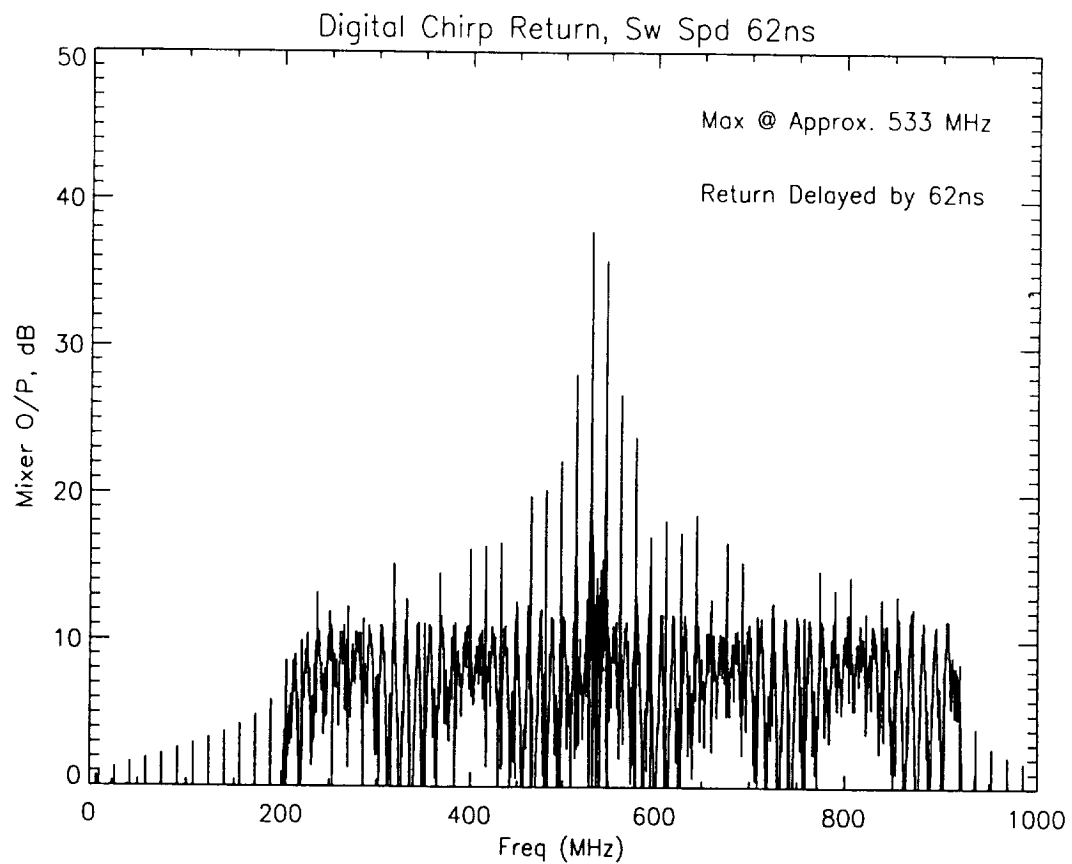
Figure 3.17 Simulated AAFE return using a digital chirp with a 62ns switching speed.
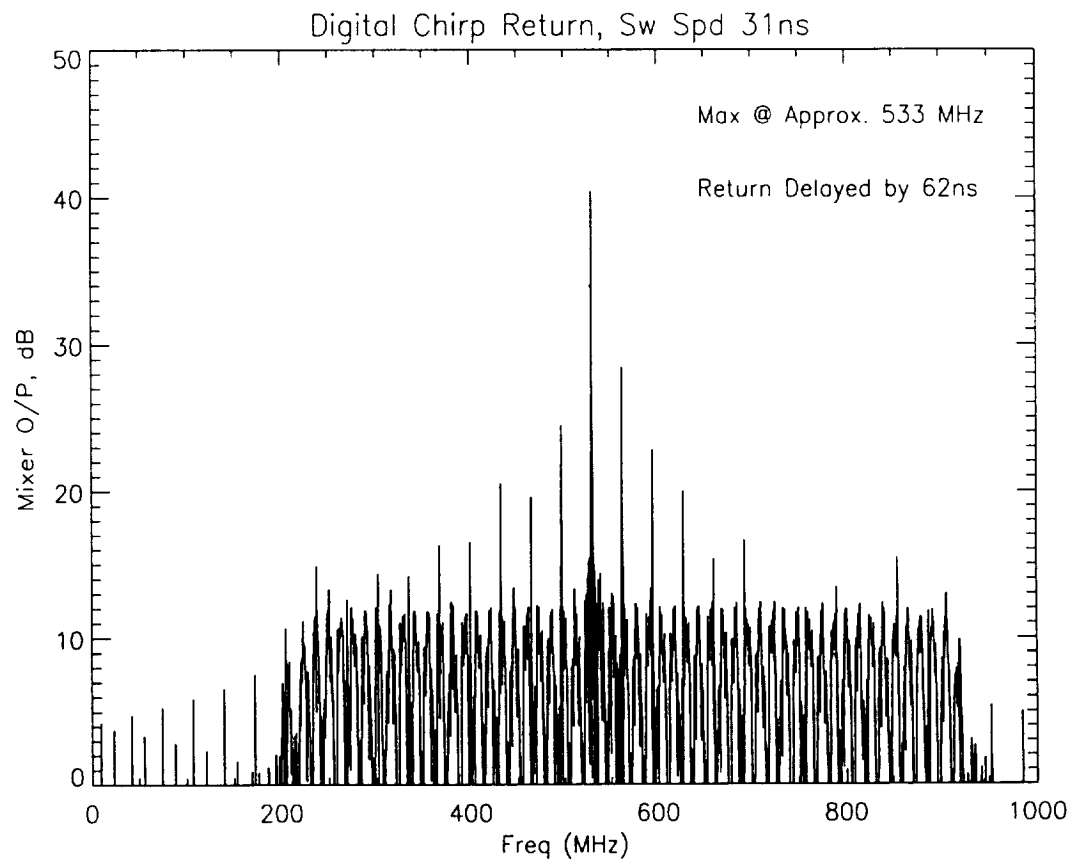
Figure 3.18 Simulated AAFE return using a digital chirp with a 31ns switching speed.
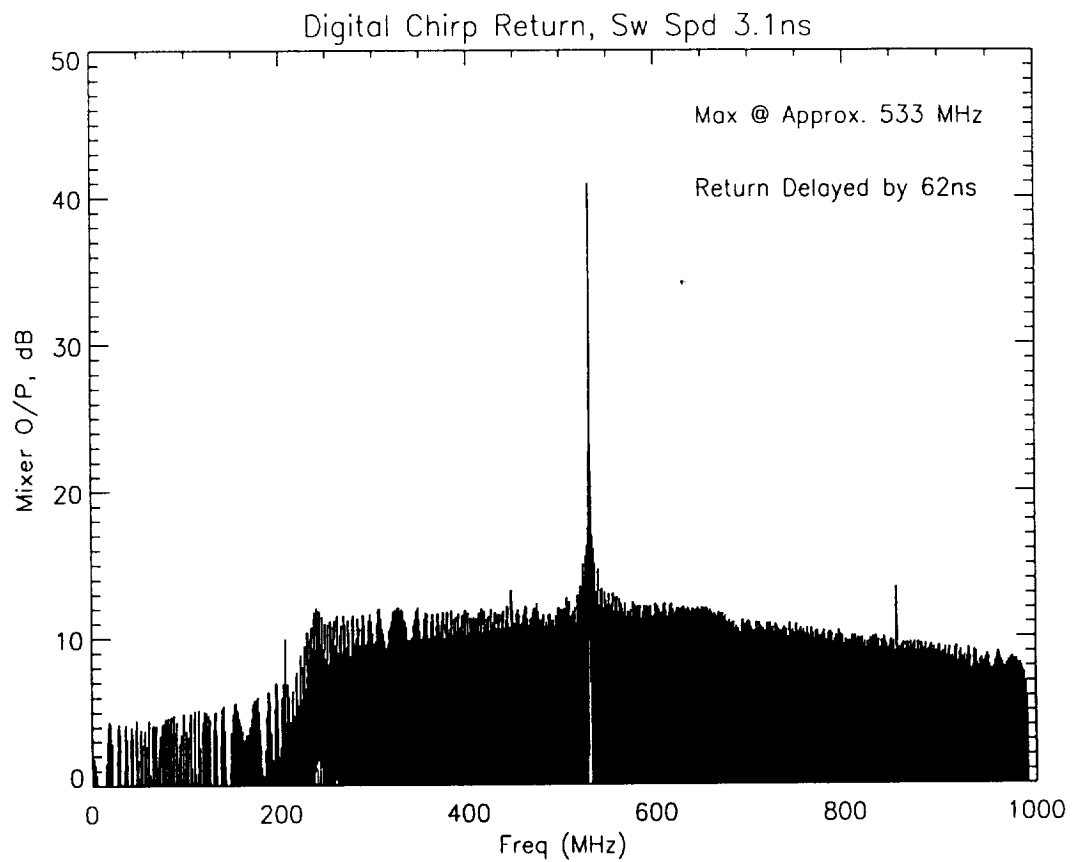
Figure 3.19 Simulated AAFE return using a digital chirp with a 3.1ns switching speed.
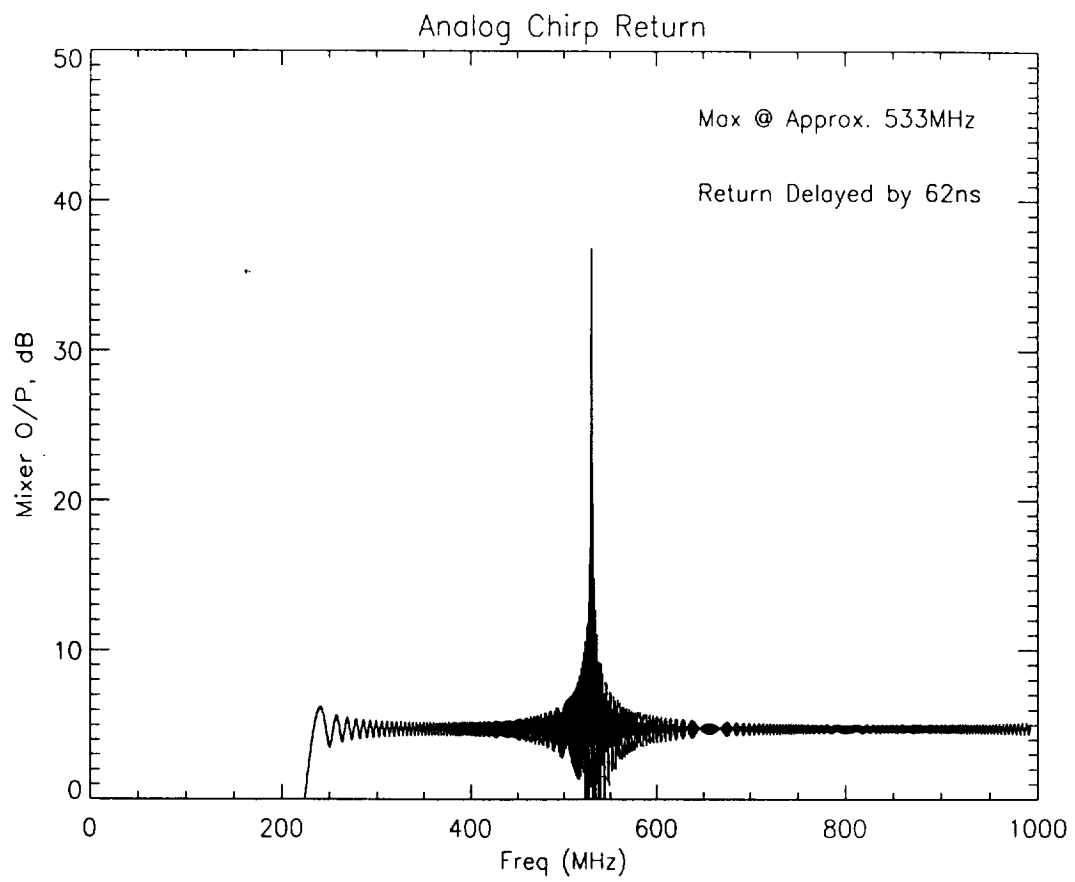
Figure 3.20 Simulated AAFE return using an analog chirp.

than 30 Hertz. Output frequencies can range from 1 to 230 MHz, and signals can pass through a smoothing low-pass filter before exiting the device. Its data sheet specifications are supplied in Appendix A.

Since the original RAC device had a center frequency of 540 MHz, some modifications to the transmitter subsystem were necessary to accommodate the digital device. In order to provide the necessary 180 MHz bandwidth, the possible center frequencies of the chirp generator output were limited to a range between 91 MHz and 140 MHz. This range is further limited to allow a buffer from interference due to other intermediate frequencies within the AAFE system, such as the baseband 27 MHz. The best, and simplest, solution would be to center the output chirp at the highest possible frequency, 140 MHz, and mix it up to 540 MHz with a new 400 MHz source. However, budgetary considerations made the acquisition of the necessary source an impossibility and another solution using the frequencies already available was needed. This design had the further requirement of changing the existing hardware as little as possible since funds for purchasing new components were limited.

## 3.2  New Design

Figure 3.21 is a simplified block diagram of the design modifications to the transmitter, focusing on the new intermediate frequency values. In order to preserve as much of the old design as possible, the digital chirp input was modified to mimic the output parameters of the original RAC device. Without these modifications, more extensive and costly adaptations to the last stages of the transmitter and receiver front end would have been necessary. This design required only minor adjustments to the last stages of the transmitter and left the receiver completely unchanged. As a result, the new components are all at lower frequencies, thus reducing costs.

Combinations of 27 MHz, 108 MHz, and 540 MHz were the only frequencies available for mixing the digital chirp signal to its required 540 MHz center frequency. Using the 567 MHz signal already generated and mixing it with the extra output available from the 108 MHz source, the main AAFE transmit pulse was changed to 675 MHz. The digital chirp input could then be centered at 135 MHz requiring only two mixers, one power splitter, amplifiers and two filters. Since the first mixing stage has a stop band of 108 MHz, its band-pass filter can have a gradual cut-off, reducing costs. For the second mixing stage, using a more economical low-pass filter allows a steeper cut-off to remove the unwanted image and 675 MHz "LO" signal.

Additional amplifiers were necessary to drive the new mixing stages properly, but since the digital chirp input does not attenuate the power level, some of the amplifiers formerly used in later stages of the transmitter were reinstalled to drive the mixers. Some new cabling was also required and these were either scavenged from now unused sections of the transmitter or purchased. A current block diagram of the transmitter subsystem is illustrated in figure 3.22 and repeated with greater detail in figure 3.23.

Once the preferred characteristics for the digital chirp output were determined, an interface could be designed to generate them. The digital chirp synthesizer (DCS) requires an involved register loading procedure before any output is produced. Subsequently, no testing of the device was possible until an interface solution could be devised. Unfortunately, its data connector, a 50 pin D type, is not a computer industry standard and required that a custom solution be built.

For preliminary testing, a circuit utilizing Altera programmable logic devices was fabricated. Figure 3.24 contains the intended waveform output which shows most of the steps necessary to program the DCS. First, a control or "ready" word (0x000040) must be sent to data lines and clocked or strobed in. The control word must be followed by a start frequency value and frequency increment value, each
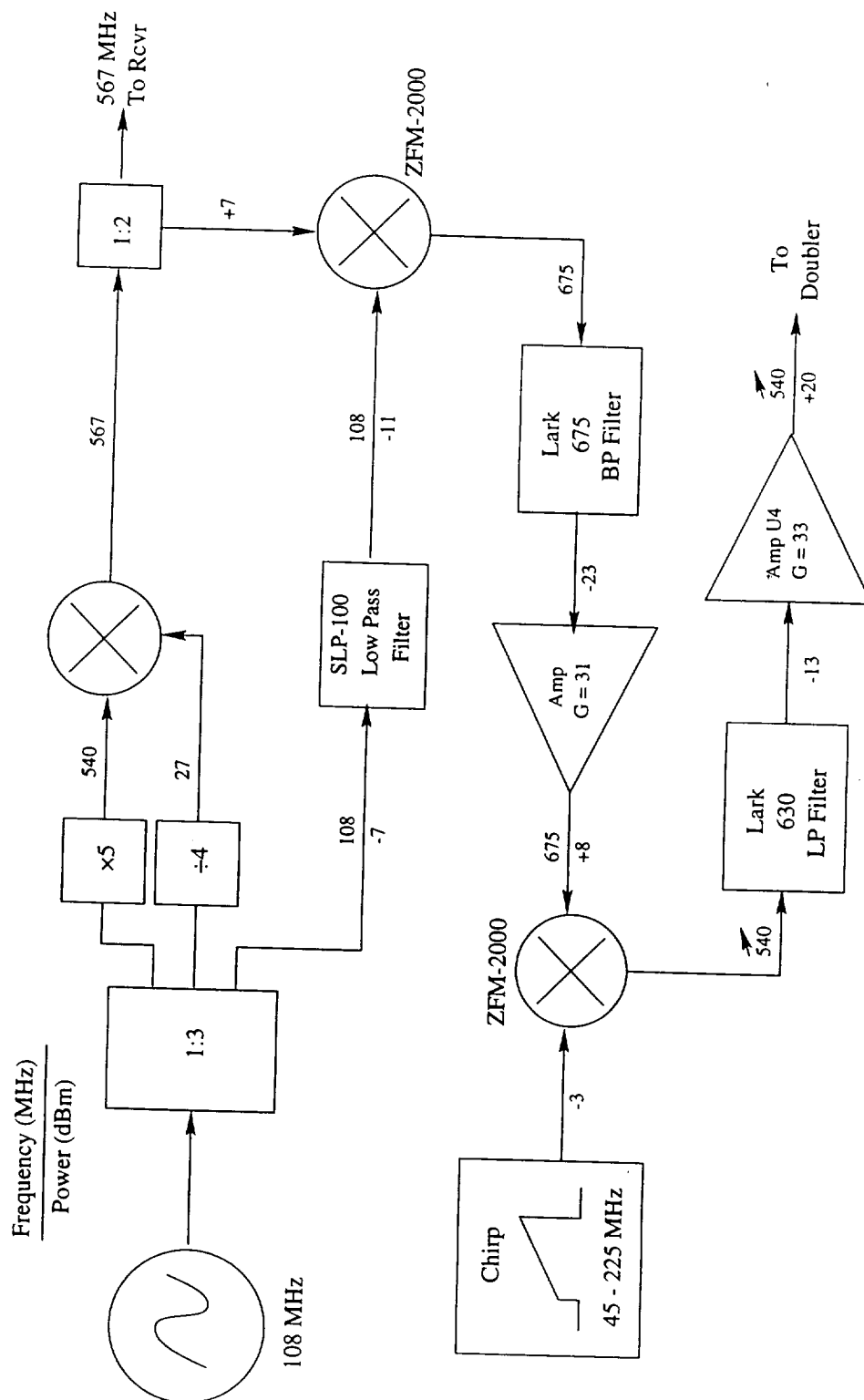
Figure 3.21 General block diagram of the updated intermediate frequency generator.

Figure 3.22 Current block diagram of the AAFE transmitter subsystem.
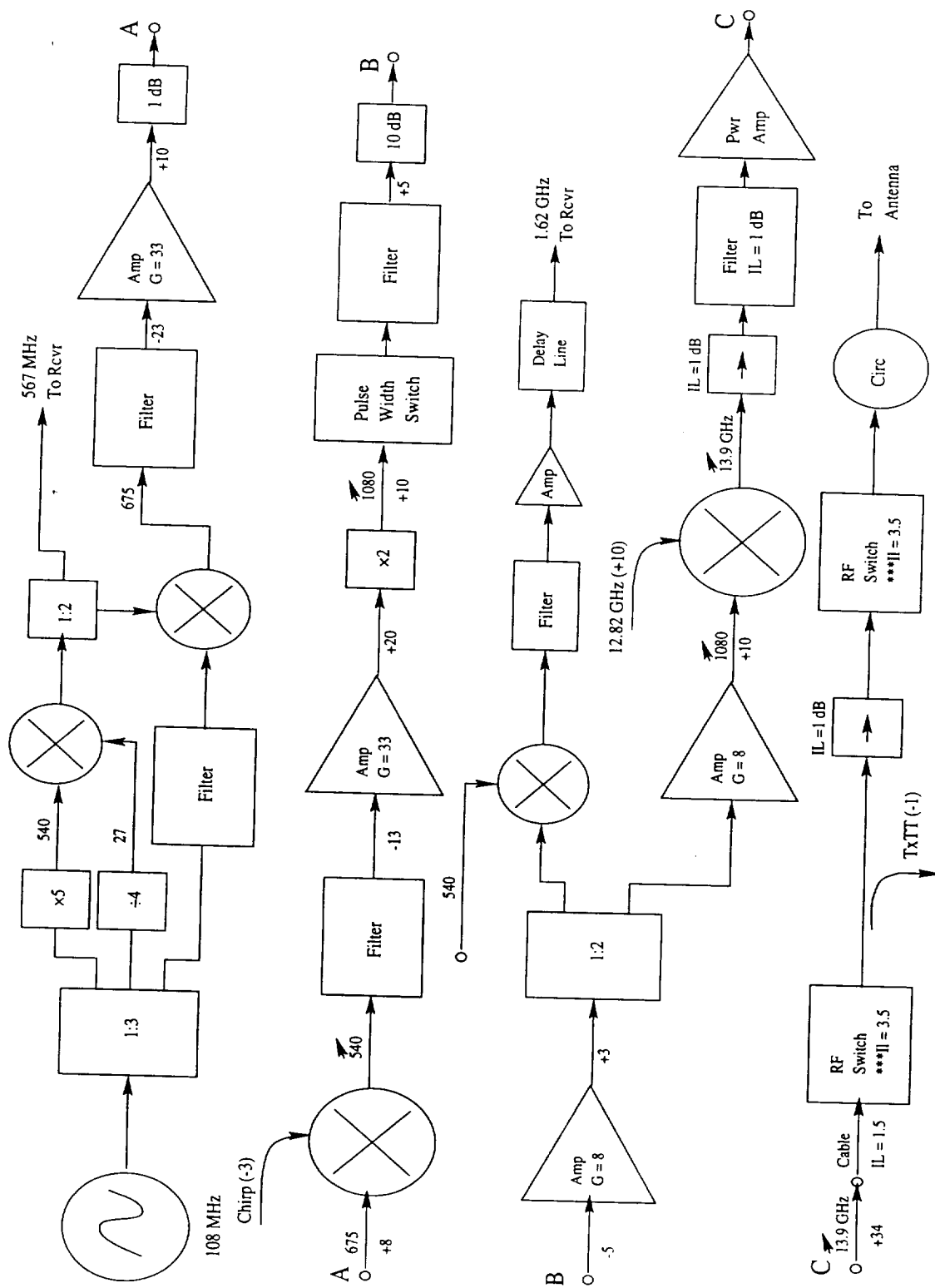
Figure 3.23 Current detailed block diagram of the AAFE transmitter subsystem.

49

strobed in with the appropriate "mode" values that determine the register being loaded. Some other lines must be held to ground or toggled to initialize the device.

Once the DCS is programmed, a select line is pulsed to produce an output. The output initiates at the start frequency and every 2 nanoseconds adds the frequency value in the increment register until the select line is released. When the select line is pulsed again, the frequency is already reset to the start frequency. There is a main and auxiliary start frequency register to allow more flexibility without reprogramming the device.

The AAFE control subsystem already sends a 50 nanosecond pulse (intended for the burst generator) to initiate the chirp or dechirp. To minimize modifications to the control subsystem, both the main and auxiliary registers were programmed with the 45 MHz start frequency. The already existing chirp and dechirp outputs could then be used to generate the transmit and deramping pulses, respectively. These pulses are elongated to the required 3.1 $\mu$second pulse width through a delay circuit in the Altera interface, as shown in the logic diagram. The pulse width can be further modified with the pulse width switch as before; however, a 3.67 $\mu$second delay is necessary to account for the delay inherent to the RAC device. The circuit was tested on a logic analyzer and its output verified.

Preliminary DCS output tests showed a general functionality of the device. Figure 3.25 illustrates a spectrum analyzer plot of the DCS output using a pulse repetition frequency of 200 kHz. This verified that the DCS was accepting and executing both the proper start and increment frequency. However, the level of low frequency components (between 0 Hertz and 45 MHz) was curiously higher than the expected noise floor value. To ensure that the presence of these low frequency components was not due to measurement inaccuracy, the chirp was observed on an oscilloscope. MIRSL does not have oscilloscope plotting capabilities, however, figure 3.26 was obtained from the manufacturer (Sciteq) and illustrates some of the
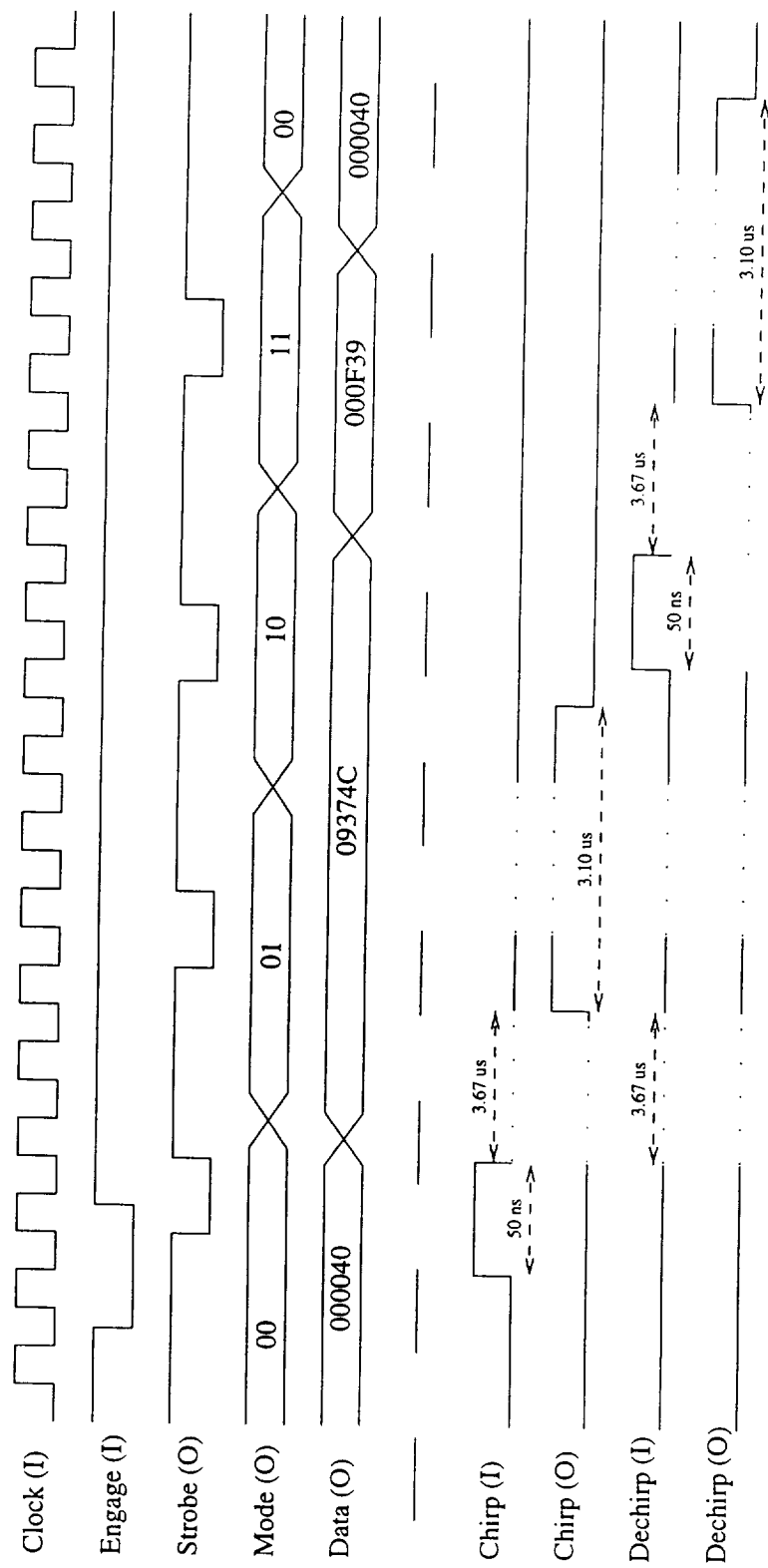
Figure 3.24 Altera programming circuit logical timing diagram.

51

interference, cutting off the more gradual "wispy" interference that could also be seen on a scope.

Moreover, as the pulse repetition frequency (PRF) was decreased, the interference worsened until there was no longer a cutoff at the start frequency, as shown in figure 3.27. The typical operating PRF of the AAFE altimeter is 750 Hertz so filtering the 200 kHz PRF output would cause aliasing. Since the DCS was programmed correctly, the DCS was sent to Sciteq for analysis.

The testing setup used by Sciteq sends a continuous PRF to the DCS unit and, as a result, a deficiency in their ROM configuration went undetected. An updated control circuit was installed in the DCS and greatly improved the functionality of the device. An updated oscilloscope (courtesy of Sciteq) and spectrum analyzer plot is shown in figures 3.28 and 3.29, respectively.

During the process of diagnosing the DCS malfunction, more attention was paid to the interface / programming circuit. A spare HP GPIO card was used to program the DCS via the computer user interface, and a circuit was designed to handshake between the GPIO and DCS and tested on a breadboard. This circuit is a much better design since it allows reprogramming of all DCS parameters in seconds. In contrast, the Altera solution eliminates much of the flexibility of the DCS since it must be reprogrammed on the ground for bandwidth and start frequency modifications. In addition, the GPIO solution allows the pulse width switch to be bypassed, adjusting the pulse width in software. As a result, any pulse width can still be obtained and we can remove the hardwired 3.67 $\mu$second delay, a possible source of ambiguity.

Another modification to the DCS interface is the method of controlling the specifications of the chirp output. Instead of programming only the start and increment frequencies, a stop frequency is also programmed, eliminating any error due to variability in the select pulse. The start and increment frequencies control

52
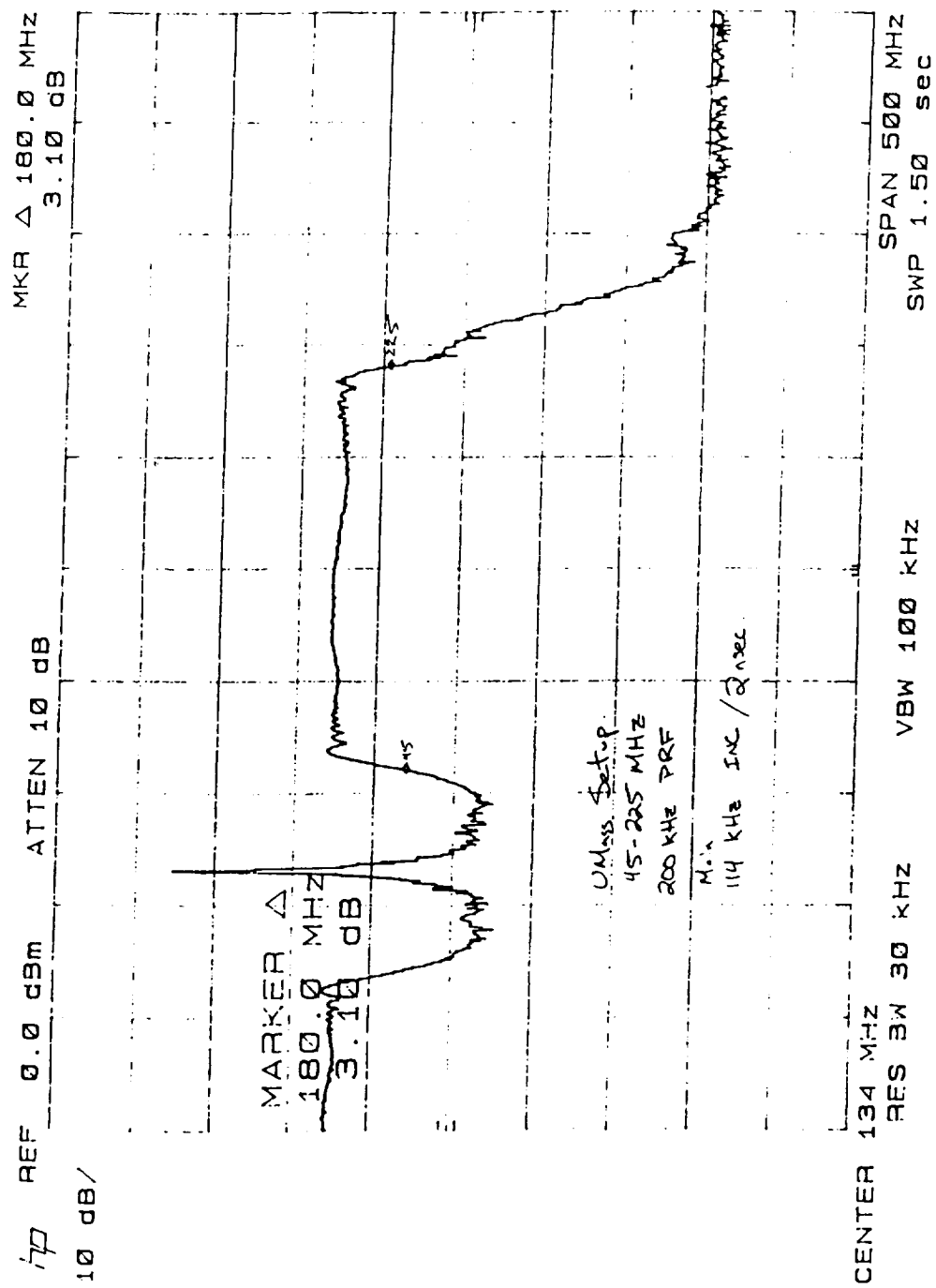
Figure 3.25 Digital chirp synthesizer output with PRF of 200 kHz.
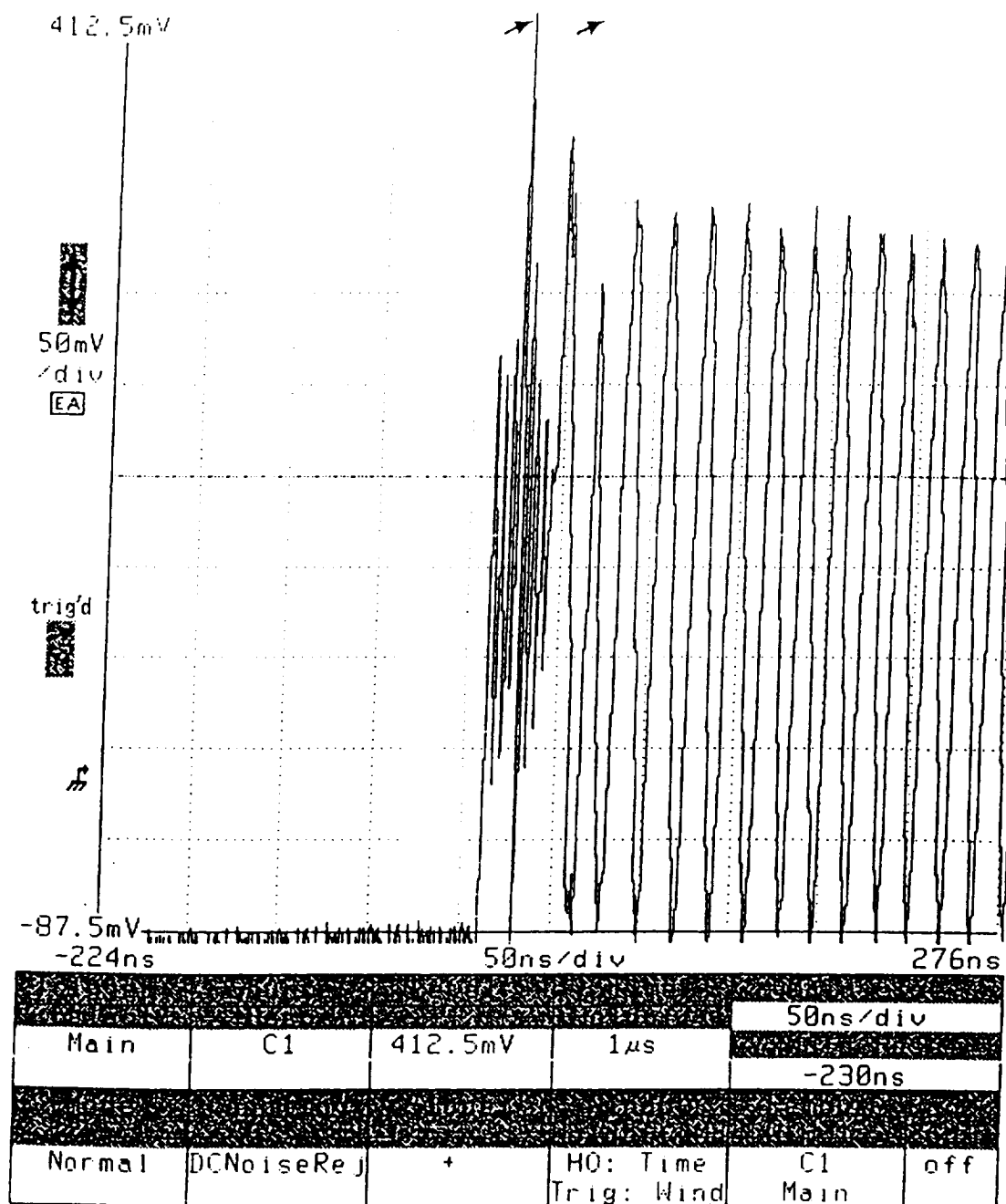
Figure 3.26 Oscilloscope plot of digital chirp synthesizer output.

54
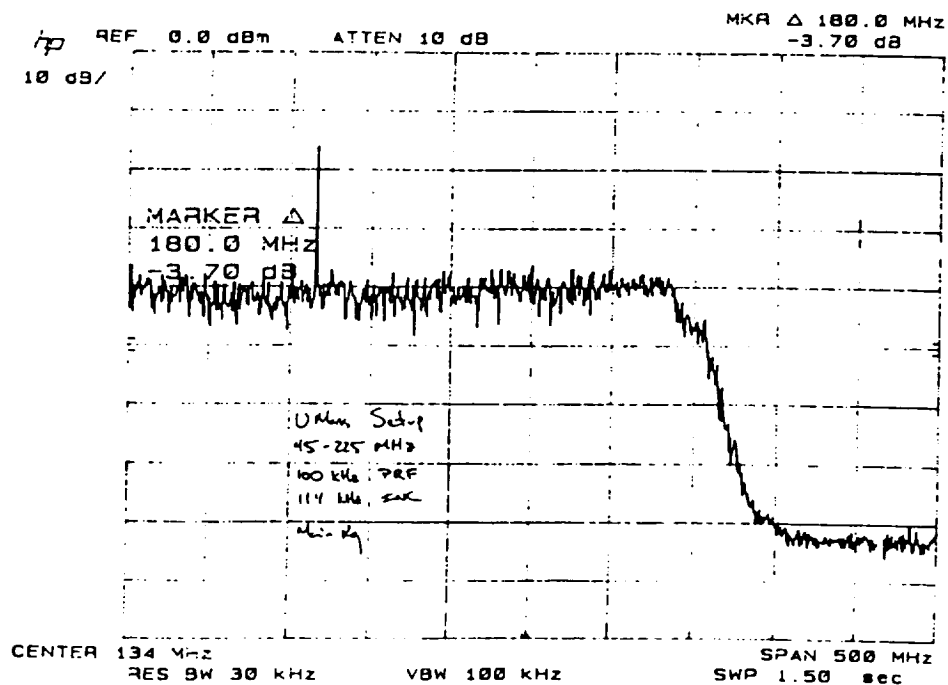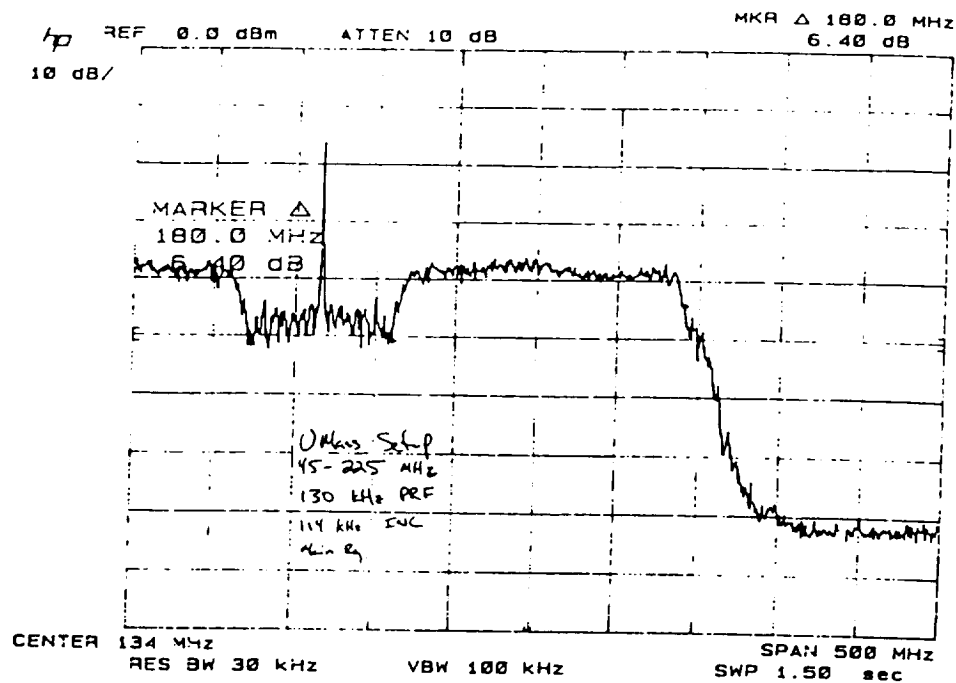
Figure 3.27 Digital chirp synthesizer outputs with PRF of 130 kHz and 100 kHz (below).
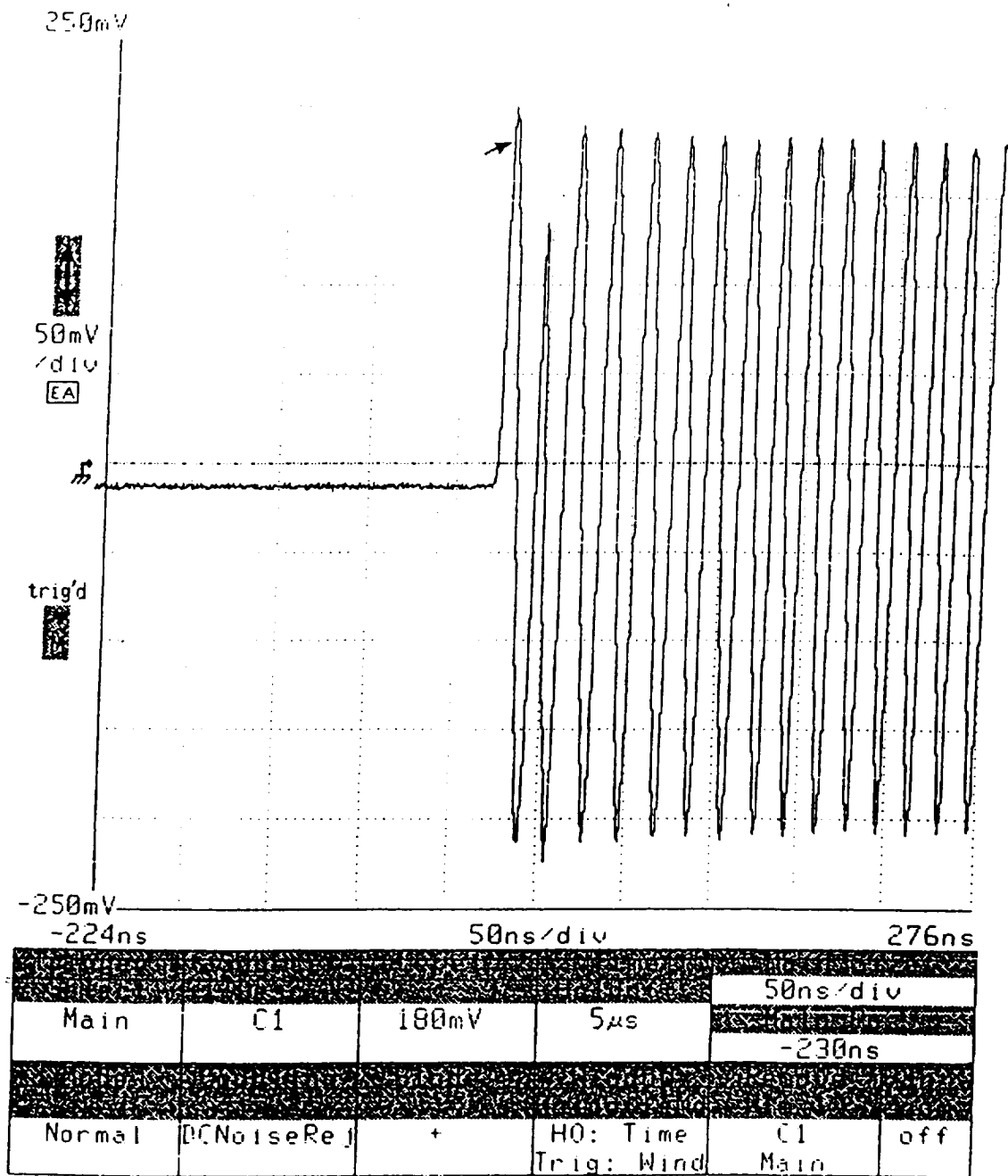
Figure 3.28 Oscilloscope plot of ROM modified digital chirp synthesizer output.
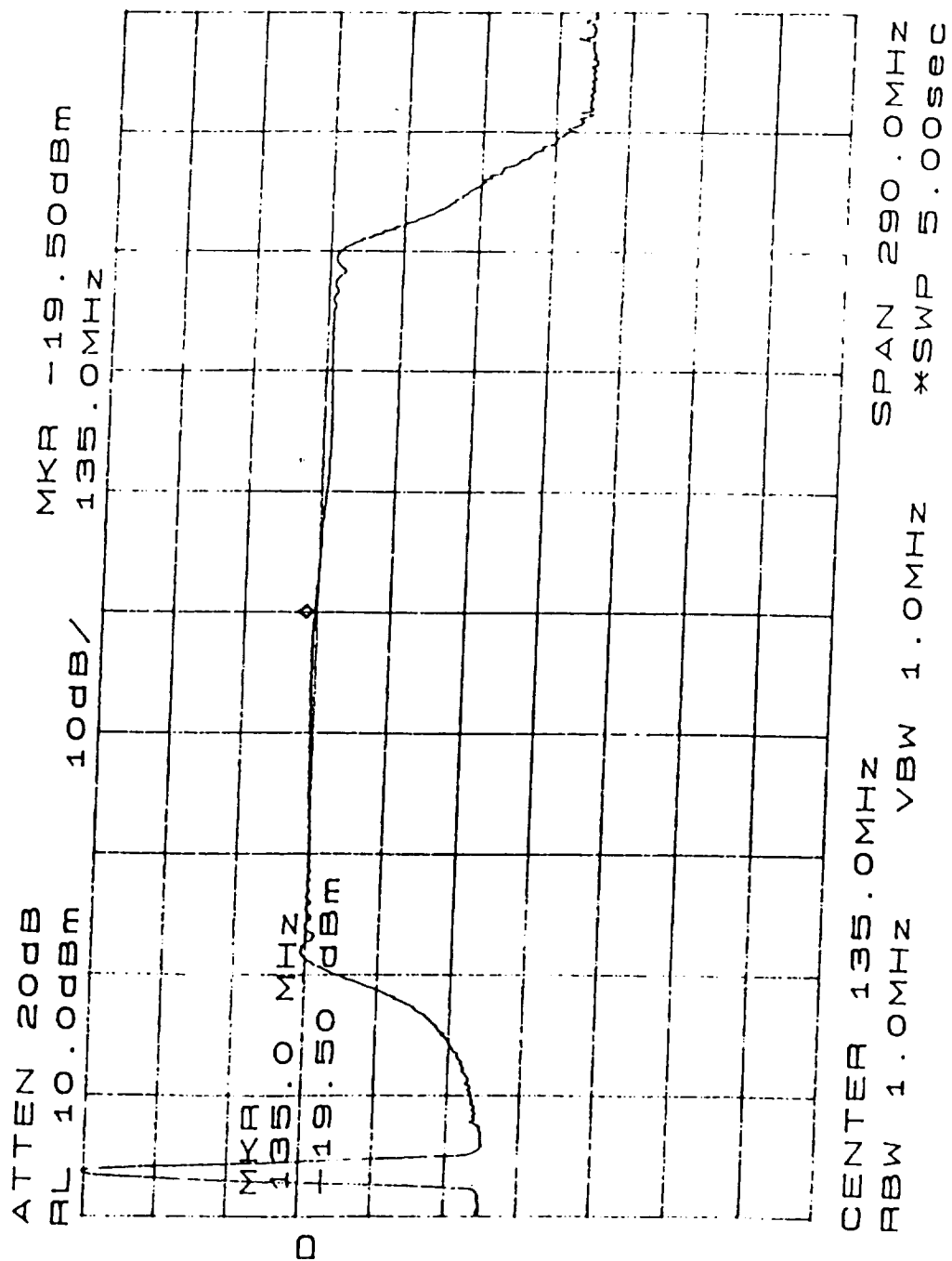
Figure 3.29 Digital chirp synthesizer output (PRF = 750 Hz) after ROM modification.
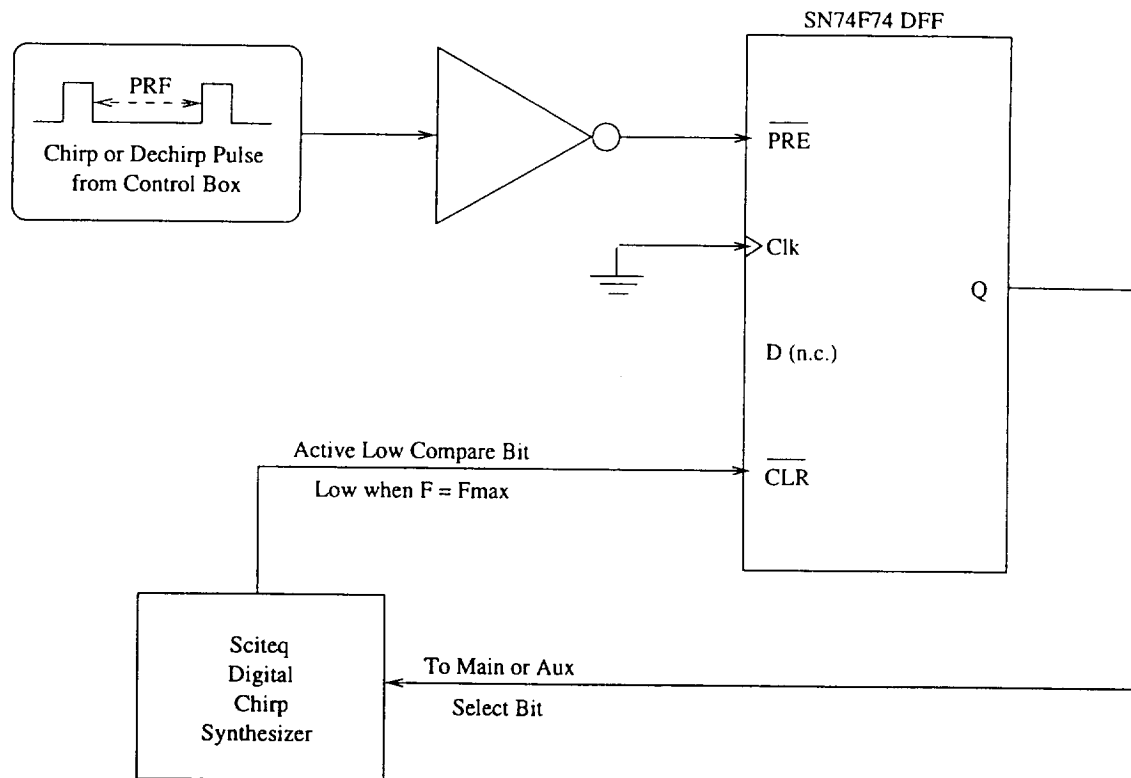
Figure 3.30 Logical representation of the GPIO digital chirp shut-off circuit.

the shape of the chirp as before, but a comparator bit goes high when the chirp reaches the stop frequency. This bit is used to turn off the select line, and therefore, the chirp pulse. The basic logic diagram of the GPIO design interface is illustrated in figure 3.30. Other pertinent information about this design can be found in Appendix B.

Once the DCS output was verified, operation of the altimeter could be tested. Until a circuit board for the GPIO interface can be fabricated and a power supply for the DCS can be assembled, a field test is not feasible. However, a combination of lab tests verified the functionality of each component of the transmit and receive sequence. First, the chirp and dechirp generation was verified on an oscilloscope. The delay of the dechirp pulse was varied and its timing in reference to the original chirp was measured to be correct.

Any possible errors in the deramping process were eliminated in the following test. A chirp pulse was generated and split using the test target section in the receiver subsystem. Instead of recombining the 102 nanosecond delayed pulse with the other pulse via the second power splitter, they were subjected to a deramping mixer. A spectrum analyzer plot of the output of this mixer is shown in figure 3.31. The chirp pulse used had a bandwidth of 180 MHz and a pulse width of 3.1 $\mu$seconds - identical to the AAFE chirp prior to the frequency doubler. After deramping, the signal should then be at a frequency calculated by

$$ F = \frac{180MHzBW}{3.1\mu seconds} \times 102nsec = 5.92MHz. \tag{3.4} $$

The spectrum analyzer plot confirms this as well as illustrating a minimum of 20 dB of suppression between the desired peak and any spurious signals. The large spike towards the left of the plot is the zero Hertz signal.

Finally, a calibration file was taken. Figures 3.33 and 3.32 show the state of the calibration output before the current upgrade. Of note are two large spurious signals, often higher than the expected return, and a miserable signal-to-noise ratio. But as figures 3.35 and 3.34 show, the radar now receives a strong, clean signal with a signal-to-noise ratio greater than 35 dB.

These tests confirm that all facets of the AAFE altimeter operate correctly on an individual basis. The only differences between calibration mode and normal transmitting mode are as follows:

- A second dechirp signal is generated at a delay specified by the tracking system. This function was verified in test one.

- The initial chirp exits the antenna, is reflected back from the surface, and received via the antenna port. No problems with the circulator and antenna were ever experienced.
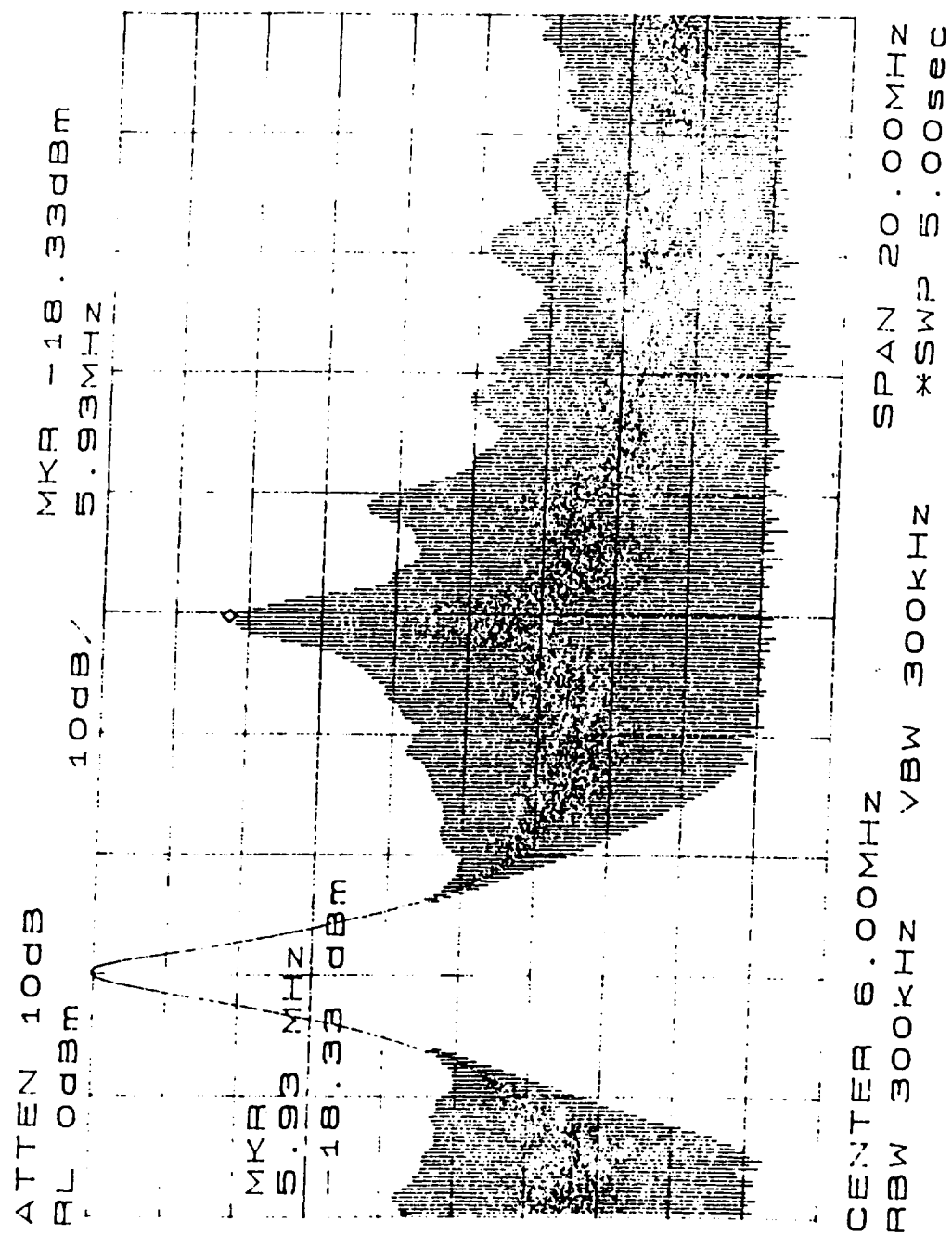
Figure 3.31 Spectrum analyzer plot of deramping test output.

Any possible data acquisition timing problems were eliminated through proper function during the calibration mode. A high degree of confidence about the operation of the radar can be assumed. The updated AAFE user's manual is included in Appendix C.
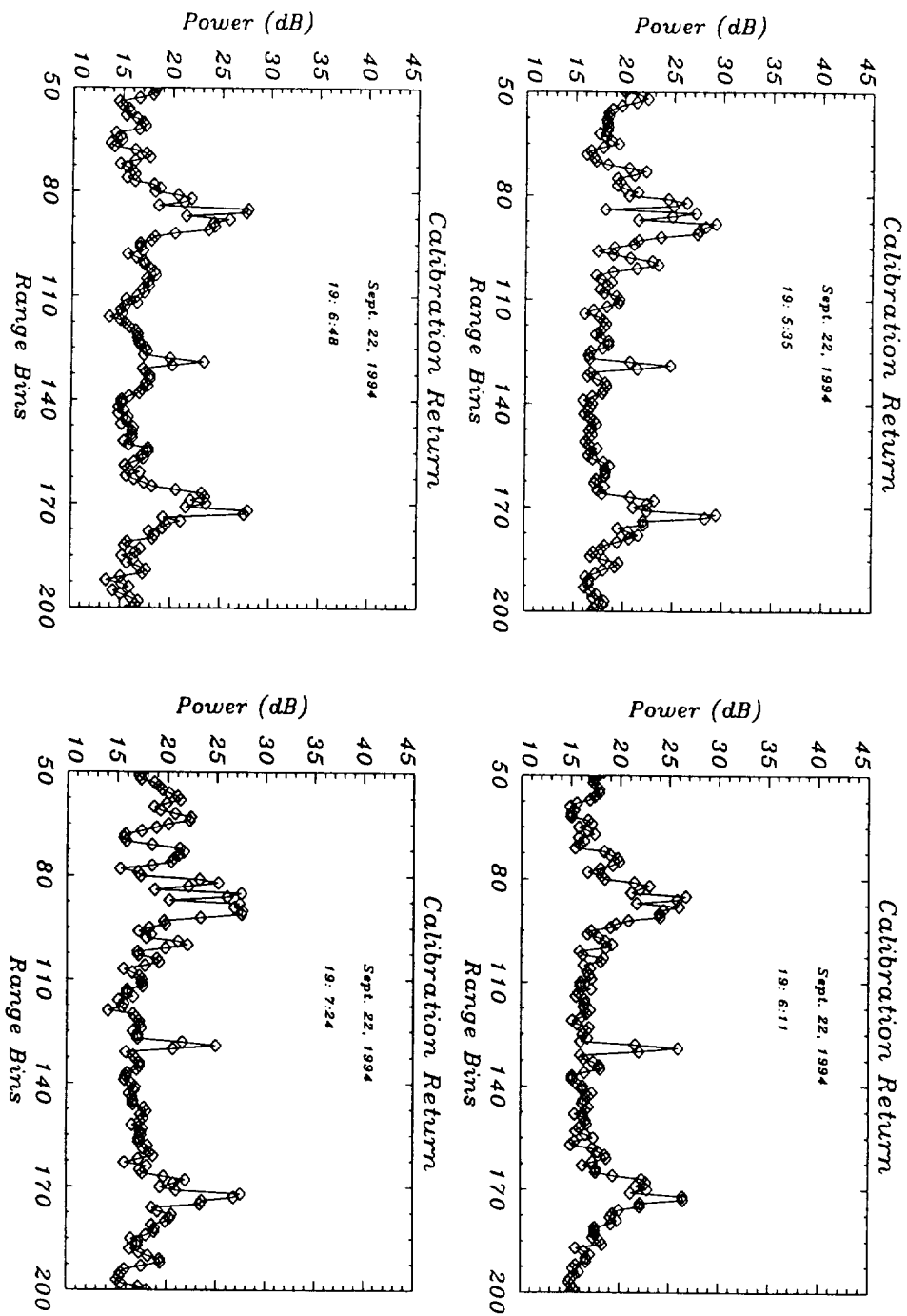
Figure 3.32 Calibration outputs of AAFE before recent modifications.
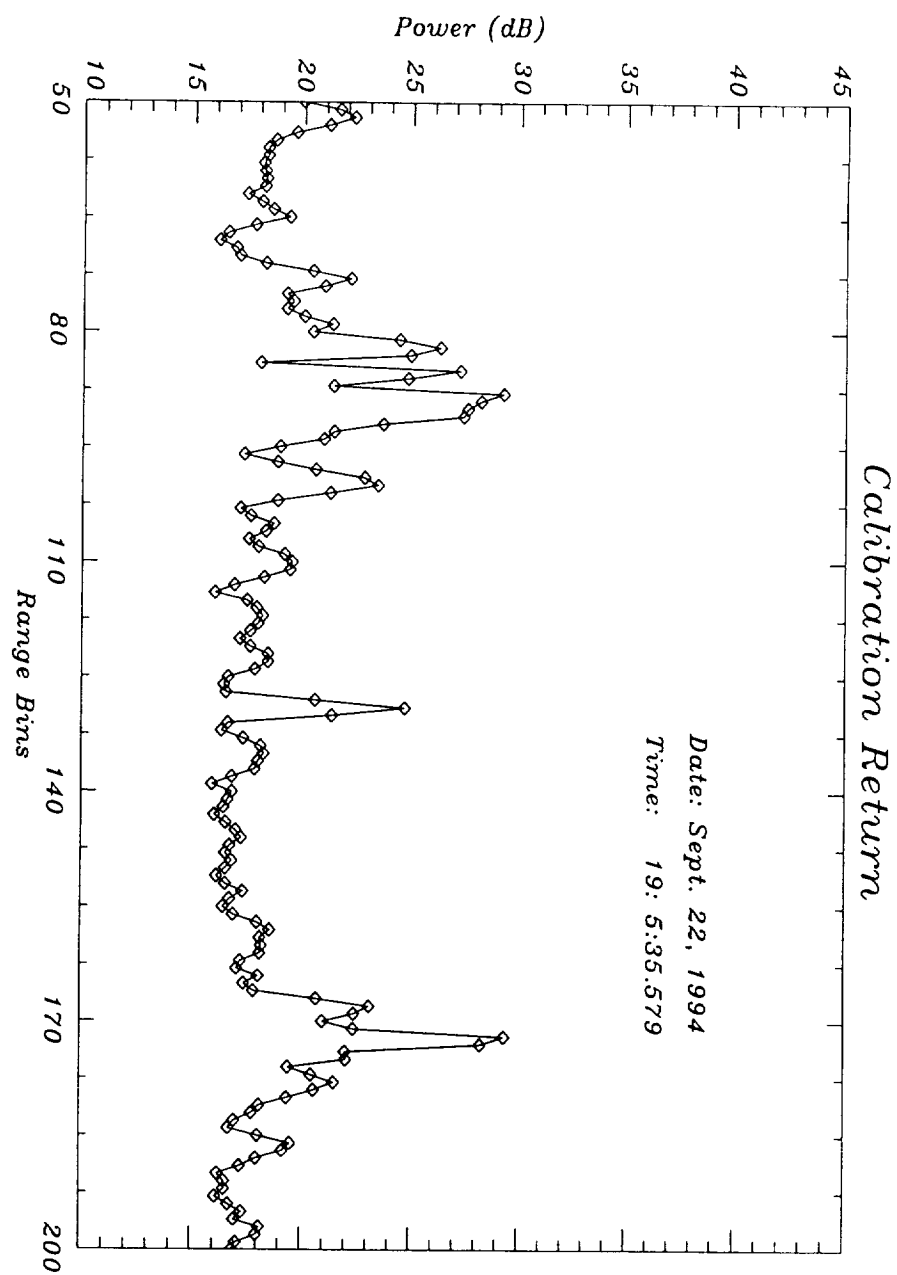
Figure 3.33 Calibration output of AAFE before recent modifications.

63
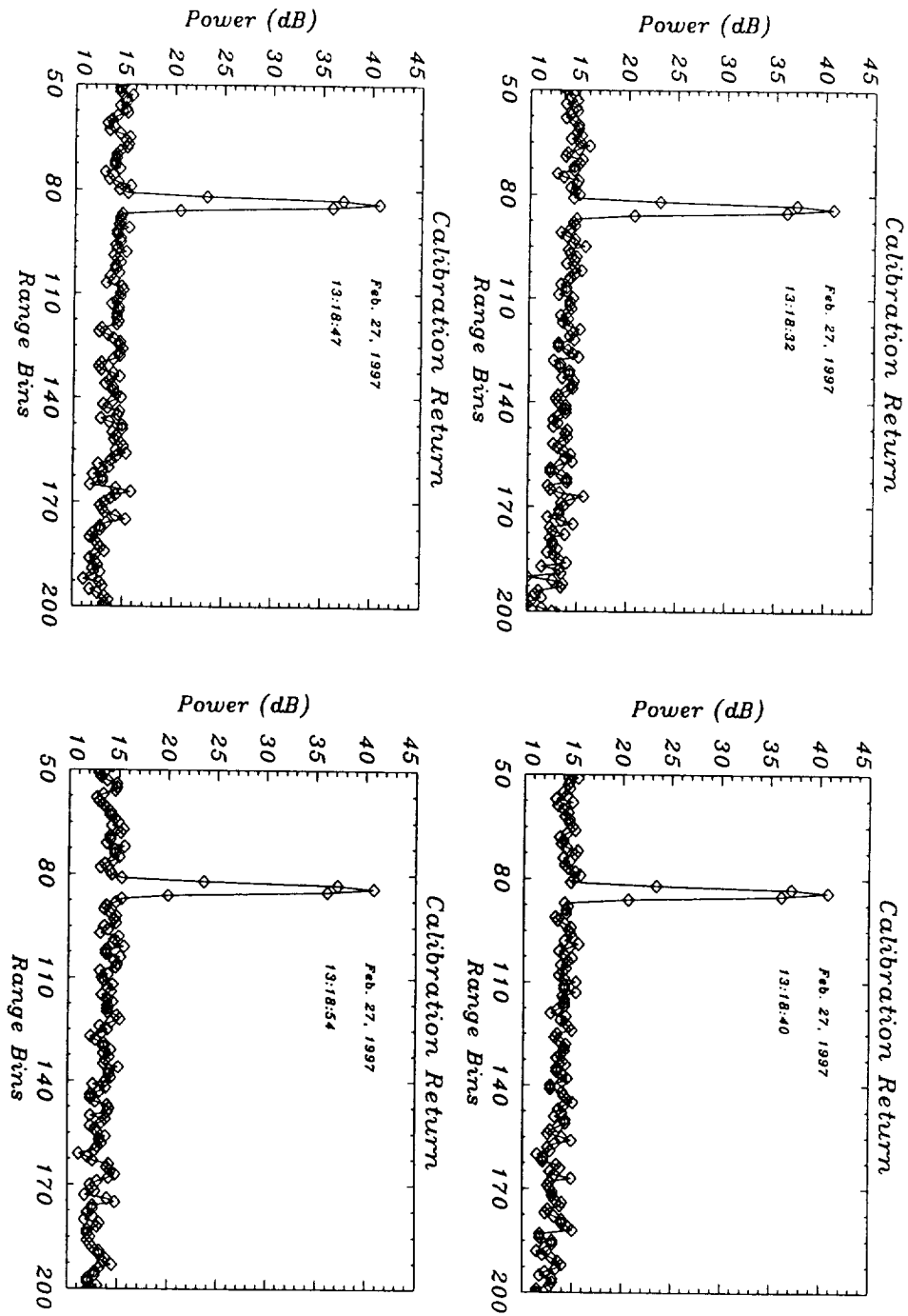
Figure 3.34 Calibration outputs of AAFE after recent modifications.
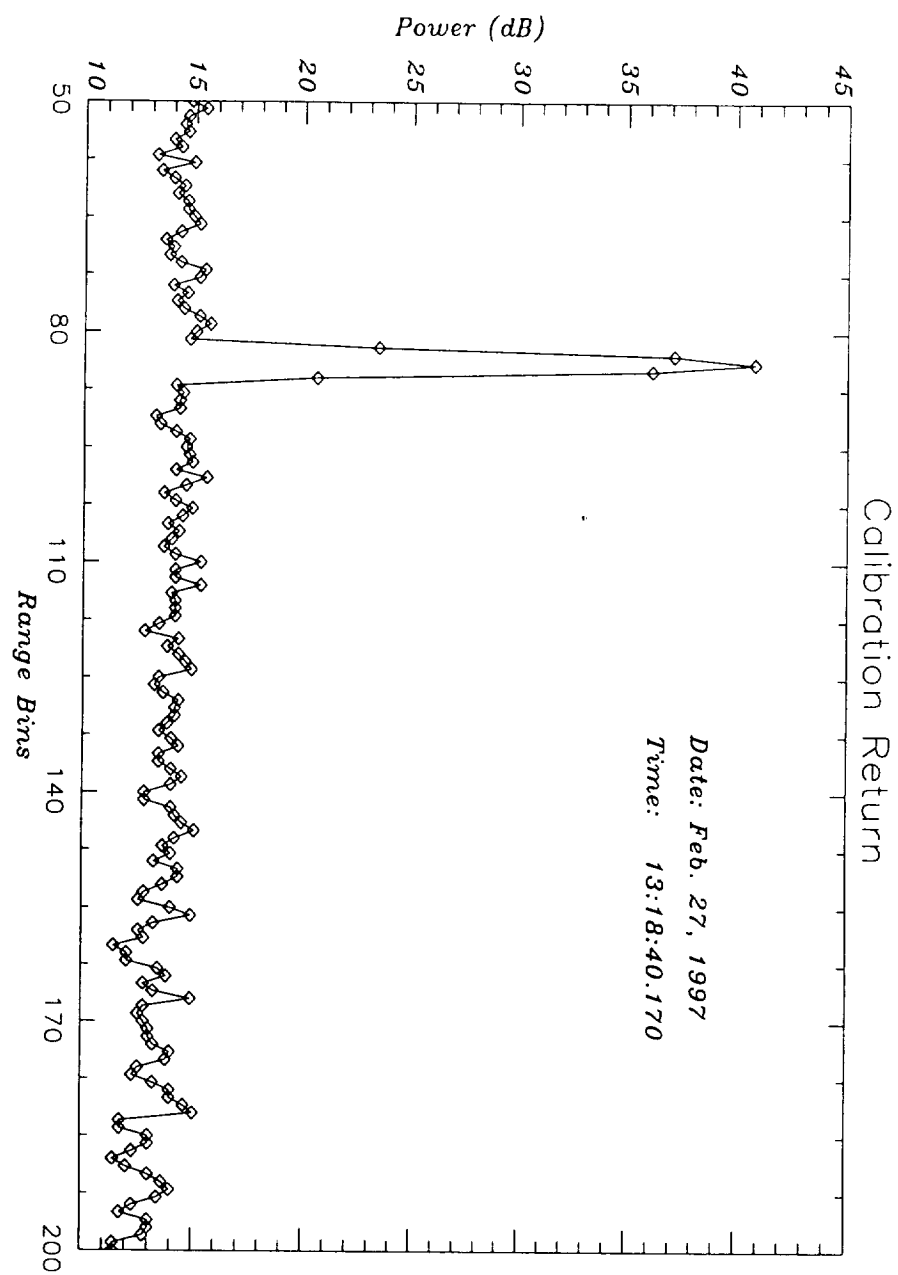
Figure 3.35 Calibration output of AAFE after recent modifications.

CHAPTER 4

PRELIMINARY RESULTS FROM THE 1994 GREENLAND
EXPERIMENT

In 1994 the AAFE altimeter participated in the NASA multisensor airborne altimetery experiment. AAFE and other remote sensing instruments, including the NASA Airborne Oceanographic Lidar (AOL), were installed on a NASA P-3 aircraft to operate over the Greenland ice mass. The experiment consisted of fourteen flights, repeating trajectories flown previously in 1991 and 1993. The mission endeavored to measure small-scale changes in the mass balance of the ice sheet through periodic measurements. Global Positioning System (GPS) receivers in differential mode were used with the aircraft's autopiloting system for accurate flight path duplication and for determining the aircraft altitude above the ellipsoid, a reference sphere around the surface of the earth. By taking the difference between the GPS altitude and altimeter measurements of the aircraft altitude above the ice sheet, the ice sheet altitude above the ellipsoid was determined.

During the 1991 and 1993 experiments, the AAFE altimeter provided extremely accurate information about the aircraft altitude above the ice sheet. Figures 4.1a and 4.1b show a comparison between AAFE altitude results and data taken with the AOL altimeter in 1991. The actual altitude measured is illustrated in figure 4.1a and 4.1b shows the difference between the two data sets.

As a result of the hardware failures mentioned previously, the AAFE altimeter was unable to repeat these results in 1994. Figure 4.2 compares 1994 AAFE data with AOL data. The drop-out of data towards the right of the plots coincides with a cloud cover through which AOL could not penetrate. As illustrated by the
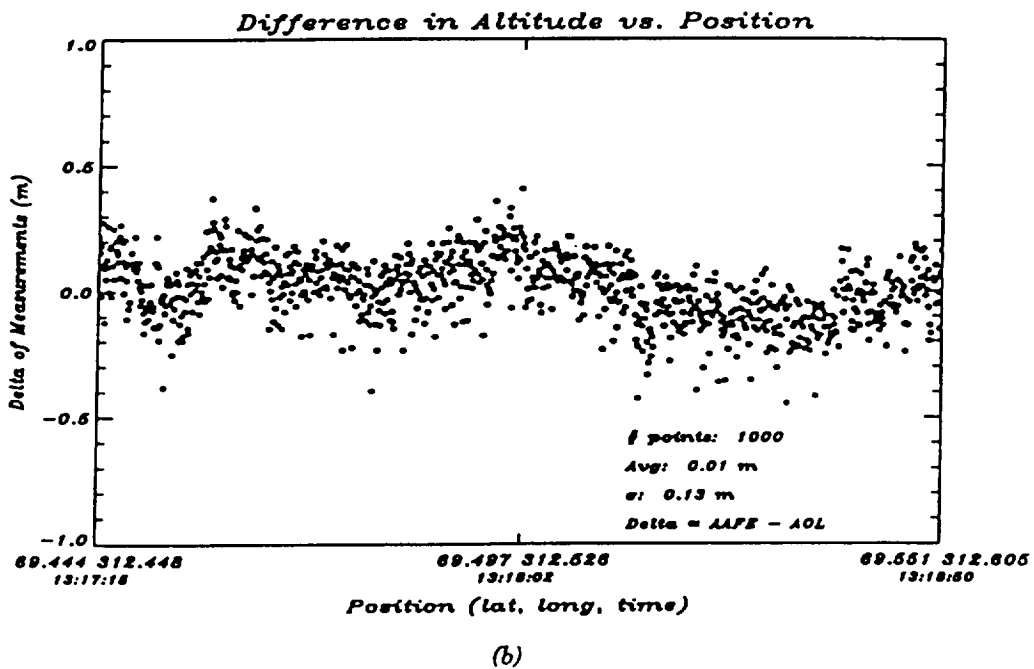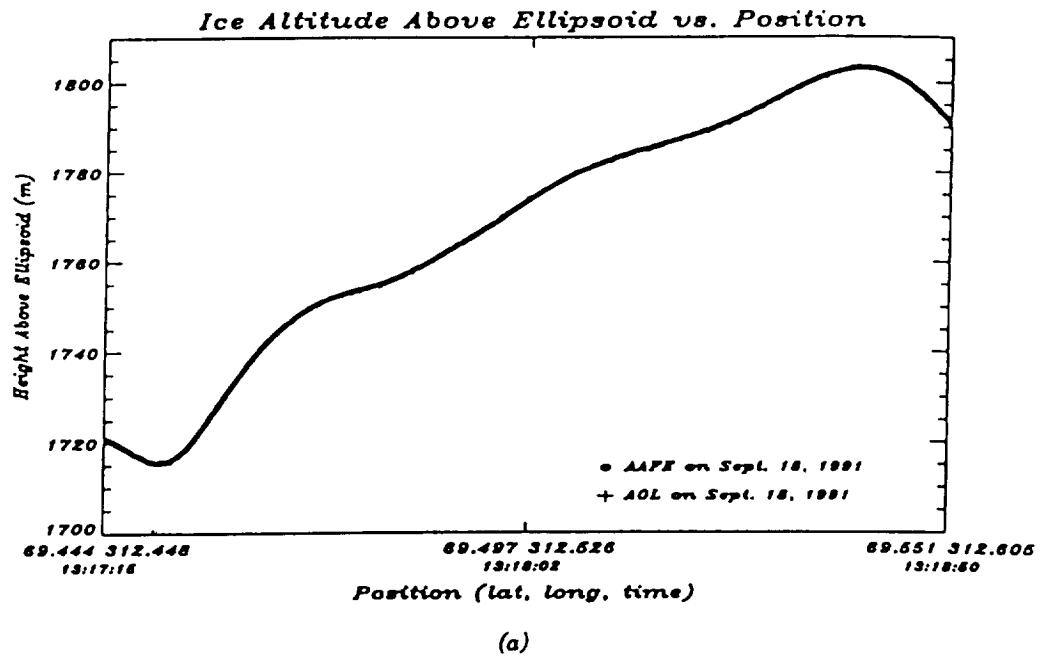
Figure 4.1 Comparison between AAFE and AOL altitude measurements during
the 1991 Greenland experiment [Ferraro, 1994]

calibration plot in figure 3.33, the AAFE altimeter was suffering from two spurious peaks, as well as a signal-to-noise ratio under 7dB. The large bias towards the left of figure 4.2 could be a result of tracking the wrong peak. Most of the data was tracked manually since the auto-tracker could not function properly due to the low signal-to-noise ratio.

In order to obtain acceptable altitude results with this data set, a massive data processing effort compensating for the transmit pulse deficiencies must be undertaken. However, other information can also be salvaged from the 1994 data set. Figure 4.3 illustrates a surface plot of AAFE returns taken within the percolation zone. There is evidence of the presence of sub-surface volume scatterers toward the chronological end of the plot, while they are notably absent from the beginning.

Although unforseen complications adversely affected results for the 1994 mission, the recent modifications to the radar hardware have returned the instrument to proper operation. When the AAFE altimeter participates in its next experiment, results similar to the 1991 mission can be expected. A catalog of AAFE data sets is listed in Appendix D.
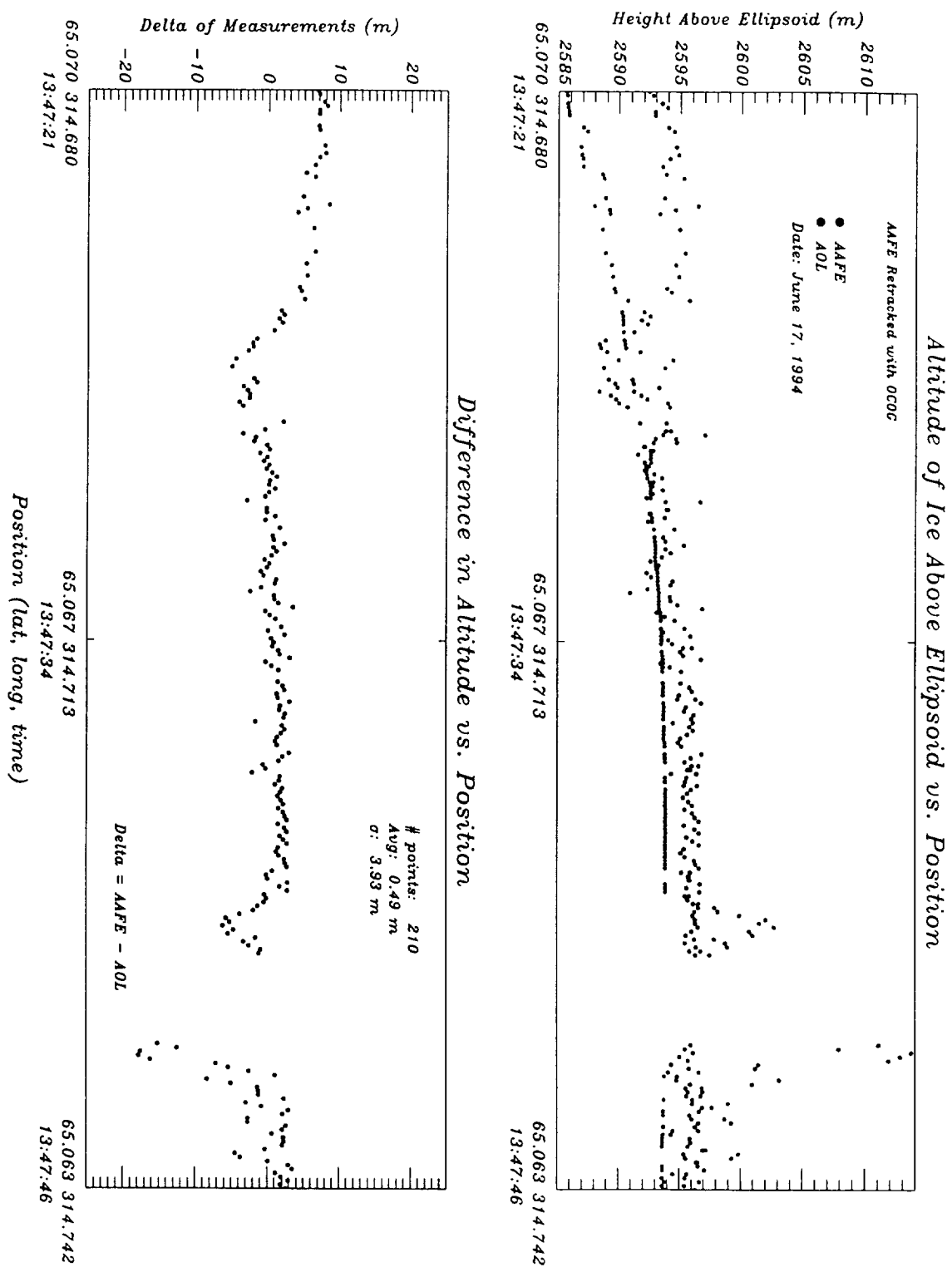
Figure 4.2 Comparison between AAFE and AOL altitude measurements during the 1994 Greenland experiment
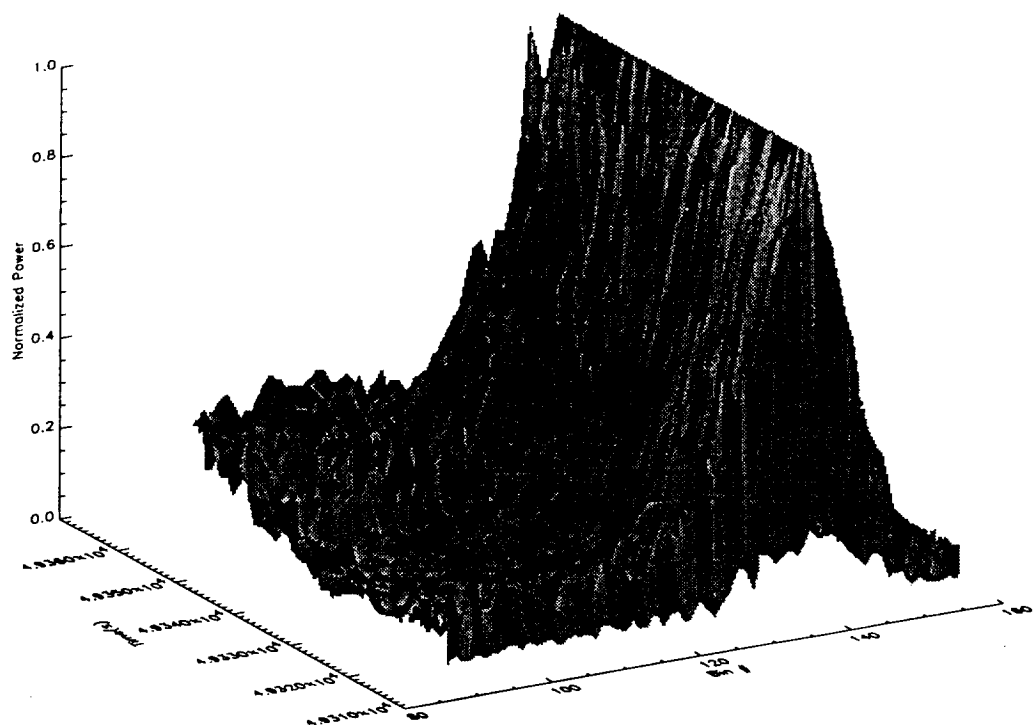
Figure 4.3 Surface plot of 1994 AAFE returns

CHAPTER 5

CONCLUSION AND SUGGESTIONS FOR FUTURE WORK

Over the past nine months, the AAFE altimeter has been returned to full operational capability by a painstakingly detailed diagnostic inspection of the radar hardware. The "detailed" transmitter and receiver block diagrams should serve as a baseline for proper hardware functionality. The receiver, in fact, has been fine-tuned starting from the analog to digital converter and working backwards. All of the mixing stages have been optimized through "LO" level to minimize insertion loss and maximize unwanted image and "LO" suppression. The amplifier stages have been optimized for maximum power output without saturation.

Currently, a conservative estimate is that the altimeter is from three to six months away from mission readiness. The following tasks, given in order of timeliness, are mandatory before AAFE can participate in any flight experiments:

- The GPIO interface circuit must be routed with PADS and sent for fabrication (possibly through ProtoExpress). Appendix B presents a tested design.

- A power supply for the digital chirp synthesizer (DCS) must be assembled. All necessary parts have been purchased except for the metal case and a means for the -2 voltage requirement. A sturdy housing for the DCS itself, complete with fan, must also be built.

- The software program "AAFE_START_NEW" must be modified to accommodate the completed GPIO interface circuit. Currently it programs the DCS via the temporary breadboard equivalent, and will need adjustment should the GPIO data pins switch from their current DCS data pin assignments, as is very likely. The DCS programming routine should be incorporated into the

"AAFE_MAIN" general radar operation code to allow reprogramming without shutting down. Both of these tasks can be accomplished in an afternoon.

If time allows, these further modifications should be completed:

- Though still functioning, the last two (identical) RF switches in the transmitter subsection are suffering from an abnormally higher insertion loss. Rated at an insertion loss of just under 2 dB, their loss consistently measures greater than 3.5 dB. This added loss halves the output power immediately prior to the antenna port, reducing operating range and the signal-to-noise ratio. Moreover, the additional loss could be a signal of component deterioration, indicating an imminent device failure.

- Much of the component-to-component wiring is old RG-316 style cable. These cables have poor isolation and their fragility makes them a source of future failure. A fair supply of semi-flex shielded cable has already been purchased and should be enough for most of the higher frequency runs.

Finally, there are some desirable improvements, but they are either expensive, extremely time consuming, or both. These include:

- The transmitter subsection has now been almost completely rearranged, leaving excessively long cable runs, components with poor anchoring, components with no current use, and a general lack of order to component layout due to repeated modifications. A complete overhaul and re-fabrication would improve system performance (through shorter cable runs, for example), facilitate diagnostics or repairs, and greatly reduce the size and weight of the transmitter. This, however, is not a small undertaking and there is the risk of component failure from of any of the custom Hughes parts.

- A more concise intermediate frequency generator could be achieved through the purchase and installation of an injection locked 675 MHz or 405 MHz oscillator. Though this would reduce the number of components, and therefore reduce failure risks and improve space and weight characteristics, there are no performance benefits for the relatively high cost.

Although the design of the AAFE altimeter can hardly be described as new technology, the numerous enhancements provided by MIRSL have enabled the radar to maintain a modern level of performance. Once again operational, the altimeter remains a powerful tool for the study of glacial ice.

# PERFORMANCE/SPECIFICATIONS: <u>DCP-1A</u>

**Output Frequency**
Range (DCP-1A) ............. 1 MHz to 250 MHz (w/o LPF)
Range (DCP-1A/LPF) ....... 1 MHz to 230 MHz (w/ LPF)
Resolution ..................... <30 Hz (Approximately 29.80... Hz)
Control........................ 24 parallel BINARY TTL bits (pos-true logic) with STROBE
**Main Output (with LPF and gain equalization)**
Level ......................... -5 dBm into 50Ω (1 MHz to 230 MHz)
Accuracy/Flatness ............ ±2 dB <Phase Control.....12 parallel TTL Binary bits (pos-
.................................. true logic)
**Spectral Purity**
Harmonics..................... -35 dBc
Spurious (typical)............. -50 dBc (@<100 MHz)
                                -45 dBc (@ >200 MHz)
Phase Noise @ 101 MHz.... <-95 dBc/Hz @ 100 Hz offset
                              <-95 dBc/Hz @ 1 kHz offset
                              <-115 dBc/Hz @ 10 kHz offset
                              <-130 dBc/Hz @ 100 kHz offset
**Clock Frequency** ............. 500 MHz
Level .......................... +5 dBm ± 2 dB
**Reference Frequency (if optional REF GEN module is supplied)**
External....................... 10.0 MHz @ 2 dBm ± 2 dB into 50Ω
or
Internal....................... 10.0 MHz @ ±1 ppm accuracy
**Frequency Switching**
Switching Speed.............. <2 NANOseconds in the chirp mode
                               <50 nsec in manual hopped CW mode
Characteristic................. Phase Continuous (Linear FM mode only)
**Connectors**
RF Sine Output ............... SMA Female (J1)
DDS Clock Ref Input ........ SMA Female (J3) - 500 MHz
Frequency Control........... 50-pin mini D-connector (P2)
Power......................... 9-pin mini D-connector (P1)
Stop Frequency .............. 15-pin mini D-connector (P3)
**Environmental**
Operating Temp............... 0°C to +50°C
Storage Temp ................. -20°C to +70°C
**Power Supply** ................. -5.2V @ 2.5A;+5V @ 150 mA; -12V @ 125 mA;-2V @ 500 mA
**Dimensions**..................... 5"(W) x 7.08"(D) x 1.125"(H);
**Weight** ........................... 2 lb (0.9 kg),net; 3 lbs (1.4 kg), shipping

# Appendix B

## GPIO Programmer Design

| Pin # | GPIO Value | Sciteq Value | Pin # | GPIO Value | Sciteq Value |
|-------|-----------|--------------|-------|-----------|--------------|
| 1 | GND | F23 | 26 | GND | GND |
| 2 | DO15 | F20 | 27 | DI15 | P10 |
| 3 | DO14 | F17 | 28 | DI14 | P07 |
| 4 | DO13 | F14 | 29 | DI13 | P04 |
| 5 | DO12 | F11 | 30 | DI12 | P01 |
| 6 | DO11 | F08 | 31 | DI11 | GND |
| 7 | DO10 | F05 | ·32 | DI10 | AuxSel |
| 8 | DO9 | F02 | 33 | DI9 | MstrReset |
| 9 | DO8 | GND | 34 | DI8 | F21 |
| 10 | DO7 | P11 | 35 | DI7 | F18 |
| 11 | DO6 | P08 | 36 | DI6 | F15 |
| 12 | DO5 | P05 | 37 | DI5 | F12 |
| 13 | DO4 | P02 | 38 | DI4 | F09 |
| 14 | DO3 | ClkReset | 39 | DI3 | F06 |
| 15 | DO2 | Mode0 | 40 | DI2 | F03 |
| 16 | DO1 | MainSel | 41 | DI1 | F00 |
| 17 | DO0 | Strobe | 42 | DI0 | GND |
| 18 | GND | F22 | 43 | SafeGND | P09 |
| 19 | PCTL | F19 | 44 | PFLG | P06 |
| 20 | IO | F16 | 45 | PSTS | P03 |
| 21 | PRESET | F13 | 46 | EIR | P00 |
| 22 | CTL0 | F10 | 47 | STI0 | GND |
| 23 | CTL1 | F07 | 48 | STI1 | Mode1 |
| 24 | GND | F04 | 49 | GND | AddZero |
| 25 | SafeGND | F01 | 50 | GND | RomReset |

Current Sciteq programming code (below) used this setup:

| GPIO Pin | Sciteq Data Bit | GPIO Pin | Sciteq Data Bit |
|---|---|---|---|
| 0 | 8 | 5 | 20 |
| 1 | 9 | 13 | Mode1 |
| 2 | 10 | 14 | 6 |
| 3 | 11 | 15 | Mode0 |
| 4 | 19 | Ctl0 | Strobe |

Basic Code:

```
10      ! ENSURE STROBE IS HIGH (INV LOGIC)

20      CONTROL 12,2;0

25      FOR I=1 TO 100

26      . NEXT I

30      !PAUSE

40      !***PROGRAM CONTROL 0x40***

50      CONTROL 12,3;16384

60      ! FLASH STROBE AFTER DELAY

70      FOR I=1 TO 100

71      NEXT I

90      CONTROL 12,2;1

100     CONTROL 12,2;0

110     !***PROGRAM MAIN REG 45 MHz - NOTE 2's Complement!***

120     CONTROL 12,3;-32720

130     ! FLASH STROBE

140     FOR I=1 TO 100

150     NEXT I

160     CONTROL 12,2;1

170     CONTROL 12,2;0

180     !***PROGRAM AUX REG 45 MHz***

190     CONTROL 12,3;8240
```

```
200     ! FLASH STROBE

210     CONTROL 12,2;1

220     CONTROL 12,2;0

230     !***PROGRAM INC 114 kHz***

240     CONTROL 12,3;-24561

250     !***PROGRAM INC 0 Hz

260     !CONTROL 12,3;-24576

270     ! FLASH STROBE

280     FOR I=1 TO 100

290     NEXT I

300     CONTROL 12,2;1

310     CONTROL 12,2;0

320     ! FLASH MASTER RESET

330     CONTROL 12,2;2

340     CONTROL 12,2;0
```

Each GPIO data line must have the following receiver built into the interface
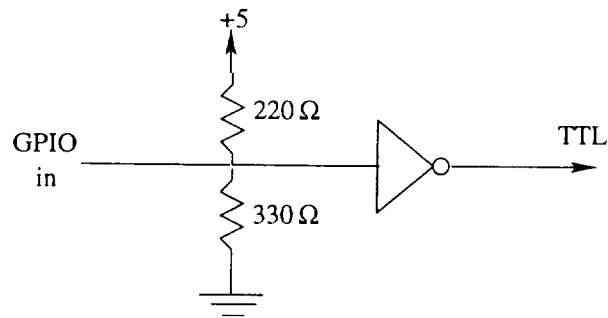


NOTE: It is better to leave out the NOT gate in the fabricated circuit board.
a complemented data word can be sent to compensate!

The following Sciteq lines must be accomodated:

Rom Reset, ADD Zero  both tied LOW
Clk Reset tied HIGH
MSTR Reset pulsed HIGH-LOW-HIGH (remains HIGH)

USER'S MANUAL

Written by Ellen Ferraro (4/29/94), Revised by Rudy Pawul (3/97)

## I. CABLE CONNECTIONS AND AC POWER CONNECTIONS

A. Front of Rack

1a. BNC-to-BNC cable from A∩B (labelled chirp) on Stanford Research Systems (SRS) Four Channel Digital Delay/Pulse Generator (referred to as SRS Pulse Generator from here on) to the BNC "T" on the Control Box input port labelled chirp.

1b. BNC-to-BNC cable from other end of BNC "T" to chirp input on GPIO/chirp interface.

2. BNC-to-BNC cable from C∩D (labelled dechirp) on SRS Pulse Generator to the Control Box input labelled dechirp.

2b. BNC-to-BNC cable from other end of BNC "T" to dechirp input on GPIO/chirp interface.

3. There must be 50 ohm loads on both the A∪B and C∪D ports on the SRS Pulse Generator. This keeps the signals from other ports clean.

4. BNC-to-SMA cable from outport port labelled trigger on Control Box to trigger port on 2000T Analytek card in top Analytek 5-slot VME chassis.

5. BNC-to-SMA cable from 3rd IF outport port on Receiver box to Ch1 port on 2004SC Analytek card in top Analytek 5-slot VME chassis.

6. 4 SMA-to-SMA cables from Transmitter box to Receiver box, labelled 3rd LO (567 MHz), 2nd LO (1620 MHz), TxTT and 1st LO (12.82 GHz). The Vtps port is

a test port and the transmitter Vtps port should have a 50 ohm load on it. There DOES NOT have to be a cable on this port from the Transmitter to the Receiver.

7. Connect an SMA-to-SMA cable from Sciteq digital chirp synthesizer (DCS) to chirp input on transmitter front panel.

8. The TWT is only a backup amplifier and does not have any connections to it. The "TO TWT" and "FROM TWT" ports on the Transmitter box may be left unconnected since they are only for back up purposes.

9. In the top Analytek 5-slot VME chassis the port 1 of the interface ports on the 2000 HA Analytek card should be connected to the J1 port on the 2004 SC Analytek card.

10. 50-pin ribbon cable from the 2000 HA Analytek card in the top VME chassis to the 2000 VIX card in the bottom 5-slot VME chassis.

11. HPIB cable from National Instrument VME GPIB card in bottom 5-slot VME chassis to HPIB card in back of computer.

12. RS-232 cable from VIPER 8704/30 card in bottom 5-slot VME chassis to RS-232 port in back of computer.

13. Connect 50-pin D-type connector from DCS to GPIO/chirp interface.

14. When system is in the aircraft, the SMA port on the 2000 AM card in the bottomm 5-slot VME chassis should be connected to the pulse-per-second (PPS) output from the GPS receiver system.

B. Back of Rack

1. HPIB cable from back of SRS Pulse Generator to HPIB card in back of computer.

2. GPIO cable from back of Control Box to GPIO card in back of computer.

2b. GPIO cable from GPIO card 12 to GPIO/chirp interface.

3. 25 pin cable from back of Control Box to back of Receiver Box.

80

4. 24 pin cable fromm back of Control Box to back of Transmitter Box.

5. There is a 4 pin connector on the back of the Receiver Box that was originally used for testing, but is NOT currently used and should not be connected for anything.

6. 24 pin cable from back of Power Supply Box to back of Transmitter Box.

7. 24 pin cable from back of Power Supply Box to back of Receiver Box.

8. HPIB cable from back of top Analytek 5-slot VME chassis to back of computer.

9. Waveguide Run from back of Transmitter Box to back of Receiver Box, (both ports face directly back).

10. Connect power cables from chirp power supply to DCS.

11. If instrument is installed in an aircraft, the other port on the circulator (the one facing to the right when looking at the back of the Tranmitter Box) should be connected to the waveguide run that goes to the antenna.

12. There should be AC power cables to the SRS Pulse Generator, the Control Box, the Receiver Box, the Transmitter Box, the Power Supply Box, the computer monitor, the GPS receiver, the HP computer, hard drive, and the other peripherals, the two Analytek 5-slot VME chassis, and the Uninterruptable Power Supply.

## II. INITIAL START-UP

### A. Power On

The power switches should be turned on as follows (all switches are on the front of the instrument except the GPS Receiver):

1. Stanford Research Systems (SRS) Pulse Generator

2. Control Box (toggle switch to green light)

3. Power Supply Box (push-button switch at far right should light up green. Red light should come on above normal/off/standby switch). Toggle switches should all be up.

4. Chirp Power Supply

5. Uninterruptable Power Source

6. Computer Monitor

7. Computer, hard drive, and all other peripherals

8. Both VME Analytek 5-slot chassis (black toggle switch)

9. Power amp in Transmitter Box (silver toggle switch should be up)

10. GPS Receiver


B. Load Software

1. When the computer is turned on it should boot up HP BASIC.

2. If this is the first time powering up the system, load the program *AAFE_START* by typing in

<p style="text-align:center">LOAD *"AAFE_START_NEW"*</p>

and hitting return.

4. If the radar has already been running, you've stopped it and you want to start it up again and change the number of averages, load *AAFE_RUN* by typing (use this only if you have not turned off the power to any part of the system)

<p style="text-align:center">LOAD *"MAIN/AAFE/PROGRAMS/AAFE_RUN"*</p>

and hitting return.

5. If the radar has already been running, you've stopped it and you want to start it up again, but do not want to change the number of averages, load *AAFE_RERUN* by typing (use this only if you have not turned off power to any part of the system)

<p style="text-align:center">LOAD *"MAIN/AAFE/PROGRAMS/AAFE_RERUN"*</p>

and hitting return.

6. Summary of AAFE programs

*AAFE_START* - inital start up

*AAFE_RUN* - re-start and change averages

*AAFE_RERUN* - re-start

## III. RUNNING SOFTWARE

A. Press RUN key using softkeys or type in RUN and hit return. Follow through the series of steps listed below (they are also explained on the computer screen).

1. Enter the number of averages (using softkeys) either 1, 16, 34; 64, 128, 256, or 512. 64 averages is recommended.

2. If running *AAFE_START* the computer will immediately start down- loading software to the VIPER board. The software will scroll by on the screen monitor as this occurs. This process will take approximately 5 minutes. Occasionally timeouts and breaks will occur, this is OK. While the software is downloading, the SYSFAIL light on the VME GPIB card in the bottom 5-slot VME chassis will be red. When the final line of code is downloaded this light will turn green.

3. If running *AAFE_RUN* or *AAFE_RERUN*, hit the abort and reset toggle switches located on the VIPER 8704/30 card in the bottom 5-slot VME chassis. Again, the software will scroll by on the monitor as the software is downloaded to the VIPER board.

4. The monitor will display a list of things to check once the software has been loaded to VIPER. In addition to checking these things, check that the SYSFAIL light on the VME GPIB board in the bottom 5-slot VME chassis is green. Then press continue on softkeys.

5. Enter desired radar rep rate, (in Hz). 750 is recommended. Hit return after entering number.

6. Enter desired pulse width with softkeys if you want a full, half, or quarter pulse width. Hit the "Enter amount" to enter any pulse width. The display on the screen shows the minimum altitude that can be flown when using each pulse width. It is recommended to use as large a pulse width as possible. When in a calibration loop, always use the full pulse width.

7. Next, the computer will ask you if an initialization should be performed on the Analytek system. This should be done every time the system is first turned on. After the initialization has been done once, it does not have to be done again if the power is not cycled. If you enter YES a calibration will be done. This takes approximately 3 minutes. As the Analytek is calibrating the STATUS lights on the Analytek 2000P card in the top 5-slot VME chassis should flicker on and off. In addition, the trigger mode and ready light on the Analytek 2000T card may also flicker. Once the calibration process is done, a Data Acquisition System Status screen will be displayed. This should read:

AC Calibration data is invalid DC Calibration date is valid AC Correction is off DC Correction is on Display is off SCSI is on Signal averaging is off Clock Frequency (MHz): 1000 Sample Frequency (MHz): 166 Segment length: 512 Process length count: 512 Trigger coupling: DC Trigger delay (usec): 4.39156626506 Trigger mode: POST Trigger offset (V): 1 Trigger slope: POS Trigger type: EXT

If they are all correct, press continue on softkeys.

8. Enter the number of records or waveforms to store in one data file. 40000 records is approximately one flight hour. 40000 is recommended during flights. Press return after entering the number.

9. The computer will come up with RADAR MODE display. Each mode is described in detail in the following sections.

B. Calibration Mode

1. When running the radar you should always start with the calibration mode to check for a clean calibration pulse. This lets you know that everything is powered up and working. This calibration loop alone DOES NOT calibrate any system delays. To calibrate system delays, such as the waveguide run, see section on Calibrating System Delays.

2. Hit the Calibrate softkey. The monitor should come up with an AAFE Radar Altimeter display, which shows the calibration pulse. This pulse should be a spike located at approximately 0.0 meters.

Some things to check for:

- The READY light on the Analytek 2000T card in the top 5-slot VME chassis should be a steady green.

- The SYSFAIL light on the VME GPIB card in the bottom 5-slot VME chassis should be a steady green.

-the USEP IND light on the VIPER 8704/30 should be rapidly flashing orange (this shows data is passing over the bus from the VIPER to the HP computer).

3. From the Calibration mode, you can adjust the AGC using the softkeys and you can adjust the pulse using a softkey. A smaller pulse width gives a wider calibration pulse. In addition, you can stop the radar using a softkey or change to the oter radar modes, which are described in the following sections.

4. The AGC setting starts at 14 dB. If you increase the AGC, you should bee the peak power level reduce. If you decrease the AGC, you will eventually start to saturate the AGC and the pulse will get noisy.


C. Radiate Mode (please ready steps 1 - 3 befor entering this mode)

1. This is the transmit mode of the radar and is the mode typically used to obtain altitude data.

2. IMPORTANT: DO NOT USE THE RADIATE MODE WHILE IN THE LAB OR ON THE GROUND! The radar should only be put in the radiate mode

when the aircraft is flying at an altitude above 100 meters. Otherwise the power level from nearby reflections in the lab or from the ground when the radar is in an aircraft may cause serious damage to the receiver and transmitter.

3. If you wish to go through the sequence of steps for the radiate mode while in the lab or on the ground, TURN OF THE POWER SWITCH ON THE POWER SUPPLY!

4. Hit the Radiate mode softkey and the computer will ask you to choose an estimator routine for tracking. OCOG is recommended for rapidly varying terrain, while MAX VAL is the best for slowly varying highly reflective terrain. The MAX VAL also takes the least computation time and is recommended whenever possible. Use the softkeys to choose a tracker.

5. Choose a smoothing method. Right now there is only one smoothing method programmed, it is alpha-beta smoothing. This does not work that well. If flying at altitudes and under conditions where a clean pulse is obtained, not smoothing is necessary. Therefore the "no smoothing" softkey is recommended. If you choose no smoothing, go on to the next step. Otherwise, if you choose alpha-beta, the computer will ask you for an alpha parameter (.5 is recommended) and then for a beta parameter (.03125 is recommended). This smoothing technique works like a two-pole filter. You will also be asked to enter an alpha and a beta for the AGC. The same values are recommended.

6. Enter the maximum altitude for the acquisition mode (in meters) This is the highest range that the acquisition mode will look at when it attempts to gain lock. An altitude of 300 to 400 meters above the intended flight altitude is recommended. Hit return after entering number.

7. Enter the minimum altitude for the acquisition mode (in meters). This is the lowest range that the acquisition mode will look at when it attempts to gain lock. An altitude 100 to 200 meters below the intended flight altitude is recommended. DO

NOT ENTER AN ALTITUDE THAT IS BELOW THE POSSIBLE ALTITUDE FOR THE TRANSMITTED PULSE WIDTH! Hit return after entering number.

8. The radar will immediately enter the acquisition mode. "Acquisition" will show up on the screen and the display screen on the SRS Pulse Generator should scroll through the delay times which correspond to the ranges in the acquisition window. Once the radar has obtained lock it will enter its normal tracking mode. The radar should automatically control the AGC and keep the waveform in the display window.

9. You can use the softkeys to manually control the AGC, the position of the waveform (delay), the transmitted pulse width and to stop the radar. If the radar stays in the acquisition mode because it can't obtain lock, there is an escape key to leae the acquisition and start over with a new min and max altitude.

10. You can also switch to the Calibrate or Rad Test mode from this mode.

11. If you have entered a maximum and minimum range that does not include the actual aircraft altitude, the radar will keep entering the acquisition mode over and over. The escape softkey allows you to leave the acquisition mode and enter a new max and min range.


D. Rad Test Mode (please read steps 1 - 3 before entering this mode)

1. This is the manual transmit mode of the radar. It transmits and receives just like the Radiate mode, but the control of the AGC and the tracking are completely manual.

2. IMPORTANT: DO NOT USE THE RAD TEST MODE WHILE IN THE LAB OR ON THE GROUND! The radar should only be put in the rad test mode when the aircraft is flying at an altitude above 100 meters. Otherwise, the power level from nearby reflections in the lab or from the ground when the radar is in an aircraft may cause serious damage to the receiver and transmitter.

3. If you wish to go through the sequence of steps for the rad test mode while in the lab or on the ground, TURN OFF THE POWER SWITCH ON THE POWER SUPPLY!

4. Hit the Rad Test mode softkey and the computer will ask you to enter the initial range to the surface. Hit return after entering the number.

5. The return from the initial range entered will be displayed on the screen. You can then adjust the delay to either put the waveform in the center of the window or find the return if there is not one present. The AGC and pulse width can also be adjusted manually.

6. The radar will not automatically track when in this mode, all tracking must be done manually by incrementing and decrementing the delay. This mode is recommended in areas where the tracking mode does not work well. Both the Calibrate and Radiate mode can be entered from this mode.

## IV. CALIBRATION OF SYSTEM DELAYS

In order to achieve as accurate altitude measurements as possible, all internal delays in the AAFE radar altimeter must be calibrated. These are three places where delays occur: the radar hardward (transmitter and receiver), the wavelength run, and the horn antenna. Once these delays have been determined, the reference plane for the altitude measurements is the aperture of the horn antenna.

THIS CALIBRATION PROCESS SHOULD BE PERFORMED EVERY DAY THAT THERE IS A TEST FLIGHT OR DATA FLIGHT!

A. Measurement of Total System Delay

1. The total delay in the system, $t_{system}$ is

$$t_{system} = t_{hardware} + t_{waveguide} + t_{antenna}$$

This can be measured by performing the following steps.

2. Place a "short" (a metal plate) over the aperture of the horn antenna.

3. Start up the radar, create a file of approximately 5000 blocks, and use a FULL pulse width.

4. MAKE SURE THE RADAR IS PUT IN THE CALIBRATION MODE.

5. Store the entire 5000 waveforms in the file and then stop the radar.

6. Rename the file to $< DATE > \_ant\_cal$.

## B. Measurement of $t_{hardware}$

1. Place a "short" (a metal plate) over the circulator port that normally goes to the waveguide.

2. Repeat steps 3 through 5 under Measurement of Total System Delay.

3. Rename the file to $< DATE > \_hard\_cal$.

## C. Measurement of $t_{waveguide}$

1. Place a "short" (a metal plate) at the end of the waveguide run (before the antenna).

2. Repeat steps 3 through 5 under Measurement of Total System Delay.

3. Rename the file to $< DATE > \_wave\_cal$.

4. This is actually a measurement of $t_{hardware} + t_{waveguide}$. To get just $t_{waveguide}$, the previous measurement of $t_{hardware}$ should be subtracted from this measurement.

5. A check on the measurement of $t_{waveguide}$ should be performed using a network analyzer.

## D. Measurement of $t_{antenna}$

1. By subtracting $t_{hardware}$ and $t_{waveguide}$ from $t_{system}$, you will have a measurement of $t_{antenna}$.

2. A check on the measurement of $t_{antenna}$ should be performed using a network analyzer.

E. External Calibration

1. Aircraft should be on the ground and stationary. Put a large piece of metal on the ground directly below the antenna.

2. Repeat steps 3 through 5 under the Measurement of Total System Delay.

3. Rename the file to $< DATE > \_ext\_cal$.

4. Measure distance from antenna aperture to ground directly below it using a tape measure and a plumb to ensure a straight line.

## DATA CATALOG

1994 AAFE Data Quick Reference Time Line

Time breakdown, by Mission, File, Time describing when AAFE data is bad enough to ignore data from 1994 data sets.

See AAFE log book for more information as only reasonably large sections of data are listed here. Times when track is temporarily lost and notes about terrain, flight maneuvers, and good returns are included.

If a file is not listed, data is worth investigating.

<u>Mission 1</u>

| | | |
|---|---|---|
| My21123046 | 12:30 to 13:08 | No Signal |
| My21134822 | 13:52 to 13:59 | Bad Signal |
| | 14:26 to 14:46 | No Signal |
| My21165433 | 17:51 to 18:02 | " " |
| My21180355 | 18:13 to 18:26 | No Signal |

<u>Mission 2</u>

| | | |
|---|---|---|
| My23125104 | 13:16 to 13:32 | Bad / None |
| My23173516 | 17:42 to 17:50 | " " |
| | 18:20 to ... | |
| My23183846 | ... to 18:42 | Bad / None |

<u>Mission 6</u>

| | | |
|---|---|---|
| My31124410 | Whole File | Tx fell off of rails |
| My31141043 | Whole File | before flight. Repaired |

| | | |
|---|---|---|
| My31151254 | Whole File | after 4th file. |
| My31161509 | Whole File | |

Mission 7

| | | |
|---|---|---|
| Jn01140306 | 14:20 to 14:53 | Bad Data |
| Jn01150717 | 16:10 to 16:20 | ”” |
| Jn01162032 | 16:20 to 16:50 | ”” |
| Jn01172309 | 17:40 to 17:47 | ”” |
| | 18:08 to 18:33 | ”” |

Mission 8

| | | |
|---|---|---|
| Jn06113756 | 13:32 to 14:12 | Bad Data |

Mission 9

| | | |
|---|---|---|
| Jn07165909 | 17:00 to 17:05 | No Signal |

Mission 10

None

Mission 11

| | | |
|---|---|---|
| Jn09110203 | 13:21 to 13:48 | Bad Signal (Clipping) |
| Jn09134913 | 13:49 to 13:53 | Bad / None |
| Jn09145152 | 14:58 to 15:15 | ”” |

Mission 12

| | | |
|---|---|---|
| Jn14160138 | 16:50 to 17:04 | Bad / None |
| Note: | Parts of this Mission were flown under 380m due to ceiling. | |

Mission 13

| | | |
|---|---|---|
| Jn16124027 | 13:25 to 13:55 | Low Altitude |
| Jn16135250 | 14:40 to 14:46 | Bad Data |

Mission 14

Lots of aerial maneuvers. See flight log (no large data lapses).

DATs for AAFE Data


1994 Data:


"Even Mission Tape"

| | | |
|---|---|---|
| Tar 1: | My21212148 | (From Mission 1) |
| | My23102850 | (Mission 2) |
| | My23125104 | |
| | My23132515 | |
| | My23140043 | |
| | My23150345 | |
| | My23163314 | |
| | My23173516 | |
| | My23183846 | |
| Tar 2: | My31115934 | (Mission 6) |
| | My31124410 | |
| | My31141043 | |
| | My31151254 | |
| | My31161509 | |
| | My31180757 | |
| | My31181325 | |
| | My31191628 | |
| | My31202622 | |
| Tar 3: | Jn06113756 | (Mission 8) |
| | Jn06141959 | |
| | Jn06152225 | |
| | Jn06162437 | |

|         |              |                         |
|---------|--------------|-------------------------|
|         | Jn06172640  |                         |
| Tar 4:  | Jn08121100  | (Mission 10)            |
|         | Jn08134732  |                         |
|         | Jn08145311  |                         |
|         | Jn08162245  |                         |
|         | Jn08172510  |                         |
| Tar 5:  | Jn09200039  | (From Mission 11)       |
|         | Jn14114003  | (Mission 12)            |
|         | Jn14135607  |                         |
|         | Jn14145838  |                         |
|         | Jn14160138  |                         |
|         | Jn14171638  |                         |
| Tar 6:  | Jn16173226  | (From Mission 13)       |
|         | Jn17101906  | (Mission 14)            |
|         | Jn17124123  |                         |
|         | Jn17124414  |                         |
|         | Jn17134719  |                         |
|         | Jn17145004  |                         |

"Odd Mission Tape"

|         |              |                         |
|---------|--------------|-------------------------|
| Tar 1:  | My06183203  | (Test Flight at Wallops)|
|         | My06184930  |                         |
|         | My06213631  |                         |
|         | My06225218  |                         |
| Tar 2:  | My21110045  | (Mission 1)             |
|         | My21123046  |                         |
|         | My21134822  |                         |

|         |              |                                       |
|---------|--------------|---------------------------------------|
|         | My21145024   |                                       |
|         | My21155230   |                                       |
|         | My21165433   |                                       |
|         | My21180355   |                                       |
| Tar 3:  | Broken Pipe  | (Just Tape Error - No Data Missing)   |
| Tar 4:  | Jn01111345   | (Mission 7)                           |
|         | Jn01124358   |                                       |
|         | Jn01140306   |                                       |
|         | Jn01150717   |                                       |
|         | Jn01162032   |                                       |
|         | Jn01172309   |                                       |
|         | Jn01183522   |                                       |
| Tar 5:  | Jn07120345   | (Mission 9)                           |
|         | Jn07135140   |                                       |
|         | Jn07145356   |                                       |
|         | Jn07155631   |                                       |
|         | Jn07165909   |                                       |
|         | Jn07180149   |                                       |
|         | Jn07190357   |                                       |
| Tar 6:  | Jn08190219   | (From Mission 10)                     |
|         | Jn09110203   | (Mission 11)                          |
|         | Jn09134913   |                                       |
|         | Jn09145152   |                                       |
|         | Jn09160259   |                                       |
|         | Jn09170528   |                                       |
|         | Jn09180743   |                                       |
| Tar 7:  | Jn14185440   | (Mission 13)                          |

Jn16102008

Jn16124027

Jn16135250

Jn16145622

Jn16161337

Opticals for AAFE Data

1991 Data:                    Side A

Greenland Data:

| | |
|---|---|
| 91_cals | 91ag13antcal1 |
| | 91ag13antcal2 |
| | 91ag28cal |
| | 91sp13antcal |
| 91sp04 | 91sp04122815 |
| | 91sp04130811 |
| | 91sp04140009 |
| | 91sp04150828 |
| | 91sp04160935 |
| | 91sp04161311 |
| | 91sp04162440 |
| 91sp12 | 91sp12125412 |
| | 91sp12135840 |
| | 91sp12150311 |
| | 91sp12160957 |
| | 91sp12171337 |
| 91sp18 | 91sp18123951 |
| | 91sp18134342 |
| | 91sp18144703 |
| | 91sp18155040 |
| | 91sp18165503 |
| 91sp19 | 91sp19123356 |
| | 91sp19133803 |
| | 91sp19144127 |

|  |  | 91sp19154449 |
|  |  | 91sp19164941 |
|  | 91sp20 | 91sp20122521 |
|  |  | 91sp20132908 |
|  |  | 91sp20143226 |
|  |  | 91sp20164519 |
|  | 91sp21 | 91sp21140624 |

1991 Data: Side B

Greenland Data:

|  | 91_test_flights |  | 91jul31150101 |
|  |  |  | 91jul31151508 |
|  |  |  | 91jul31153123 |
|  |  |  | 91jul31155921 |
|  |  |  | 91jul31160236 |
|  |  |  | 91jul31160905 |
|  |  |  | 91jul31161338 |
|  |  |  | 91jul31161842 |
|  |  |  | 91jul31162043 |
|  |  |  | 91jul31163656 |
|  |  |  | 91jul31164051 |
|  |  |  | 91jul31172525 |
|  |  |  | 91jul31172952 |
|  |  |  | 91jul31173236 |
|  |  |  | 91jul31174639 |
|  |  | 91aug02 | 91aug0275449 |
|  |  |  | 91aug0281202 |

|          | 91aug0282307   |
|----------|----------------|
|          | 91aug0282558   |
| 91aug07  | 91aug07173315  |
|          | 91aug07173818  |
|          | 91aug07174153  |
|          | 91aug07204505  |
| 91aug08_09 | 91aug08235656 |
|          | 91aug09100708  |
|          | 91aug09151415  |
| 91aug13_14 | 91aug13235747 |
|          | 91aug14163841  |
|          | 91aug14164208  |
|          | 91aug14175857  |
|          | 91aug14184646  |
|          | 91aug14192359  |
|          | 91aug14193722  |
| 91aug15  | 91aug15164535  |
|          | 91aug15190441  |
|          | 91aug15201531  |
| 91aug23  | 91aug23130938  |
|          | 91aug23143325  |
|          | 91aug23145557  |
|          | 91aug23145733  |
|          | 91aug23150345  |
|          | 91aug23150654  |
|          | 91aug23150956  |
|          | 91aug23152307  |

|  |  | 91aug23160853 |
|---|---|---|
|  |  | 91aug23161339 |
|  |  | 91aug23161739 |
|  |  | 91aug23170253 |
|  | 91ag24 | 91ag24135355 |
|  |  | 91ag24143820 |
|  |  | 91ag24145816 |
|  |  | 91ag24160823 |
|  | 91ag28 | 91ag28152500 |
|  |  | 91ag28163115 |
|  |  | 91ag28180052 |
|  |  | 91ag28193040 |
|  | 91ag29 | 91ag29161611 |
|  |  | 91ag29174809 |
|  | 91ag30 | 91ag30132103 |
|  |  | 91ag30152036 |
|  | 91ag31 | 91ag31132637 |
|  |  | 91ag31142813 |
|  |  | 91ag31161256 |
|  |  | 91ag31174716 |

Newfoundland Data:

| 91_test_flight | nv09212129 |
|---|---|
| 91_transit_flight | nv13154532 |
|  | nv13164948 |
| 91nv14 | nv14131927 |
|  | nv14135333 |

|  |  |
|---|---|
|  | nv14145829 |
| 91nv14_91nv15 | nv14235556 |
|  | nv15002543 |
|  | nv15010916 |
| 91nv17_91nv18 | nv17223216 |
|  | nv17232406 |
|  | nv18002418 |
|  | nv18012448 |
| 91nv20 | nv20125356 |
|  | nv20135356 |
|  | nv20205901 |

1993 Data, Optical 1 of 2:

Side A

| MISSION6 | 93Jn23102345 |
|---|---|
|  | 93Jn23103332 |
|  | 93Jn23105019 |
|  | 93Jn23105727 |
|  | 93Jn23110916 |
|  | 93Jn23112247 |
|  | 93Jn23120316 |
|  | 93Jn23130232 |
|  | 93Jn23142651 |
|  | 93Jn23152604 |
|  | 93Jn23154010 |
| MISSION1-5 | 93Jn27120925 |
|  | 93Jn27132314 |

|  |  |
|---|---|
|  | 93Jn27143113 |
|  | 93Jn27144625 |
|  | 93Jn27155540 |
|  | 93Jn27170428 |
| MISSION3-10 | 93Jn28102007 |
|  | 93Jn28104004 |
|  | 93Jn28114558 |
|  | 93Jn28124655 |
|  | 93Jn28134728 |
|  | 93Jn28144800 |
|  | 93Jn28150759 |
|  | 93Jn28161009 |
|  | 93Jn28164640 |
| MISSION4X | 93Jl03112821 |
|  | 93Jl03123917 |
|  | 93Jl03135154 |
|  | 93Jl03145317 |
| 93cal_files | 93sp23broad_bm_antcal |
|  | 93sp23internal_cal |
|  | 93sp23nar_bm_antcal |
|  | 93sp27_107.3cm_extcal |
|  | 93oc08_plate_at_Xcm |
|  | 93oc18new_108cm_cal |
|  | 93oc18new_plate_cal |

Side B

|  |  |
|---|---|
| MISSION7 | 93Jn24133312 |

|  |  | 93Jn24143531 |
|--|--|--------------|
|  |  | 93Jn24145951 |
|  |  | 93Jn24151425 |
|  |  | 93Jn24154516 |
|  |  | 93Jn24161540 |
| MISSION11 |  | 93Jn25121609 |
|  |  | 93Jn25122932 |
|  |  | 93Jn25133413 |
|  |  | 93Jn25143823 |
|  |  | 93Jn25154511 |
| MISSION10Y |  | 93Jl01122411 |
|  |  | 93Jl01134059 |
|  |  | 93Jl01141923 |
|  |  | 93Jl01154742 |
|  |  | 93Jl01164815 |
| MISSION9Y |  | 93Jl08113227 |
|  |  | 93Jl08121404 |
|  |  | 93Jl08131513 |
|  |  | 93Jl08141659 |
|  |  | 93Jl08152021 |
|  |  | 93Jl08162105 |

1993 Data, Optical 2 of 2:

Side A

| MISSION1-5 | As in Optical 1 |
|------------|-----------------|
| MISSION7 | As in Optical 1 |
| MISSION10Y | As in Optical 1 |

| | |
|---|---|
| MISSION11 | As in Optical 1 |
| MISSION5Y | 93J102112407 |
| | 93J102121709 |
| | 93J102124313 |
| | 93J102134421 |
| | 93J102144923 |

Side B

| | |
|---|---|
| MISSION5Y | As above |
| MISSION9-4 | 93J107095039 |
| | 93J107101753 |
| | 93J107114039 |
| | 93J107124132 |
| | 93J107134805 |
| | 93J107145003 |
| | 93J107160208 |
| MISSION11A | 93J109095902 |
| | 93J109105533 |
| | 93J109113342 |
| | 93J109120815 |
| | 93J109130906 |
| | 93J109135604 |
| | 93J109141658 |
| | 93J109153351 |
| | 93J109163423 |

## Bibliography

[1] NASA, . *Final Report of the Advanced Application Flight Experiment Breadboard Pulse Compression Radar Altimeter Program*, 1976. NASA Contractor Report CR-141411.

[2] Zwally, H. J. Growth of greenland ice sheet: Interpretation. *Science*, 246:1589 – 1591, December 1989.

[3] Ferraro, Ellen. *Analysis of Airborne Radar Altimetry Measurements of the Greenland Ice Sheet*. PhD thesis, University of Massachusetts, Amherst, MA, 1994.

[4] Skolnik, Merril I. *Introduction to Radar Systems*. McGraw Hill Inc., New York, 2nd edition, 1980.

[5] Ulaby, F. T., Moore, R. K., and Fung, A. K. *Microwave Remote Sensing, Active and Passive*, volume II: Radar Remote Sensing and Surface Scattering and Emission Theory, chapter 7: Measurement and Discrimination. Artech House, Inc., 1986.